2015-09-30

Modelling Tumour Control in External Beam Radiotherapy for Prostate Cancer

Balderson, Michael

UNIVERSITY OF CALGARY

Modelling Tumour Control in External Beam Radiotherapy for Prostate Cancer

by

Michael John Balderson

A THESIS

SUBMITTED TO THE FACULTY OF GRADUATE STUDIES

IN PARTIAL FULFILLMENT OF THE REQUIREMENTS FOR THE

DEGREE OF DOCTOR OF PHILOSOPHY

GRADUATE PROGRAM IN PHYSICS AND ASTRONOMY

CALGARY, ALBERTA

SEPTEMBER, 2015

Abstract

Modeling tumour control for prostate treatments can be challenging. Models used to predict tumour control are typically based on the well known linear-quadratic (LQ) model for cell survival. The LQ model accurately predicts cell killing for a given radiation dose in most cases, however in some cases the LQ model falls short and LQ model predictions differ from what has been observed experimentally. Cell survival following low radiation doses ($\sim$ <1Gy) and radiation induced bystander effects are two examples where the LQ model potentially falls short at modelling cell survival following an absorbed radiation dose.

Using mathematical models that account for radiation induced bystander and low dose hypersensitivity effects, we look at how these effects potentially change predicted outcomes of tumour control when compared to standard LQ predictions. We start by investigating how the basic LQ model predicts tumour control under large geometric miss errors under intensity modulated radiation therapy (IMRT) and volume modulated arc therapy (VMAT) modalities. Next, we look at the geometric miss scenario again, but rather than compare two different delivery techniques we investigate how radiation induced bystander effects potentially change predicted tumour control under geometric miss cases. We then expand on this idea and study how radiation induced bystander effects potentially influence predicted outcome under heterogeneous dose distributions. Finally, we compare the relative biological effectiveness (RBE) of bystander effects with low dose hypersensitivity effects and spectral effects for out-of-field radiation doses.

The majority of this work focused on how radiation induced bystander effect changed biological modeling of tumour control in external beam radiotherapy for prostate cancer. This work ultimately demonstrates that bystander effects can modify predicted outcomes of tumour control. We have shown that bystander effects potentially improve TCP under

geometric miss and that bystander effects may relax the common planning constraint of aiming for dose homogeneity within a target volume.

Acknowledgements

First, I would like to thank my supervisor Dr. Charlie Kirkby. I could not have asked for a better and attentive PhD supervisor. Your door was always open to me and I felt comfortable asking you any question regardless how "dumb" it may have seemed to you. More than once I received an email on the weekend with an idea regarding the project or Monday morning would role around and you would come find me, excited to discuss some idea you had been thinking about over the weekend or had been pondering over a vacation. I don't think I could have had a more caring, attentive, and kind supervisor. Whenever I needed feedback, comments on the project, or a reference letter, you provided them within 24 hrs. Other graduate students were envious of this efficient turn around time. I will miss our "soap box" discussion about life in general as well as the ongoing within the Medical Physics Community. It was an honour and privilege to be your fist PhD graduate student. I would like to also thank the other members of my PhD committee Dr. Derek Brown, Dr. Peter Dunscombe, and Dr. Abhijit Ghose for providing such valuable insight and expertise which helped keep me on track and allowed this project to move forward.

I would like to acknowledge the University of Calgary, the Tom Baker Cancer Centre, the staff at the Jack Ady Cancer for their support and friendship. I would also like to thank all my fellow graduate students at the TBCC for their support and friendship as well, particularly Nathan Becker, Dal Granville, and Sarah Quirk for the total team effort during our time together in Calgary.

I would not be where I am today without my family, especially my lovely wife Amy and my two boys Carter and Nate. This year will mark our 10 year wedding anniversary and the last 10 years have been quite a journey (living in 3 cities, 6 different houses, 2 kids and one on the way). I would not have been able to accomplish what I have without

the support of my wife Amy.

To my lovely Family - Amy, Carter, Nate, and baby number 3 :) .

This work would not have been possible without you!

Table of Contents

List of Tables

List of Figures and Illustrations

List of Symbols, Abbreviations and Nomenclature

Symbol	Definition
AAPM	American Association of Physicists in Medicine
AP	Anterior Posterior
ATM	Ataxia Telangiecatasia Mutated
AXB	Acuros XB
BER	Base Excision Repair
CBCT	Cone Beam Computed Tomography
CTV	Clinical Target Volume
dDVH	Differential Dose Volume Histogram
DVH	Dose Volume Histogram
DNA	Deoxyribonucleic Acid
DSB	Double Strand Break
EBRT	External Beam Radiation Therapy
EUD	Equivalent Uniform Dose
gEUD	Generalized Equivalent Uniform Dose
gLQ	Generalized Linear Quadratic
GJIC	Gap Junction Intercellular signalling
Gbp	Giga base pair
GTV	Gross Tumour Volume
HRR	Homologous Recombination Repair
HRS	Hyper-Radiosensitivity
ICRU	International Commission on Radiation Units & Measuremen
IGRT	Image Guided Radiation Therapy
IM	Internal Margin

IMRT	Intensity Modulated Radiation Therapy
IJRB	International Journal of Radiation Biology
IRR	Increased Radioresistance
ITV	Internal Target Volume
LINAC	Linear Accelerator
LQ	Linear Quadratic
LR	Left Right
mLQ	Modified Linear Quadratic
MRI	Magnetic Resonance Imaging
NTCP	Normal Tissue Complication Probability
NHEJ	Nonhomologous End Joining
PET	Positron Emission Tomography
PRV	Planning Rectal Volume
PTV	Planning Target Volume
QA	Quality Assurance
QC	Quality Control
RBE	Relative Biological Effectiveness
SBRT	Stereotactic Body Radiation Therapy
SD	Standard Deviation
SF	Surviving Fraction
SF_{LQ}	Surviving Fraction Linear Quadratic
SI	Superior Inferior
SRS	Stereotactic Radiosurgery
SSB	Single Strand Break
SSBR	Single Strand Break Repair

TBCC	Tom Baker Cancer Centre
TCP	Tumour Control Probability
TG	Task Group
U of C	University of Calgary
PDF	Probability Distribution Function

Chapter 1

Introduction

1.1 Cancer in Society

In 2014 were was an estimated 191,300 new cases of cancer diagnosed and 76,600 cancer related deaths in Canada [3]. According to the Canadian Cancer Society the lifetime probability of developing cancer in Canada is 45 % for men and 42 % for women. Within Alberta there were an estimated 16,500 new cases of cancer diagnosed in 2014 [3]. Cancer currently is the leading cause of death within Canada with 29.9 % of all deaths being cancer related. Cancer is caused when cells within the body begin to proliferate in an uncontrolled manner when regular control mechanisms fail. These abnormal cells can invade other healthy tissues and/or metastasize to other parts of the body. There are many different types of cancer and generally speaking the specific type of cancer is named after the specific organ of issue in which the cancerous cells originated. For example, prostate cancer is so named because the abnormal cells originated from the prostate gland even though they may have metastasized to other organs within the body. Prostate and breast cancer are the most frequently diagnosed cancers for males and females respectively, followed by lung and colorectal cancers [3].

In addition to being personally costly, cancer has major economic ramifications on society at large. In 2000, cancer was the fourth most costly disease in Canada, accounting for $17.4 billion. These costs include $2.6 billion in direct healthcare costs, which included physician and hospital expenses, and $14.8 billion in indirect costs from lost productivity and premature death [4].

1.1.1 Prostate Cancer

Among men, prostate cancer is the most diagnosed form of cancer accounting for almost 25% of new cancer cases. The lifetime probability of developing prostate cancer in Canada is 13.1% whereas the lifetime probability of dying from prostate cancer is 3.6% [3]. The vast majority of new prostate cancer cases occur in men over the age of 50. Prostate cancer in Canada is the third most common cause of cancer deaths in men, preceded by lung and colorectal in terms of cancer-related deaths.

Typically the main treatment options for prostate cancer include surgery, chemotherapy, radiation, hormone therapy, and watchful waiting [5]. Treatment methods are determined once the cancer has been staged and the risk to the patient has been assessed. Staging is generally based on three main categories known as T, N, and M categories. T Categories assess the size, extent, and involvement of the tumour, N categories look at the lymph node involvement, and M categories consider if the cancer has metastasized outside the primary site. Often a combination of methods is used in the treatment of prostate cancer such as surgery followed by radiation, particularly if the surrounding lymph nodes have been compromised.

1.1.2 Surgery

If the cancer is confined to the prostate gland a common procedure to control the disease is by removing the prostate gland through a radical prostatectomy. Radical prostatectomys involve removing the prostate, seminal vesicles, and surrounding tissues. Patients undergoing this type of procedure are typically in relatively good health.

1.1.3 Chemotherapy

Chemotherapy refers to chemical drugs which are administered by intravenous injection or by pills taken orally and these drugs often target the deoxyribonucleic acid (DNA).

Docetaxel (Taxotere), Cyclophosphamide (Cytoxan), and Doxorubicin (Adriamycin) are common chemotherapy drugs. In prostate cancer, chemotherapy may be given if the prostate cancer cells have metastasized outside the prostate gland and the cancer is not responding to hormonal therapy. Chemotherapy drugs typically target rapidly diving cells cancer as well as rapidly dividing normal cells such as hair follicles and cells inside the lining of the stomach and intestine. For this reason patients undergoing chemotherapy often lose hair and can experience nausea and diarrhea.

1.1.4 **Radiation Therapy for Prostate Cancer**

Roughly 50% of all incident cases of cancer require radiation treatment at some point during the management of the disease [6]. There are two main types of radiation therapy for the treatment of prostate cancer: external beam radiation (teletherapy) and internal radiation therapy (brachytherapy). In external beam radiation therapy (EBRT) the radiation source is outside the patient and the radiation is typically delivered through use of a linear accelerator known as a LINAC (see figure 1.1), It can be delivered externally by way of a radioactive source such as Cobalt 60, however this is less common. When a patient receives EBRT to treat prostate cancer, the prostate receives a prescribed radiation dose which is delivered over a number of fixed fractions. For example, intermediate risk prostate cancer patients at our centre typically receive a total dose of 78 Gy which is delivered over 39 fractions of 2 Gy/fraction.

Another option for the treatment of prostate cancer, other than EBRT, is the use of brachytherapy. In prostate brachytherapy, the radiation is delivered internally using implanted radioactive seeds (about the size of a grain of rice), which are surgically implanted inside the prostate gland. Iodine^{125} and Palladium^{103} are common radioactive materials used in prostate brachytherapy. This treatment method exposes the prostate cells to a continuous radiation dose rate that diminishes with time due to the radioactive

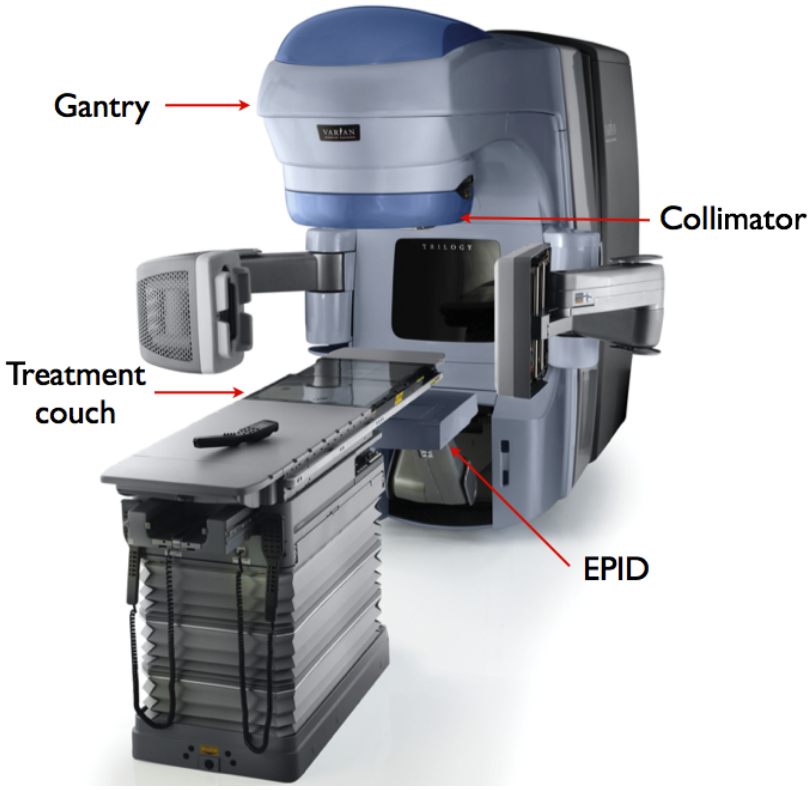

Figure 1.1: Varian Trilogy Linear Accelerator. Image courtesy of Varian Medical Systems, Inc. All rights reserved.

decay of the seeds. In this work however we have not touched on prostate brachytherapy treatments, but focused on EBRT of intermediate risk prostate treatments receiving a prescribed dose of 78 Gy delivered over 39 fractions. Prostate can also be treated using high dose rate brachytherapy.

1.1.5 Watchful Waiting

Prostate cancer is considered a relatively slow growing cancer. As a result, an elderly person or someone with major health complications might decide that instead of actively treating the cancer they will just monitor the slow progression of the cancer. In some cases, healthy patients might choose watchful waiting as well. This approach gives patients the option to avoid the negative side effects often associated with treatment with the understanding that other factors like age or other health circumstances will likely cause a person's death. If the cancer starts to spread more rapidly or aggressively then the patient still has the choice to take a more active treatment approach.

1.2 Current trends in Radiotherapy for Prostate Cancer

1.2.1 Intensity Modulated Radiation Therapy

For the treatment of prostate cancer, Intensity Modulated Radiation Therapy (IMRT) is a very common treatment approach in EBRT [7]. IMRT is an advanced form of 3D conformal radiation where the intensity of the radiation beam is modulated using mulitleaf collimators (MLC). IMRT has become a very common treatment for prostate cancer because by modifying both the shape and intensity of the incoming radiation one can achieve a highly conformal dose to the prostate gland, while at the same time limit dose to the surrounding normal tissues, such as bladder and rectum, which are particularly sensitive to radiation. In fact, IMRT radiation treatment for early stage

prostate cancer has been shown to be as effective as surgery [8].

1.2.2 **Volumetric Modulated Radiation Therapy**

Currently many IMRT prostate plans are delivered as the gantry moves around the patient in arc while the MLC modulates the beam intensity. This type of treatment approach is commonly refered to as volumetric modulated arc therapy (VMAT). Typically VMAT can deliver a slightly more conformal radiation dose compared with static gantry IMRT, while adequately sparing the surrounding normal tissues. There is some evidence to suggest that VMAT results in a lower normal tissue complication probability (NTCP) without compromising tumour control compared with IMRT [9, 10, 11]. VMAT plans typically take less time to deliver then conventional radiotherapy which is beneficial to a busy clinic with long wait times. One potentially negative side effect of VMAT is that there may be increased amounts of low dose radiation to the rest of the body [12]. The increased amount of low radiation dose received by the body is not without concern particularly because of the potential of increased induction of secondary malignancies especially for young people [13, 14]. Hall and Wuu even predicted a 1-1.75 % increase in radiation-induced secondary malignancies for patients living 10 years [15].

1.2.3 **Image-Guided Radiotherapy Therapy**

One of the major improvements in the treatment of prostate cancer has been through better use of imaging techniques. Many modern LINAC's are equipped with cone beam computed tomography (CBCT) scanners. CBCT gives the radiation therapist the ability to quickly acquire an image of the patient's internal anatomy including bony landmarks and soft tissues prior to treatment and adjust the position of the patient if necessary to conform to the planned geometry. This ensures that the radiation fields hit the target volume while at the same time minimize radiation dose to surrounding normal tissues

such as the bladder and rectum.

Often a combination of imaging techniques such as magnetic resonance imaging (MRI) and positron emission tomography (PET) are used in combination with CT images to help better identify the cancerous tumour during the diagnostic phase, as well as track the progression of the tumour during the treatment. As better imaging techniques are used throughout the course of treatment, there is potential to adapt the treatment accordingly on a patient-by-patient basis. This is known as adaptive radiotherapy and will likely play a large role in radiation treatments in the future.

Another major advantage of using image-guided radiation therapy (IGRT) is that it helps mitigate potential geometric errors. Geometic miss errors may occur because the cancerous volume has been misidentified and it extends beyond the planning target volume (PTV), an error of initial target definition [16]. In other cases, the target volume may be appropriately identified, but the miss stems from an extreme in the combination of random and systematic positioning errors. Protocols have been established to add appropriate treatment margins to account for these types of error [17, 18, 16, 19].

1.2.4 **Stereotactic Body Radiotherapy**

Currently there is an increasing trend to use stereotactic radiosurgery (SRS) as well as stereotactic body radiation therapy (SBRT) protocols in the management of human cancer [20, 21]. Historically, the different radiosensitivities of tumors and normal tissues allows one to maximize the therapeutic ratio by delivering a small dose ($\sim$1.8 - 2.0 Gy) over n fractions. This has been the standard of care for radiotherapy treatments over the past 90 years [21]. However, in recent years with the advent of newer technologies and better imaging capabilities like IMRT and IGRT, we are able to accurately deliver highly conformal treatments with a steep dose gradient outside the target. This has allowed for much higher dose per fractions to be delivered while maintaining reasonable sparing

of normal tissues. The ability to deliver high dose/fraction treatments is shifting the paradigm in radiotherapy treatment.

It is generally accepted that prostate cancer has a relatively low $\frac{\alpha}{\beta}$ ratio [22, 23, 24]. The $\frac{\alpha}{\beta}$ ratio is a parameter comprised of both the linear (α) and quadratic (β) parts of the Linear Quadratic model (see section 1.5.2). SBRT is an attractive option for treatment and is gaining the interest of many scientific investigators and there is potential that SBRT will become the standard of care in the management of prostate cancer [1, 20]. For prostate cancer, SBRT potentially offers improved outcomes while minimizing toxicity to normal tissues compared to other modalities like IMRT. Meier looked a different toxicity studies for stage l-ll prostate cancer and found the rates of late GU toxicity are similar to those seen with IMRT, and rates of late rectal toxicity may be less than with IMRT and low-dose rate brachytherapy (see figure 1.2) [1].

1.3 Errors in Radiotherapy

Errors in radiation therapy can never be completely eliminated and one of the major roles of the medical physicist is to establish proper quality assurance (QA) and quality control (QC) protocols to reduce the frequency and severity of errors [25]. In this work, one error we looked at was that of geometric miss. A geometric miss error might occur because the cancerous volume has been misidentified when first diagnosed [16] or it might occur if there is an extreme in the combination of positioning uncertainties and motion that results in a misalignment of the clinical target volume (CTV) with the radiation fields [26, 27, 28, 29, 30, 31, 32]. A major advantage of IGRT is that it helps mitigate potential geometric miss errors. A large part of this work investigated the impact geometric miss errors have on predicted outcome under different biological models.

Poisson-based tumour control probability (TCP) models are typically very sensitive

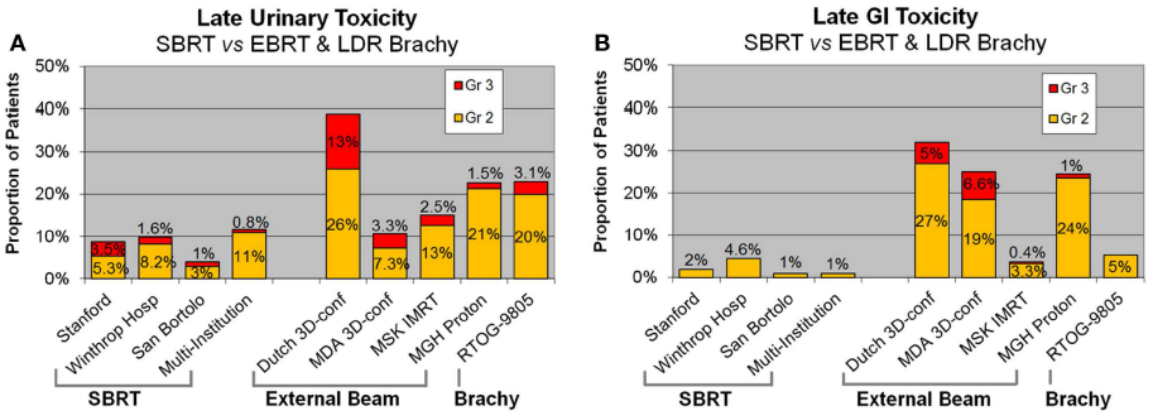

Figure 1.2: Late urinary (A) and GI (B) toxicity rates following SBRT, external beam radiotherapy, and brachytherapy. *SBRT, stereotacticbody radiotherapy* Source: Robert Meier: Dose-escalated robotic sbrt for stage l - ll prostate cancer -[1] used with permission.

to geometric miss. In order for the tumour to be controlled, all cells within the tumour must be exposed to a sufficiently high radiation dose otherwise some clonogenic cells will likely survive. For example, if a geometric miss results in even 1 % of the tumour cells not receiving the prescribed dose, then the TCP prediction will likely be extremely low [33].

Errors in radiotherapy are generally rare, however in some cases radiotherapy errors cause extreme harm to the patient and can even be fatal especially if the error results in the misadministration of the intended dose [34]. Errors can occur at any stage of the radiotherapy process from the initial planning stages to the administration of the radiation dose.

1.4 Biological Response to Radiation

Biological damage occurs when energy from ionizing radiation is absorbed in biological material. There is compelling experimental evidence that DNA is the most sensitive component of a cell [35]. The amount of energy absorbed per unit mass is termed the radiation dose and has units of Gy, where 1 Gy $= 1\frac{J}{kg}$. If the absorbed energy is sufficient to cause a break in or otherwise alter a DNA strand, damage may occur. Two mechanisms for breaking DNA strands exist: (1) direct, in which ionizing radiation interacts directly with atoms of the DNA and (2) indirect, in which ionizing radiation interacts with atoms in the cell producing free radicals which then can diffuse to the DNA and cause biological damage. A diagram of these two mechanisms is shown in figure 1.3. Damage from ionizing radiation my cause a single strand of the DNA to break (SSB) or may cause a double strand break (i.e. both strands of the DNA to break in close proximity to each). Single strand breaks in the DNA are almost always efficiently repaired. Many double strand breaks are also efficiently repaired. Ionizing radiation induces many more SSBs in the

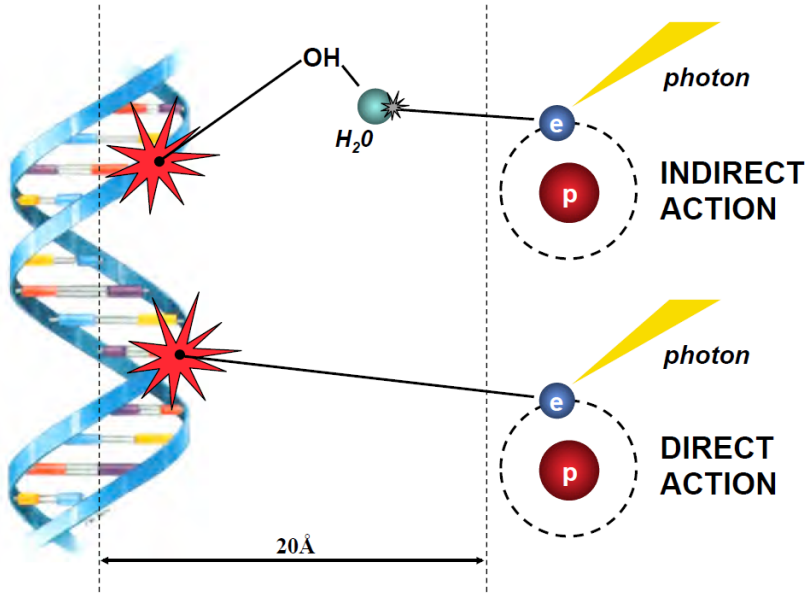

Figure 1.3: Direct and indirect action of gamma rays and X-rays on the DNA (source: T. Lawrence, Slideshow is from the University of Michigan Medical, open source; http://www.slideshare.net/ openmichigan/ 010709tlawrenceintroradoncologypreclin).

DNA compared with with DSB's, however it is the number of DSB's which is closely related to the probability the cell survival. For example, 1 Gy of radiation will induce about 1000 single-strand breaks in the DNA and only about 20-40 double-strand breaks [36]. To put this into perspective, 1 Gy of radiation will kill $\sim 30\%$ of cells [36]. Radiation damages both cancer cells as well as healthy normal cells and therefore an important goal of treatment is to deliver a lethal dose to the treatment site while minimizing the dose to surrounding normal tissue. When considering the time-dependent repair of DSB as it relates to the temporal delivery of the radiation beam as well as the intrinsic DSB repair kinetics of the cell the terms of sublethal and potentially-lethal damage are used. This can be modeled quite well in the LQ model using the Lea-Catcheside dose protraction factor G [54].

1.4.1 The four R's of Radiobiology

The goal of radiation therapy is to deliver a lethal radiation dose to the tumour while at the same to time minimizing the dose to surrounding normal tissues. In EBRT, this is accomplished by breaking up the radiation dose into multiple fractions. Delivering multiple fractions of radiation helps maximize the therapeutic ratio by taking advantage of some basic radiobiology properties. These basic radiobiology properties are known as the four R's of radiobiology and were first proposed by Withers [37]. Steel et al., have suggest there is a fifth R to account for the intrinsic property of cell radiosensitivity [38]. More details of the four main R's of radiobiology are provided below.

Repair of sublethal damage

Damage from ionizing radiation my cause a SSB or may cause a DSB. Single strand breaks in the DNA are almost always efficiently repaired. Many double strand breaks are also efficiently repaired. Ionizing radiation induces many more SSBs in the DNA compared with with DSB's, however it is the number of DSB's which is closely related to the probability the cell survival. Normal tissues are typically more efficient than cancer cells at recognizing and repairing damage caused by radiation. Delivering fractionated radiotherapy improves the thereputic ratio by killing more cancer cells compared with normal tissue cells because of the more efficient repair mechanism in the normal cells.

Cell cycle progression is controlled by molecular checkpoint genes. When radiation has dammaged a cell, these molecular checkpoint genes might prevent the cell from progress through the mitotic cycle. P53 is an important gene in this process. P53 can activate DNA repair proteins when damage has occurred, can arrest as cell at the G1/S phase of the mitotic cycle, and can initiate apoptosis. Ataxia telangiectasia mutated (ATM) protein also plays an important role in repairof DNA damage. Patients with autosomal recessive syndrome ataxia telagiectasia have a increased risk of developing caner and are

highly radiosensitive [36].

Reoxygenation effect

The presence of oxygen plays an important role in radiotherapy. Cells that are hypoxic are much more radioresistant to radiation damage than non-hypoxic cells [39, 40, 41, 42]. The presence of oxygen is an essential component in creating reactive oxygen species as well as free radicals which are key elements in the biological damage process from ionizing radiation. Damage produced by free radicals in DNA may be repaired under hypoxic conditions but may be "fixed" (made permanent and irreparable) if molecular oxygen is available [43]. Delivering multiple fractions of radiotherapy, gives time for previously hypoxic cells to become reoxygenated and therefore more radio sensitive.

Repopulation

Fractionated radiotherapy reduces the total number of clonogenic cells in the tumour following each radiation fraction. However, any surviving clonogenic cells have the potential to reproduce and therefore repopulate the tumour. Because tumour cells can continue to repopulate during treatment a higher dose of radiation than that required to kill "N" initial clonogens may be needed to achieve local control to successfully eradicate the remaining clonogenic cells.

In some cases it has been shown that some tumours experience accelerated repopulation. Accelerated repopulation is a phenomenon where cells proliferate faster following, or during, radiation treatment than they did prior to receiving treatment. Wither al el., looked at head and neck cancers and found that they experience accelerated repopulation about 28 days after the start of the 1st fraction of radiation [44]. To compensate for the accelerated repopulation, an additional dose of 0.6 Gy per day is required [43].

Reasortment within the cell cycle

Cells progress through different phases of their mitotic cell cycle. The mitotic cycle consists of mitosis (M), gap phase one (G1), DNA synthetic phase (S), and gap phase two (G2). The radiosensitivity of cells depends on what stage the cell is at in its mitotic cycle. Cells in the G2 phase or very close to the M phase are most radiosensitive whereas cells in the latter part of the S phase of the cycle are more radio resistant [36]. Fractioned radiotherapy can take advantage of this effect by allowing time for cells who were previously in a radioresistant phase in the mitotic cycle to progress and be in a more radio sensitive part of the mitotic cycle for the next fraction of radiotherapy.

1.4.2 Repair pathways

Double-strand break repair

When ionizing radiation damages both strands of the DNA in close proximity to each other, this is considered a double strand break (DSB). Many DSB are efficiently repaired using two main repair mechanisms known as homologous recombination repair (HRR) and nonhomologous end joining (NHEJ). HRR uses an undamaged DNA strand as a template to repair the DSB. HRR is essentially an error free process but takes 6 or more hours to complete. HRR will likely happen when the damaged cell is in the late S/G2 phase of the cell cycle. NHEJ is a much faster process than HRR but there is much higher probability that errors will occur making NHEJ less accurate than HRR [43]. NHEJ typically will be the repair mechanism for DBS if the cell it is the G1 phase of its cycle but can happen at any phase of the cell cycle.

Single-strand break repair (SSBR) and Base excision repair (BER)

Theses repair mechanisms are very efficient and damages to bases or single strands on the DNA often happen as a normal metabolic process in the body. It is estimated that 100,000 such damages occur each day in every cell in the body [36].

Base damage can be repaired using various enzymes. When damage to a base has happened, glycosylases proteins will remove the damaged base from the DNA without breaking the DNA structure and then endonuclease enzymes will come and cut the DNA backbone creating a clean SSB in the DNA. These clean SSB are then efficiently repaired using the complementary strand of the DNA using short or long patch process. Short patch process replaces only the damaged base whereas long patch process involves removing and replacing up to 10 bases. Short patch repairs involve ligation by ligase3 and long patch repair involves ligation by ligase1. SSBR is similar to BER but involves an extra step. In SSBR the SSB was caused by ionizing radiation rather than a cellular repair mechanism itself and as a result the SSB are often dirty so an extra step is needed to clean the ends of the damaged DNA strands before the SSB is fully repaired.

1.5 Biological Modeling of Cancer Outcomes in Treatment Planing

Alfred North Whitehead commented that "There is no more common error than to assume that, because prolonged and accurate mathematical calculations have been made, the application of the result to some fact of nature is absolutely certain."[45]. This quote highlights one of the major challenges with biological modeling. Historically, the quality of a radiation treatment plan has been judged by physical quantities, i.e., dose and dose-volume (DV) parameters, thought to correlate with biological response rather than by estimates of the biological outcome itself. It is widely recognized that the DV criteria, which are merely surrogadouble strand break repair te measures of biological responses, should be replaced by biological indices in order for the treatment process to more closely reflect clinical goals of RT [46, 47]. Like any model, biological modeling outcomes are highly dependent on parameters that often are difficult to quantify or differ

significantly among different investigators. This makes the modelling of any biological process difficult. This makes the absolute predicted outcome from biological models less robust. Some have used biological models to help determine the effectiveness of different treatment plans [48, 49], while others have cautioned against this approach [50].

In 1961, Munro and Gilbert proposed that the number of surviving cells after irradiation would follow a Poission distribution [51]. This concept has been incorporated into the majority of TCP models used today [46]. Common dose response models would include linear quadratic (LQ) models, TCP models, NTCP models, and equivalent uniform dose (EUD) models. Specific details of these models are provided below.

1.5.1 **Monte Carlo Method**

In much of this work, we were interested in how a population of patients would respond in cases of geometric miss or increasing dose heterogeneity scenarios. To account for the variability of biological parameters which might be found across a population of patients we used the Monte Carlo methodology. We assumed that the various biological parameters used in this work would follow a Gaussian distribution characterized by a mean and standard deviation (SD). The population of patients response can be accounted for by randomly drawing biological parameters from a probability distribution function (PDF) that corresponds to each biological parameter.

For example, if we wanted to determine the surviving fraction (SF) following a 2 Gy radiation dose, for a population of patients, and are given the mean and SD values for each biological parameter, we could look at 200 different intermediate risk prostate patients but for each individual patient the biological parameters would be generated by randomly selecting from the defined PDF function corresponding the the mean and SD of each parameter. Once the response for all 200 patients has been determined, the population response can be determined by aggregating the results of the individual

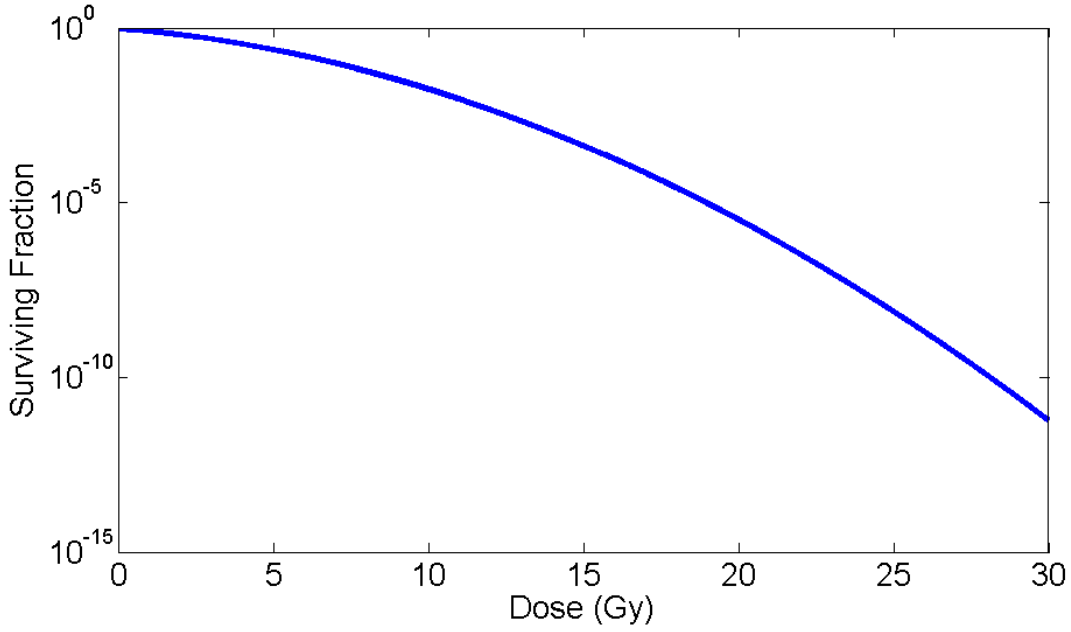

Figure 1.4: Surviving Fraction vs. Dose using the LQ model.

responses.

1.5.2 **Linear Quadratic Model**

The LQ has emerged as the most popular model to describe the relationship between total isoeffective dose and dose per fraction in fractionated radiotherapy [36, 52, 53, 54]. It has the advantage of being a relatively simple model described by only two parameters α and β, yet still generally works well in describing the response for both experimental and clinical radiobiology for both *in vitro* as well as *in vivo* scenarios. The α and β parameters represent the proportionality coefficients for the linear and quadratic components of a plot of SF vs. Dose when the SF axis is plotted using a log scale (see figure 1.4). In our context, SF refers to the fraction of surviving clonogenic cells following radiation. The $\frac{\alpha}{\beta}$ ratio is a radiosensitivitiy parameter and represents the curviness of the LQ curve [55].

There has been much debate however as to whether the LQ model can be applied

at the higher dose per fraction (∼8 - 30 Gy) often seen in SBRT or SRS treatments [56, 57, 58, 59, 60, 61, 62, 63, 21, 64]. Guerrero and Li proposed a modified LQ model (MLQ) to account for larger dose per fraction [65], Park et al. proposed a Universal Survival Curve (USC) for determining surviving fractions [66], and more recently Wang et al. proposed a generalized LQ (gLQ) for a wide range of doses including higher dose per fraction associated with SBRT [67]. However, Brenner et al. and others have argued that the LQ model is an appropriate model for high dose per fraction treatments up to 18 Gy per fraction [58, 68, 21].

According to the LQ model the SF following 'n' fractions is given by equation 1.1. Here D is the total dose.

$$SF = exp\left(-\alpha D - \frac{\beta D^2}{n}\right) \tag{1.1}$$

1.5.3 **Tumour Control Probability**

The probability that radiation will control the tumour relates to the probability that no surviving clonogenic cells remain at the end of treatment. If the initial number of clonogenic cells is 'N' and the surviving fraction of clonogenic cells following radiation is 'SF', then the probability that the radiation treatment approach has controlled the tumour is represented by equation 1.2.

$$TCP = exp\left(-SF * N\right) \tag{1.2}$$

If the α and β parameters are known or can be reasonably estimated, then the SF can be found using the LQ equation (see equation 1.1). Often information regarding the N, and other biological parameters are not known specifically and in these cases TCP can be approximated using empirical methods. TCP curves typically follow a sigmoidal shape, which can mathematically be defined by two basic parameters, D_{50} and γ_{50}. D_{50}

is the dose for 50% control, γ is the slope of the dose response curve at D_{50}. In practice a tumour volume is comprised of different volume elements and so TCP is generally formulated as the product over the structure's voxels weighted probability functions:

$$TCP = \prod_{i=1}^{M} P(D_i)^{v_i} \tag{1.3}$$

1.5.4 **Equivalent Uniform Dose**

The concept of EUD, was first proposed in 1997 by Niemierko [69] (see equation 1.4). The basic idea of EUD is to describe what uniform dose would result in the same biological effect as the heterogeneous dose distribution of interest. Often when different treatment plans are compared with each other, the dosimetric advantage of one plan over the other is not clearly discernible. For example, a complicated 3D dose distribution can be represented by a 2D dose volume histogram where in some regions of the dose volume histogram (DVH) plot of one plan might have a dosimetric advantage over another, but in a different region that plan might have a dosimeric disadvantage [70]. In this respect, EUD has an advantage in that the two different plans with different dose distributions can be represented by a single number, making comparisons between treatment plans from an EUD perspective relatively straight forward.

$$EUD = D_{ref} \frac{ln[\sum_{i=1}^{N} \nu_i \times SF_i]}{ln\,(SF_2)} \tag{1.4}$$

1.5.5 **Treatment Margins**

Generally, clinicians follow guidelines from the International Commission on Radiation Units and Measurements (ICRU) Report 62 for defining targets [71]. The gross tumour volume (GTV) is defined as tumour that is visible by any imaging modality or palpable to touch. In order to properly treat possible microscopic disease not visible during imaging,

a margin of a few millimeters is added around the GTV, creating the clinical target volume (CTV).

Once the CTV is defined an additional margin known as an internal margin (IM) is added to the CTV to account for motion and tumour motion throughout the course of treatment. The CTV, with the addition of the IM, is known as the internal target volume (ITV). Finally, a set-up margin is added to the ITV to account for different random or systematic uncertainty. The final volume after adding the different treatment margins is defined as the planning target volume (PTV) [71]. In many cases a single margin is added to the CTV to create the PTV and this is know as the PTV margin. Van Herk et al., have developed margin recipes to determine the appropriate CTV-PTV treatment margin to cover the CTV for 90 % of patients with 95 % isodose (see equation 1.5 [18].

$$PTV margin = 2.5\Sigma + 0.7\sigma \tag{1.5}$$

Here Σ is the quadratic sum of the SD of all preparation (systematic) errors, and σ is the quadratic sum of the SD of all execution (random) errors

1.6 Low Dose Hypersensitivity

It is generally well accepted that radiation doses above 1 Gy are well described by the LQ model [36]. However, over the past three decades investigators have discovered different cell lines are more radiosensitive to radiation doses below 1 Gy compared to what would be expected by extrapolating back from the high dose region using the LQ model [72, 73]. It has been shown that over fifty different cells lines exhibit this increased radiosensitivity to these low doses[74, 75]. The induced repair model accurately predicts the SF at both low and high radiation doses. This model has a similar functional form to the LQ model, however in the induced repair model, α is a function of dose $\alpha\,(D)$, whereas in the LQ

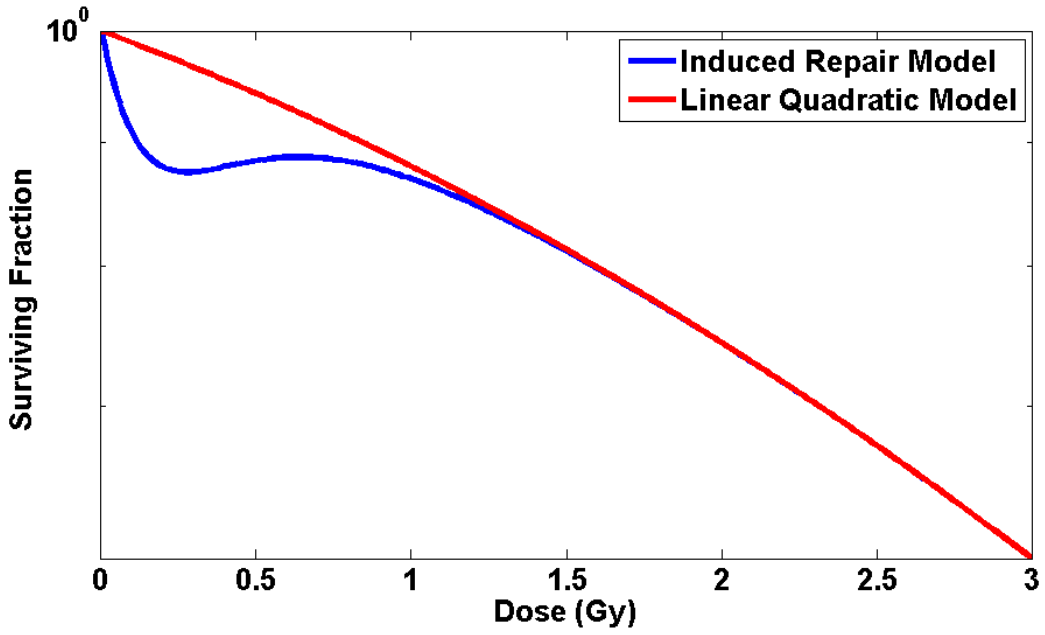

Figure 1.5: Surviving Fraction vs. Dose. The red line was modelled using the basic LQ model and the blue line was modelled using the Induced Repair Model. Parameters used in the figure are those for normal tissue prostate cells RWEP1 [2].

model α is a constant parameter that does not change with dose (see equation 1.7).

$$\alpha(D) = \alpha_r - (\alpha_r - \alpha_s)\, e^{\frac{D}{D_c}} \tag{1.6}$$

Phenomenologically, this model suggests that at low doses cells experience a hyper radio-sensitivity (HRS) and as the dose increases they experience an increased radio-resistance (IRR) [36]. On a cell survival curve, this initial increase in radio-sensitivity at very low doses is manifest as a steeper initial slope on the survival curve (α_s) compared with what would be extracted from extrapolating back from higher dose regions using the LQ model which have more gradual slope (α_r). The more radiosensitive phase happens for dose up to around 10 cGy. As doses begin to increase the cells become more radio resistant. The point where the transition from α_s to α_r is 63% complete is defined by D_c.

The transition from the more sensitive to more resistance biological response typically happens between approximately (20 cGy - 80 cGy) [36]. The SF according to the induced repair model is therefore:

$$SF = e^{-\left(\alpha_r - (\alpha_r - \alpha_s)e^{\frac{D}{D_c}}\right)D - \beta D^2} \tag{1.7}$$

1.7 Radiation Induced Bystander Effects

An inherent assumption of the LQ model is that radiation damage is caused solely from the absorbed radiation dose that disrupts the DNA of cells. DNA damage can also occur due to respiration and other metabolic processes. However, starting in the 1990's researchers began to find that in some cases cells outside the direct radiation beam could have adverse effects (i.e. chromosomal aberrations, reduced SF) if they were in proximity to cells which had been directly exposed to radiation. This has become know as Radiation Induced Bystander Effects. In simple terms, a radiation induced bystander effect, is an effect where "a cell that responds to the fact that its neighbours have been irradiated" [76]. Radiation induced bystander effects have been extensively reviewed in the literature [77, 78, 79, 80, 76, 81, 82, 83].

In 1992 Nagasawa and Little published a paper showing that when less than 1 % of the cells had been exposed to a low dose of α-particles, up to 30% of the cells showed chromosomal damage [84]. Other evidence of bystander effects have come from media transfer experiments. Mothersill and Seymour did media transfer experiments where the medium of irradiated human epithelial cells was transfered to unirradiated cells [85]. In their experiment, it was shown that the medium from the irradiated cells had a toxic effect on the unirradiated cells, suggesting that some signal had been secreted from the irradiated cells into their surrounding medium, which the unirradiated cells responded

to. More recently Butterworth et al.,[86] did modulated field exposures. In their work part of the cells were shielded from direct radiation exposure while the remainder of the cells were directly exposed. In the modulated field exposures, it was shown that the overall surviving fraction of cells in the shielded portion was much lower than what could be accounted for using the LQ model. Like before, it was assumed that some bystander signal had been released from the directly irradiated cells and that the released bystander signal had a toxic effect on the adjacent cells shielded from the primary radiation beam.

Numerous groups have proposed various mathematical modeling approaches to investigate the bystander response [87, 88, 89, 90, 81, 91, 92, 93]. Recently, McMahon et al., have developed a computational model of cellular response that accurately predicts cell survival for modulated fields for both cells in and out of the primary treatment field [94]. In a follow up to the original bystander model proposed by McMahon et al., [94], they published a more general mechanistic model of bystander response which can be applied generally to a variety of different *in vitro* or *in vivo* experiments and models [93]. The general bystander model proposed by McMahon et al., served as a starting foundation for much of the work presented in this thesis.

1.8 Overview of the Thesis

In addition to the introductory and concluding chapters, this work is comprised of four core chapters (chapters 2-5). Two of the core chapters have already been submitted and accepted into peer reviewed journals, the 3rd is in review and we strongly suspect will be accepted shortly as we recieved positive comments from the reviewers at the initial review. The fifth chapter is under review with *Physics in Medicine and Biology.*

1.8.1 Chapter one

This chapter provides the reader some basic background information which is necessary to build a proper foundation to understand the results presented herein and gives context as to where this work fits into current modalities for the treatment of prostate cancer.

This thesis work primarily looks at how radiation induced bystander effects modify predicted outcome in EBRT for prostate cancer compared with commonly used LQ based models such at TCP models. We also look at other effects such as low dose hypersensitivity and spectral effects and quantify the magnitude of these effects compared to bystander and LQ model predictions.

1.8.2 Chapter two

Geometric miss errors have the potential to influence out-of-field doses, particularly doses on the periphery of the target volume and this was the focus of chapter 2. Chapter 2 looked specifically at how geometric misses changed tumour control under common dose delivery techniques, namely IMRT and VMAT.

1.8.3 Chapter three

LQ models of tumour control are inherently sensitive to geometric miss errors such as those presented in chapter 2. Radiation-induced bystander effects have potential to influence cell survival particularly on the periphery of the primary radiation field. Chapter 3 investigate how radiation-induced bystander effects potentially change tumour control when portions of the target volume are missed because of a geometric miss error.

1.8.4 Chapter four

In addition to geometric misses, bystander effects may play an important role when considering dose heterogeneity throughout the target volume. This final core chapter looks

at how bystander effects changed tumour control under increasing dose heterogeneity cases.

1.8.5 Chapter five

Our results have shown that radiation-induced bystander effects have the potential to change current biological models of tumour control. This chapter looked at how the relative biological effectiveness (RBE) of radiation-induced bystander effects compare with other out-of-field effects such as low dose hypersensitivity and spectral effects.

1.8.6 Chapter six

This chapter summarizes the results present in this thesis and provides guidance on potential next steps necessary to validate our bystander model.

Chapter 2

Under conditions of large geometric miss, tumour control probability can be higher for static gantry IMRT compared to VMAT for prostate cancer

2.1 General Introduction to Chapter 2

The work presented in this chapter investigated potential biological consequences of common perturbations to an ideal dose distribution for cases of geometric miss. A linear quadratic-based model for tumour control probability (TCP) was constructed which simulated consequences on patient outcome of various perturbations when considering both intensity modulated radiation therapy (IMRT) as well as volume modulated arc therapy (VMAT). In this work, we focused on modeling typical intermediate risk prostate treatments treated receiving 78 Gy in 39 fractions. Both systematic and random geometric shifts were considered. The goal was to investigate these two modalities (IMRT and VMAT) under geometric miss scenarios to determine whether one was more robust than the other in terms of TCP.

This work has been submitted to the peer reviewed journal *Medical Dosimetry*. The review came back with positive feedback with some suggested minor changes. We anticipate this paper will be accepted shortly. I was the first author of this work and prepared the main manuscript. The other contributing authors were Dr. Charles Kirkby, Dr. Derek Brown, and Patricia Johnson. I developed the main algorithm for modelling the consequences of geometric miss and generated all the results under the supervision of Dr. Charles Kirkby. Patricia Johnson was a summer student working at the TBCC under

the supervision of Dr. Derek Brown, Dr. Charles Kirkby, and myself. She performed some of the initial modelling work. I collaborated with Dr. Charles Kirkby, Dr. Derek Brown, as well as Patricia Johnson on the design and implementation of our biological modeling study. All authors contributed to the review of the results and development of the final manuscript.

2.2 Under conditions of large geometric miss, tumour control probability can be higher for static gantry IMRT compared to VMAT for prostate cancer

MJ Balderson[1,2,4], P Johnson[1,5], DW Brown[6], C Kirkby[1,2,3,4]

[1] Department of Medical Physics, Tom Baker Cancer Centre, Calgary, Alberta, Canada

[2] Department of Physics and Astronomy, and [3]Oncology, University of Calgary, Alberta

[4] Department of Medical Physics, Jack Ady Cancer Centre, Lethbridge, Alberta, Canada,

[5] Department of Medical Biophysics, University of Western Ontario, Londan, Ontario, Canada

[6] Department of Medical Physics, University of South California San Diego, San Diego, California, USA

2.2.1 Abstract

The purpose of this work was to compare static gantry intensity modulated radiation therapy (IMRT) with volume modulated arc therapy (VMAT) in terms of tumour control probability (TCP) under scenarios involving large geometric misses, i.e. those beyond what are accounted for in the clinical target volume (CTV) to planning target volume (PTV) when margin expansion. Using a planning approach typical for these treatments, a linear quadratic-based model for tumour control probability (TCP) was used to compare mean TCP values for a population of patients that experiences a geometric miss (i.e. systematic and random shifts of the clinical target volume (CTV) within the planning target dose distribution). A Monte Carlo approach was used to account for the different biological sensitivities of a population of patients. Interestingly, for errors consisting of coplanar systematic target volume offsets and three dimensional random offsets, static gantry IMRT appears to offer an advantage over VMAT in that larger shift errors are

tolerated for the same mean TCP. For example, under the conditions simulated, erroneous systematic shifts of 15 mm directly between or directly toward a static gantry IMRT fields result in mean TCP values between 96% and 98%, whereas the same errors on VMAT plans result in mean TCP values between 45% and 74%. Random geometric shifts of the target volume were characterized using normal distributions in each Cartesian dimension. When the standard deviations were doubled from those values assumed in the derivation of the treatment margins, our model showed a 7% drop in mean TCP for the static gantry IMRT plans but a 20% drop in TCP for the VMAT plans. While adding a margin for error to a clinical target volume is perhaps the best approach to account for expected geometric misses, this work suggests that static gantry IMRT may offer a treatment that is more tolerant to geometric miss errors than VMAT.

Key words: Monte Carlo; Prostate Cancer; Modelling; Tumour Control Probability (TCP)

2.3 Introduction

When radiation therapy fails to control a cancer, one of the potential reasons is that the target, the volume of cancerous stem cells, has not received the intended radiation dose because a portion of that volume ended up outside the directly irradiated volume. In some cases such errors occur because the cancerous volume is misidentified and it extends beyond the planning target volume (PTV) an error of initial target definition [16]. In other cases, the target volume is appropriately identified, but the miss stems from an extreme in the combination of positioning uncertainties and motion that results in a misalignment of the clinical target volume (CTV) with the radiation fields [26, 27, 28, 29, 30, 31, 32], despite any robust analysis of setup uncertainty and motion used in deriving the expansion to the PTV from the CTV [18, 17, 16, 19]. In other words, the

target was accurately identified, but a portion of it was missed because it moved well beyond the expected range of uncertainty in position.

Both conventional intensity modulated radiotherapy (IMRT) where the gantry maintains a static position during field delivery, and volumetric modulated arc therapy (VMAT), where the gantry changes position during field delivery, offer highly conformal dose distributions. In both cases, the radiation dose falls off quickly outside the directly irradiated volume in order to reduce toxicities to surrounding healthy tissues. This work considers whether one of these delivery approaches offers an advantage over the other when portions of the tumour have been under-dosed resulting from a geometric miss error (i.e. where a portion of the tumour has moved outside the radiation field or the radiation beam has been misaligned). Tumour control probability (TCP) calculations were used as an endpoint to compare IMRT and VMAT delivery techniques.

Our methodology was straight forward and follows the general approach used for the derivation of CTV to PTV expansion margins under consideration of setup and motion uncertainties [27, 28, 32, 17, 18, 16]. First, treatment plans using each approach were generated for a model case of a spherical target inside a cylinder. Second, dose distributions were calculated under conditions of rigid translation of the target volume where the translations derived from assumptions of setup uncertainty and motion. Third, using the resulting dose distributions within the target volume, a tumour control probability (TCP) was calculated. A Monte Carlo approach was used to average the results over a robust set of parameters. Our results are broken into cases of systematic errors, random errors, and combined errors. Each set of results considers static gantry IMRT deliveries using 5, 7 or 9 fields as well as VMAT deliveries using one or two arcs.

2.4 Materials and Methods

2.4.1 Establishing Dose Distributions: Geometric Miss

We consider the consequences of geometric shifts of the CTV within a dose distribution optimized to deliver at least 95 % of a prescribed dose to the PTV. Shifts of this nature (see figure 2.1) would potentially result from incorrect setup, organ motion, bias in image guidance systems, and biases in various geometric parameters such as MLC leaf position, jaw position, couch position, or even from incorrect delineation of the cancerous volume. Generally, such geometric misses are accounted for by adding a margin to the CTV based on estimations of the magnitudes of such errors. However, in extreme circumstances the shift can move the CTV beyond the PTV, resulting in under-irradiation of portions of the CTV. We have focused on the treatment of prostate cancer because prostate cancer is commonly treated with IMRT and VMAT techniques. We assumed a simplified model of the problem with a spherical CTV with a 2.5 cm radius (r) representing the prostate, which is centred inside a cylindrical phantom of 15 cm radius (see figure 2). The simplified model should be sufficient to grossly determine the impact of a CTV shift on TCP under the different techniques (see figure 2.2).

IMRT dose distributions were generated using the Eclipse treatment planning system (AAA version 11.0.31). Five, seven, and nine field static gantry IMRT plans with equally spaced beams, as well as single and dual arc VMAT plans were created all using 6 MV fields on a Varian iX accelerator. To be consistent with the standards at our center, a 7mm CTV-PTV margin was applied. A prescription of 78 Gy in 39 fractions was assumed. Optimization was performed to obtain a dose distribution as shown for the 7 field plan in figure 2. The optimization objectives were set such that 0 % of the target volume was to receive a dose higher than 81.9 Gy (105 % of the prescription dose) and 100 % of target volume was to receive a dose of at least 78 Gy and each constraint was assigned a

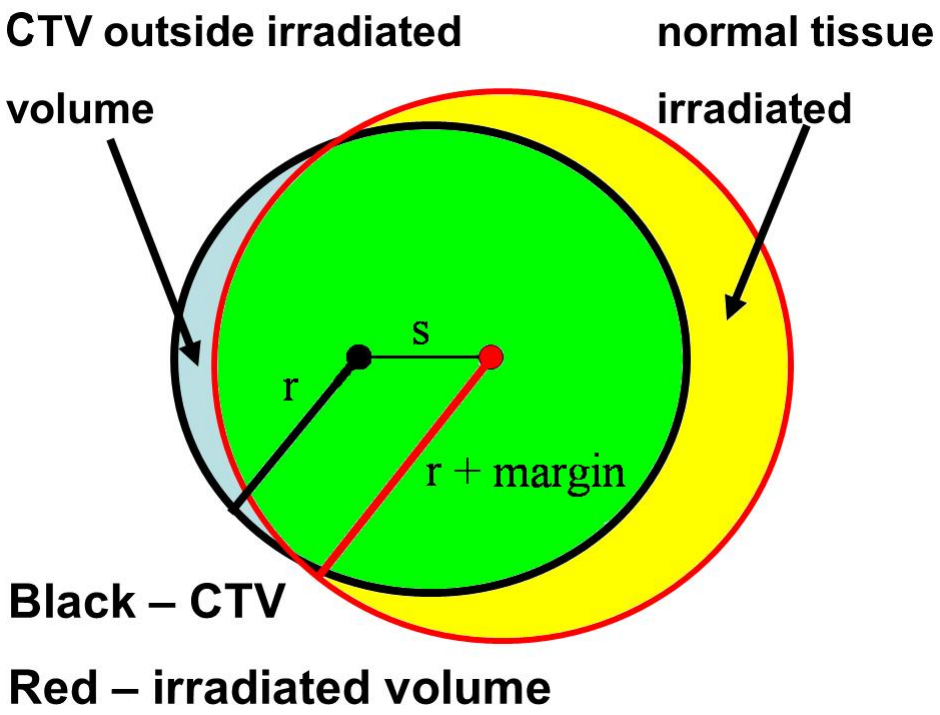

Figure 2.1: Geometric miss: CTV and irradiated volume off set.

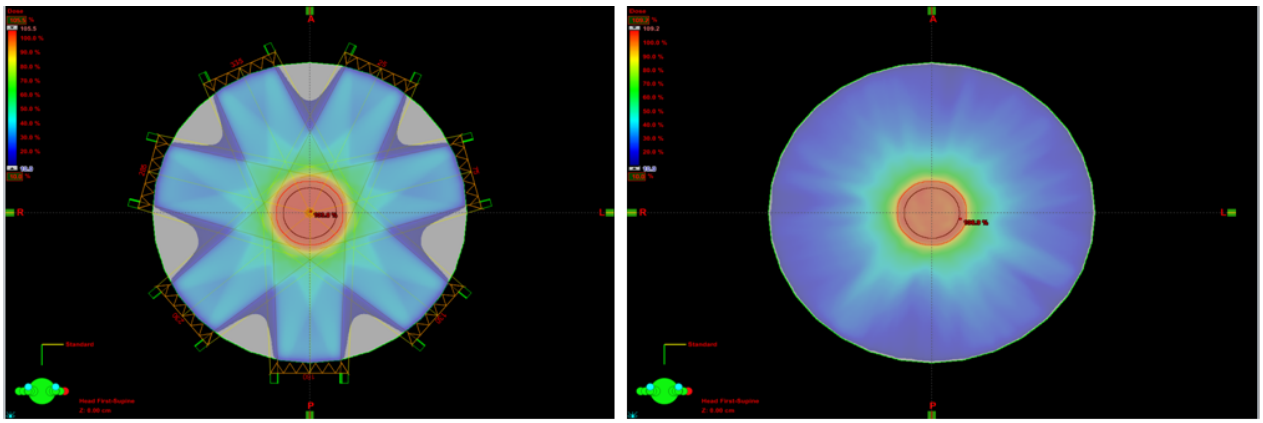

Figure 2.2: Dose distributions calculated in Eclipse. The left image is the 7 Field IMRT plan and the on the right image is the dual arc VMAT plan.

priority of 100. As no organs at risk were specifically defined, a normal tissue objective was applied allowing 105 % out to 1 cm from the target border, dropping down to 60 % with a fall-off parameter of 0.05. This constraint priority was 150. Beamlet smoothing priorities were set to 55 (X) and 45 (Y). Final dose distributions were normalized (prior to any shift) such that the 78 Gy isodose covered 95 % of the PTV.

Systematic Positioning Errors

A MATLAB program (The Math Works, Natick, MA, USA) was created to model the effect of systematic displacement of the CTV. The three dimensional dose distributions calculated on the treatment planning system were imported into the MATLAB environment. Rigid body shifts, s, were applied in (i) a direction directly between two fields (e.g. CTV would be shifted directly posterior as inset in figure 2.3), (ii) in a direction directly toward one of the fields (e.g. CTV would be shifted directly anterior as inset in figure 2.4), and (iii) perpendicular to the beam delivery plane, towards the superior. Because arc plans do not have between two fields or toward one field orientations, when

we shifted the dual and single arc plans, we did so in a manner consistent with shifts for a 7 field IMRT plan. Values of s were varied in each direction from 0 to 30 mm in 1.0 mm increments. The range of 0 to 30 mm was necessary to fully characterize the drop in TCP and allowed us to investigate the potential impact large geometric errors may have on outcome. The maximum value of 30 mm is well outside of a normal clinical range but could be possible in cases of wrong treatment sites or gross errors in image guidance. For each shift, the MATLAB program interpolated a new dose distribution within the shifted CTV and generated a new differential dose volume histogram (dDVH). A mean TCP was then calculated from the modified CTV dDVH corresponding to each value of the systematic shift error.

Random Positioning Errors

A similar program was developed to model the effect of random positioning errors in all three dimensions. Many studies have investigated prostate set-up error and reported mean systematic displacement values in the superior-inferior (SI), anterior-posterior (AP) and left-right (LR) directions [27, 95, 96, 97, 30, 98, 99]. Byrnes review of prostate motion from the literature included 6 studies that reported the standard deviation (SD) of movement in the AP, LR, and SI directions. Based on the values reported in these studies we assumed a model where the SDs of daily prostate movement in the AP, LR, and SI directions were 3.12 mm, 2.21 mm, and 3.26 mm respectively. The program randomly selected a shift in each direction from a set of Guassian probability density distributions (centered at 0 with standard deviations derived from Byrnes work), which was applied to each treatment fraction. The dDVH delivered to the CTV under each shift was tallied into a cumulative overall treatment dDVH for each patient and subsequently used as input into the TCP calculation. To simulate errors where random shifts exceeded these typical expectations, we introduced a scaling factor to widen the random shift probability

density functions, i.e. a scaling factor of 2 would double the standard deviation for each function. The ratio of potential shift magnitudes remained constant, but the general effects of allowing larger or smaller random position errors were reduced to dependence on a single parameter. The scaling factor was varied from 0 to 10 in increments of 0.5. A third MATLAB program was generated where random offsets with a scaling factor of 1.0 were also superimposed on the systematic offset cases.

TCP Model

TCP was calculated from the dDVHs extracted from each case of cumulative shifts. In the presence of a heterogeneous dose distribution TCP is generally calculated as:

$$TCP = \prod_{i=1}^{M} P(D_i)^{v_i} \tag{2.1}$$

where M is the number of volume elements, or voxels, and v_i is the relative volume of the voxel. We apply the linear quadratic formulation to the probability function. As described by the AAPM report TG 166 [46], this is:

$$P\left(D_i\right) = exp\left(-exp\left(\mathrm{e}\gamma - \alpha D_i - \frac{\beta D_i^2}{n}\right)\right) \tag{2.2}$$

$$\alpha = \frac{\mathrm{e}\gamma - ln\left(ln2\right)}{D_{50}\left(1 + \frac{2}{\frac{\alpha}{\beta}}\right)} \tag{2.3}$$

$$\beta = \frac{\mathrm{e}\gamma - ln\left(ln_2\right)}{D_{50}\left(2 + \frac{\alpha}{\beta}\right)} \tag{2.4}$$

D_{50} is the dose for 50% control, γ is the slope of the dose response curve at D_{50}. The ratio (α/β) of the linear (alpha) and quadratic (beta) terms is a tissue specific radiosensitivity parameter and is a useful measure of the curviness of such dose effect curves [55].

Two recent studies aimed to quantify the dose response of prostate cancer by determining D_{50} and γ. Levegrun et al. acknowledge that the dose response parameters vary by prognostic subgroup and they quote D_{50} and γ values for various risk groups. For all prostate patients they determined D_{50} to be 70.5 Gy and γ to be 2.9 [100]. Cheung et al. studied high risk patients only and determined D_{50} and γ to be 75.5 Gy and 1.7 respectively for this subgroup [101].

There has been much debate in recent years over the $\frac{\alpha}{\beta}$ ratio for prostate tumours. The $\frac{\alpha}{\beta}$ parameter of a cell is a measure of its sensitivity to changes in fractionation [102]. Most tumour types have high $\frac{\alpha}{\beta}$ ratios and are not very sensitive to alterations in fraction size or dose-rate. Studies suggest that this is not the case for prostate tumours, and that for prostate the $\frac{\alpha}{\beta}$ ratio is comparable or even lower than that of late responding normal tissue [103, 102, 22, 23, 104, 105, 106]. Oliveira et al. summarized the extensive debate on the value of this parameter. They calculated an arithmetic mean of all the reported values and obtain an $\frac{\alpha}{\beta}$ value of 2.73 Gy with a standard deviation of 1.96 [102]. In this work we used the self-consistent set of radiation response parameters provided by Pedicine [24] for intermediate risk prostate cancer. According to Pedicine et al., intermediate risk prostate cancer has a $\frac{\alpha}{\beta}$ ratio of 3.12 Gy (95% CI 2.71-3.60 Gy), and a γ value of 5.29 (95% CI 4.85-5.65). From these numbers we are able to derive a D_{50} value of 59.9 Gy. To account for the differences within a population for each radiobiological parameter a Monte Carlo approach was used. For each case investigated, 200 sets of parameters were generated by randomly sampling a normal distribution for each model parameter. The standard deviations for $\frac{\alpha}{\beta}$, D_{50} , and γ were 0.22 Gy, 2.0 Gy, and 0.20 respectively and were derived from the 95% confidence intervals reported in Pedicines work [24]. A TCP was calculated for each of these parameter sets, resulting in a distribution of TCP values for the population exposed under a given condition. For each condition examined, the mean TCP was then plotted against changes in the condition.

2.5 Results

2.5.1 Geometric Uncertainty

Systematic Positioning Errors

The plots in figures 2.3 and 2.4 plot the mean TCP vs. systematic positioning error coplanar with the radiation field. In figure 3, shifts directly between two static gantry IMRT fields are considered, and in figure 4, shifts directly toward one of the static gantry IMRT fields are considered. As expected, the mean TCP for co-planar shifts remains close to its theoretical maximum for small systematic shifts (those less than or equal to the errors accounted in deriving the PTV margin). However, for larger systematic shifts, around 12 mm for the IMRT cases and 10 mm for the VMAT cases, the mean TCP begins to drop. A mean TCP of 50 % is calculated for systematic posterior shifts of 14.9 mm (single arc) and 16.6 mm (dual arc) for the VMAT cases. The 50 % mean TCP occurs at 19.2 mm (5 field), 19.9 mm (7 field), and 20.2 mm (9 field) shifting posterior between the fields. When shifting anterior, the VMAT cases result in 50 % mean TCP at 16.8 mm (dual arc) and 17.7 mm (single arc). The same anterior shifts towards the static gantry IMRT fields result in 50 % mean TCP at 19.9 mm (9 field), 20.3 mm (7 field), and 20.9 mm (5 field). Seen another way, a systematic shift of 15 mm directly between static gantry IMRT fields results in a mean TCP of 96 %. A 15 mm shift directly into a field results in a TCP of 98 %. The same 15 mm translation on VMAT plans drops the mean TCP to 45 % (single arc) and 74 % (double arc).

The variation in the VMAT cases when comparing anterior and posterior shifting is due to the non-uniformity in the optimization process. More important is that 50 % TCP VMAT range of 14.9 mm 17.7 mm is consistently less than the static gantry IMRT ranges 19.2 20.2 mm (between fields) and 19.9 20.9 mm (towards fields). This suggests that the static gantry IMRT technique may be more forgiving of large systematic shift

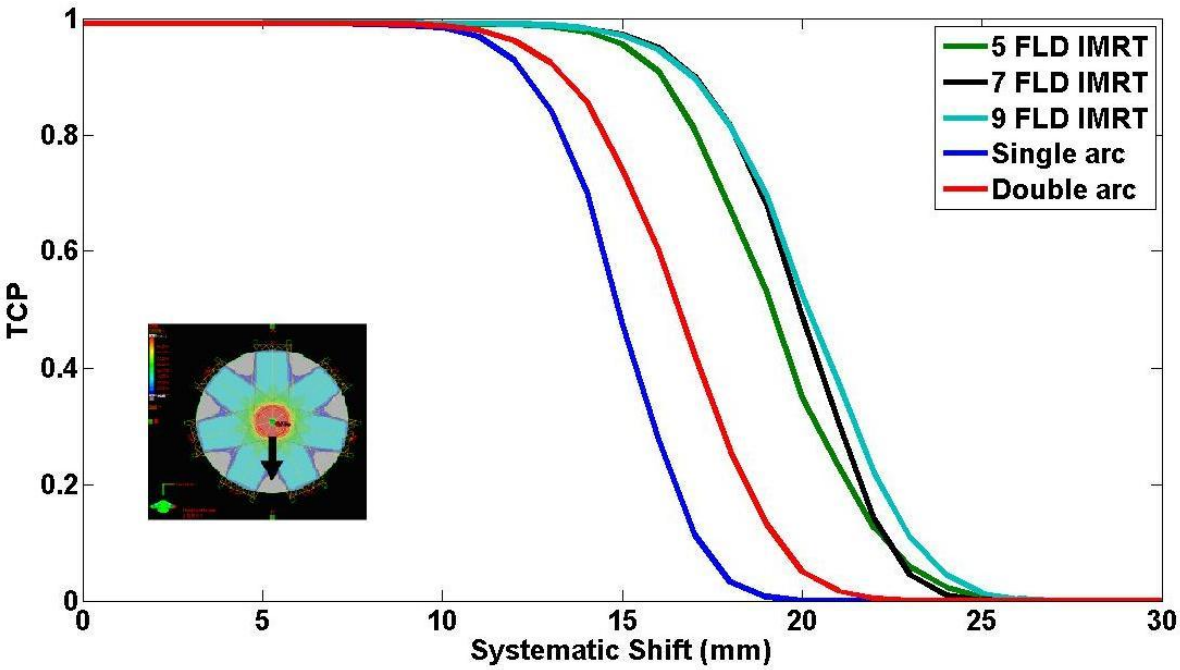

Figure 2.3: Mean TCP vs. systematic shift directly between two fields. Shifts for the dual and single arc plans were consistent in direction with shifts between fields for a 7 field IMRT plan.

errors coplanar with the treatment fields.

Figure 2.5 shows the effect on mean TCP when the systematic shift occurs perpendicular to the treatment field plane. In this situation the dose outside the PTV is to a much larger extent characterized by the properties of the 6 MV photon beam (i.e. the dose profile within the treatment planning system) than by the specific approach to the treatment. Outside of the penumbra, dose differences between profiles taken along the centre of the phantom vary by less than 0.5 % of the prescription dose. Within the penumbra the profiles easily meet a 2 mm distance-to-agreement criteria (plots not shown). Hence it is not surprising that the differences in mean TCP vary little between each other.

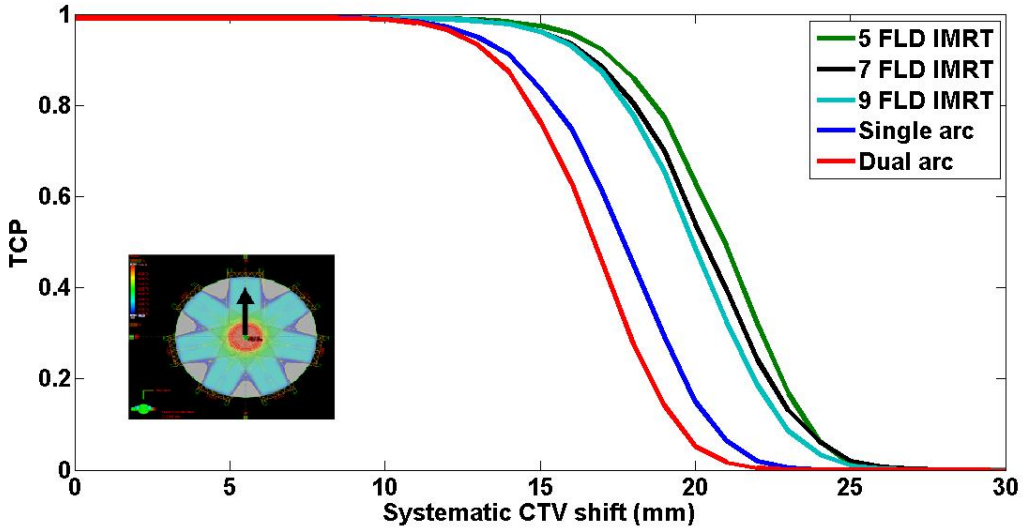

Figure 2.4: TCP vs. systematic shift directly toward one of the fields. Shifts for the dual and single arc plans were consistent with shifts toward fields for a 7 field IMRT plan.

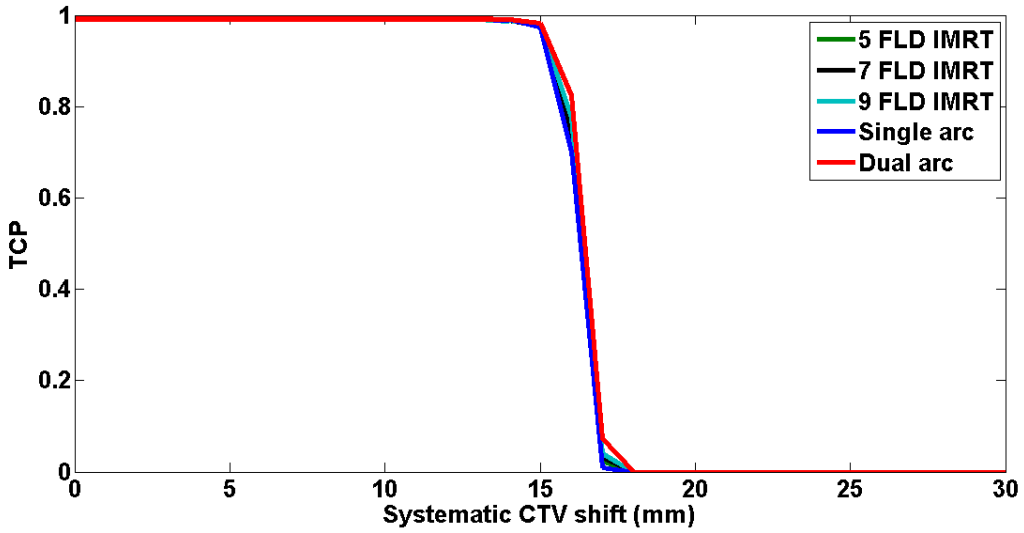

Figure 2.5: Mean TCP vs. shift in the SI dimension. Since the dose falloff outside of the PTV is dictated by the physical properties of the beam interacting with the medium and not the irradiation geometry, differences in mean TCP are minimal.

Random Positioning Errors

Figure 2.6 plots mean TCP as a function of the scaling factor for the standard deviation of the probability density functions used to sample day-to-day rigid translation errors in each of the three Cartesian dimensions. Here, the mean TCP remains close to its theoretical maximum for standard deviation scaling factors up to approximately 1.5 and then begins to decrease. In general, variation comparing the VMAT plans against each other (single arc vs dual arc) or the static gantry IMRT plans against each other (5, 7 or 9 field) was minimal. However differences between VMAT and IMRT were more obvious. When the SD for random motion was doubled our model showed that the mean TCP decreases to 79 % and 92 % for the VMAT and IMRT cases respectively. For a mean TCP of 50 %, the scaling factors were 2.3 for VMAT and 2.7 for the static gantry IMRT. This suggests that the static gantry IMRT approach is more tolerant of random errors that fall outside of expectation - at least in terms of predicted tumour control.

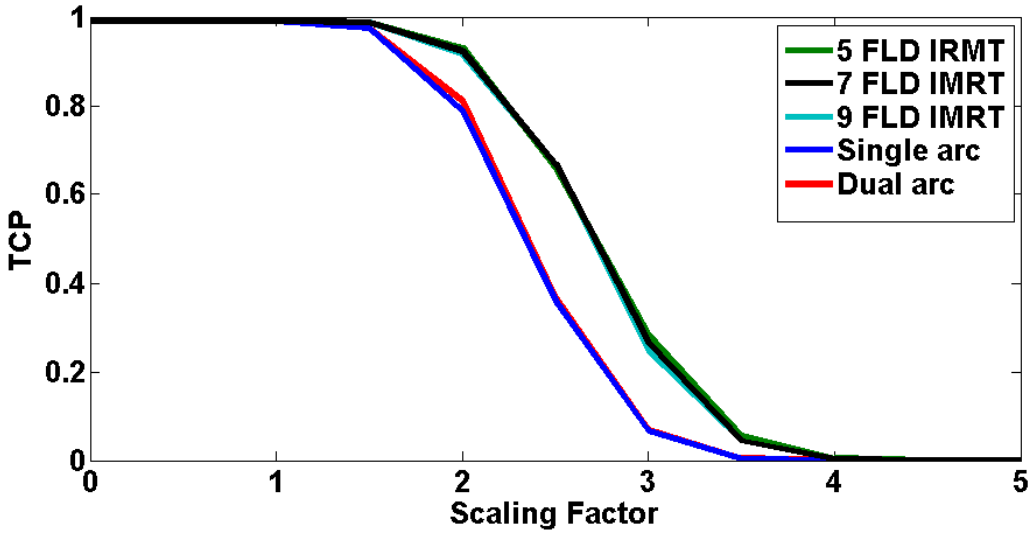

Figure 2.6: TCP vs. standard deviation scaling factors for random setup errors using the symmetric 7 field IMRT plan.

The effect of adding random positioning errors to the systematic positioning errors is plotted in figure 2.7 for the 7 field IMRT and the VMAT cases. For all cases mean TCP remains close to its theoretical maximum up to systematic shifts of 7 mm and then the mean TCP drops beyond this point. This would be consistent with the 7 mm CTV - PTV margin applied in the treatment plan. Both single and dual arc VMAT plans showed greater sensitivity to combined random and systematic positioning errors compared to the 7 field IMRT plans. Mean TCP drops to 80 % at systematic shifts between 13-15 mm for the 7 field IMRT case compared to 10-13 mm for the VMAT plans.

2.6 Discussion

Using a Monte Carlo approach to integrate the diversity in tumour response, we have quantified mean TCP as a function of systematic and random errors in cases of static gantry IMRT and VMAT. Because of uncertainty in target delineation, machine preci-

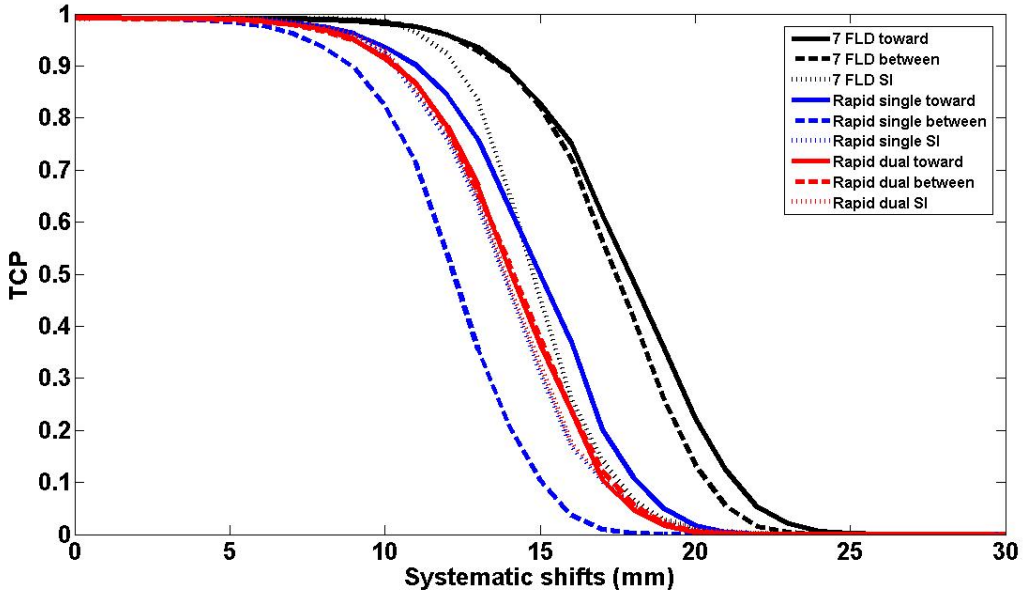

Figure 2.7: Mean TCP as a function of systematic shifts when random daily shifts are also incorporated for the 7 field IMRT, single and dual arc VMAT plans.

sion, patient setup, and target motion, such errors are naturally incorporated into the treatment planning process in the form of a margin that expands the targeted volume from what is clinically identified. Typical CTV-PTV margins for prostate treatment are on the order of 5-10 mm and therefore it is shifts beyond these limits that we are concerned with in this study. Unfortunately not all errors are predictable and naturally some are going to fall outside even the anticipated limits. With such cases in mind, it is valuable to understand how different treatment approaches compare to one another. This work has suggested a distinct difference in mean TCP between static gantry IMRT and VMAT, when errors have occurred beyond what is accounted for in the CTV PTV expansion margin. For example, Shah et al. [107] monitored prostate displacements using the Calypso RF tracking system and reported a maximum case where a displacement of >10 mm was observed for 28 % of the treatment time, and on average displacements of >10 mm occur about 0.2 - 0.3 % of the time. These large geometric shift errors are rare but our study suggests that static gantry IMRT may be a more robust treatment to use on a population that is at greater risk for large intrafraction motion compared with VMAT

Current radiotherapy techniques typically use some form of image guided radiotherapy (IGRT) as part of their treatment protocols. With this in mind, the large geometric miss errors reported in this study would, already very unlikely, be even that much more unlikely to occur clinically because such errors should be caught during the IGRT process. However the focus of this work was not to investigate those errors which can be anticipated and therefore accounted for in the planning process, but looked at those extremely rare errors which fall outside these anticipated limits.

It is important to note that this work has focused exclusively on TCP and has not addressed normal tissue complication probabilities (NTCPs), the other factors that are critical to designing optimal radiotherapy treatments. The problem with addressing this

in a model study is that a translation of the target does not necessarily correlate with an equal or even predictable translation of the nearby organs at risk. There is evidence to suggest that, in general, VMAT results in lower NTCP for a given TCP in prostate treatments compared with static gantry IMRT which allows for more sparing of normal tissues while doses to the target volume doses are escalated [9, 10, 11]. Whether large translation errors might change this remains an open ended question. Never-the-less, the central concern in this work is addressing the notion that when treatments fail to control the tumour, at least in some instances it is because the target is under-dosed due to a geometric miss that went beyond what was accounted for in the planning process. When considering between an IMRT or VMAT treatment approach, a full evaluation of the pros and cons of each modality is warranted and we suspect that under normal conditions VMAT would be a preferred treatment option in most situations. Retrospectively speaking, this work is very useful in understanding the potential consequence a large geometic miss will have on treatment outcome of prostate patients. In this respect, this work would suggest that static gantry IMRT may actually result in less failures to achieve tumour control.

Naturally, there are other errors to consider in the context of external beam radiation therapy treatments for prostate cancer. The volume of the CTV can vary, the CTV can rotate or otherwise deform, and other shifts in the anatomy resulting in changes of the source-to-surface distance or heterogeneities in the beam path can alter the distribution of dose deposited in the target. However, for the case of the prostate, which is deeply embedded in the pelvis, in this study we treat these as higher order effects. Mutanga et al., for example, found almost no noticeable difference in their dose-derived parameters when comparing both translations plus rotation correction with translation alone corrections [28].

Biological parameters used in this model pertained specifically to intermediate risk

prostate treatment [24]. In order to investigate the sensitivity of our results to the chosen values, we looked at how our results changed when values for low and high risk prostate treatments were used [24]. Sensitivity was quantified by comparing the geometric shift associated with a 50% drop in TCP. The reported trends did not change (i.e. IMRT was more robust than VMAT for large shifts). The TCP curves shifted on the order of around 2 mm. For example, using low risk parameters, a 50 % drop in TCP occurred at shifts around 2 mm larger than that of the intermediate risk population and similarly, using high risk parameters a 50 % drop in TCP occurred at shifts around 2 mm smaller than that of the intermediate risk population.

In our modelling we have used a simple 3 parameter linear-quadratic TCP formulation. More complicated formulations that account for factors such as cell re-population and hypoxia have been developed and a similar analysis could be performed using these models and respective model parameters - particularly if this work were to be extended to other cancers. However, for the population under investigation here, we would not expect the results to change dramatically since prostate cancer is not typically a fast-growing cancer.

Finally we introduce a note about the interpretation of these results. Generally speaking, VMAT offers advantages in terms of requiring shorter treatment times, delivering less monitor units, and by allowing for more degrees of freedom in gantry angle it can achieve the same target dose goals while delivering lower doses to organs at risk, compared to static gantry IMRT. Under conditions of large geometric misses, both modalities quickly drop to minimal probabilities of tumour control. This work shows that static gantry IMRT can result in a couple extra mm of latitude for geometric misses compared with VMAT, however all advantages and disadvantages of each modality need to be weighed when deciding on the most appropriate modality to apply. We assume that as we add more and more treatment fields, generally speaking the 95 % isodose lines essentially

encompass smaller volumes, and therefore offer less room for the CTV to shift without consequence, or when large shifts occur in error, a smaller volume of the CTV is directly irradiated. As a result VMAT seems to be less robust than IMRT for large geometric shifts.

2.7 Conclusions

Failure of radiation therapy to achieve tumour control is a serious concern, particularly when it occurs in treatments for low or intermediate risk prostate cancer where the target is relatively straight-forward to delineate and control rates are generally very high. This work investigated cases where geometric miss errors went beyond the uncertainties typically accounted for in treatment planning and resulted in less than optimal tumour control for two common approaches to treatment: static gantry IMRT and VMAT. A Monte Carlo-based model of biological response predicted mean TCP changes when systematic and random geometric miss errors were introduced into a model test case. Directly comparing static gantry IMRT with VMAT treatment deliveries suggests that static gantry IMRT can result in higher mean TCP values than VMAT for given large errors, or that the static gantry IMRT approach offers an increased latitude for forgiveness, to the order of 2 mm, over VMAT.

2.8 General Conclusions to chapter 2

The work presented in this chapter demonstrated how TCP begins to degrade once geometric shift are such that the CTV moves outside the PTV dose distribution. This work also demonstrated that more conformal VMAT plans are slightly more sensitive to geometric shifts compared to IMRT treatment plans when large systematic and random shifts are considered. The results presented in this chapter pertain to commonly used treatment methods (i.e. IMRT and VMAT) for controlling prostate cancer. Biological outcomes were modeled using the standard LQ formalism. The results presented in this chapter serve as a starting point for comparing other biological models such as those that incorporate bystander effects (see chapters 3 and 4).

Chapter 3

Potential implications on TCP for external beam prostate cancer treatment when considering the bystander effect in partial exposure scenarios

3.1 General introduction to chapter 3

The previous chapter looked at modelling potential consequences of geometric misses for intermediate risk prostate cancer and was based on a Linear Quadratic (LQ) model in determining bioeffect estimations following a course of radiotherapy. One of the main assumptions used in the LQ model is that biological damage occurs solely as a function of locally absorbed physical dose. However, the concept of radiation-induced bystander effects has started to challenge the main assumption that cellular damage is a function of only the locally absorbed dose. This current chapter looks at the potential consequence of geometric miss but incorporates a bystander effect derived from *in vitro* experiments.

The work presented in this chapter has been peer-reviewed and published in the *International Journal of Radiation Biology (IJRB)* [33]. I was the first author of this work and the other contributing author was Dr. Charles Kirkby. I developed the models used in this work and prepared the main manuscript for this work. I collaborated closely with Dr. Charles Kirkby on the design and implementation of this bystander biological modeling for geometric miss. Both Dr. Kirkby and I contributed to the review of the results as well as the draft of the final manuscript.

3.2 Potential implications on TCP for external beam prostate cancer treatment when considering the bystander effect in partial exposure scenarios

MJ Balderson[1,2,4], **C Kirkby**[1,2,3,4]

[1] Department of Medical Physics, Tom Baker Cancer Centre, Calgary, Alberta, Canada

[2] Department of Physics and Astronomy, and [3]Oncology, University of Calgary, Alberta

[4] Department of Medical Physics, Jack Ady Cancer Centre, Lethbridge, Alberta, Canada,

Running title: Implications on TCP when considering the bystander effect

Key words: Bystander Effect; Prostate Cancer; Modelling; Tumour Control Probability (TCP)

Declaration of Interest: The authors declare no conflicts of interest with the work presented herein.

3.3 Abstract

Purpose : This work investigates the potential implications on tumour control probability (TCP) for external beam prostate cancer treatment when considering the bystander effect in partial exposure scenarios.

Materials and methods: The biological response of a prostate cancer target volume under conditions where a sub-volume of the target volume was not directly irradiated was

modelled in terms of surviving fraction (SF) and Poisson-based TCP. A direct comparison was made between the linear-quadratic (LQ) response model, and a response model that incorporates bystander effects as derived from published in vitro data [94, 93]. Scenarios of random and systematic misses were considered.

Results : Our results suggest the potential for the bystander effect to deviate from LQ predictions when even very small ($< 1\%$) sub-volumes of the target volume were directly irradiated. Under conditions of random misses for each fraction, the bystander model predicts a 3% and 1% improvement in tumour control compared to that predicted by a LQ model when only 90% and 95% of the prostate cells randomly receive the intended dose. Under conditions of systematic miss, if even a small portion of the target volume is not directly exposed, the LQ model predicts a TCP approaching zero, whereas the bystander model suggests TCP will improve starting at exposed volumes of around 85%.

Conclusions: The bystander model, when applied to clinically relevant scenarios, demonstrates the potential to deviate from the TCP predictions of the common local LQ model when sub-volumes of a target volume are randomly or systematically missed over a course of fractionated radiation therapy.

3.4 Introduction

In radiation therapy it is generally accepted that the mechanism causing genetic damage and subsequent cell death is strictly a function of the radiation dose delivered to cells [43]. Based on this assumption, empirical models like the popular linear-quadratic (LQ) models have been developed to explore the biological effects of the radiation dose on cells. Endpoints like tumour control probabilities (TCP) are commonly calculated to

predict the probability of tumour control after a tumour has been exposed to a specific radiation dose. However, since the 1990's there has been evidence that unexposed cells can be affected by signals they receive from neighbouring cells that have been directly exposed to radiation. This is commonly known as the bystander effect or radiation induced bystander effect. This phenomenon has been extensively reviewed in the literature [77, 76, 78, 79, 81, 80, 108, 82].

Some of the earliest evidence of a bystander response came from media transfer experiments. Mothersill et al. [85] did medium transfer experiments where medium from irradiated epithelial cells were transferred to unirradiated cells. They found that the medium from the epithelial cells had a toxic effect on unirradiated cells. Little and colleagues showed that in some cases, where only 1 % of a cell population was irradiated, 30 % showed chromosomal changes [84]. Butterworth et al. looked at the cell survival for human prostate cancer (DU-145), and normal human fibroblast (AG0-1522) cell lines exposed to modulated fields. In their experiments, cells were grown in T25 or T80 culture flasks and then exposed to radiation where a portion of the flask was shielded from direct radiation exposure creating a non uniform radiation field. In their work, they found the surviving fraction (SF) of cells in the out of field portion of the flask was much lower than what would be predicted from a LQ model [86].

Numerous groups have proposed various mathematical modeling approaches to investigate the bystander response [89, 81, 92, 88, 94, 87, 109, 91, 90, 110]. Recently, McMahon et al. have developed a computational model of cellular response that accurately predicts cell survival for modulated fields for both cells in and out of the primary treatment field [94]. Many bystander studies are limited in the sense they use empirical methodologies to develop a relationship between exposed dose, bystander signal, and cellular response, making comparisons with other models difficult and reducing the scope in which they

might be applied. However, McMahon et al., in part to address theses limitations have published a more general mechanistic model of a bystander response which can be applied generally to a variety of different in vitro or in vivo experiments and models [93].

It is clearly of interest to consider what relevance the bystander effect might have on current cancer therapy practice, especially at a clinical level [76]. Current models of biological outcomes based solely on locally absorbed radiation dose might be inaccurate if the bystander effect plays a significant role in vivo. Of particular interest are (i) scenarios where portions of the target volume may be missed, either through systematic and random physical errors or by errors in contouring, (ii) scenarios where portions of the target volume may be selectively boosted, and (iii) predictions of response in normal tissues that receive partial or no direct exposure including toxicity complications and the induction of secondary cancers. Conceivably, one could imagine exploiting the bystander effect, once well-understood, to reduce radiation dose to portions of a tumour in order to spare normal tissues while maintaining an acceptable TCP or to boost TCP by selectively boosting the dose to subvolumes of a given target. It is stressed however that even though there is evidence of a radiation induced bystander effect, a lot more research and strong clinical evidence would have to be available before altering any current clinical practices.

The goal of this work is to extrapolate an established in vitro model of the bystander effect in in-vivo scenarios, particularly scenarios (i) and (ii) above, and estimate the potential for the bystander effect to influence TCP. Particular emphasis has been placed on modelling prostate cancer response. In this context we establish the magnitude of effect this model predicts in vivo, and ultimately demonstrate that further research is justified.

3.5 Methods and Materials

3.5.1 Bystander model

Our bystander model was taken and adapted from the published mechanistic model developed McMahon at el, [93]. In their work they provided a sample of their code written in the python environment (Python Software Foundation, Beaverton, OR, USA) and that was used as a starting point for our model which was written in a Matlab environment (The MathWorks, Natick, MA, USA). In order to verify consistency between our code and the code provided by McMahon at el. we verified that given the same initial conditions, both models would predict similar outcomes. The model is then expanded so as to predict potential consequences the bystander effect might have on patient outcome as measured by TCP in scenarios where less than the full target volume is directly irradiated. Specific details of the bystander effect model are given in McMahon at el. [93]. However, for completeness and to demonstrate how the model was extrapolated a basic summary is provided here.

3.5.2 Basic Assumptions

In the bystander model damage accumulates as an integer number of hits to a sensitive target within the cell. The precise definition of a hit is purposefully left ambiguous as it is simply a convenient quantity by which damage can accumulate, allowing for end-points to be determined. The bystander effect model proceeds under four basic assumptions [93]. 1) Cells exposed to radiation will both experience damage directly from the radiation and generate a signal for an extended period of time which is proportional to the delivered dose (D). This signal enters the medium in which the exposed cells are suspended and freely moves to other cells. Diffusion of the signal is assumed to be efficient, such that an equilibrium concentration is quickly obtained within a target volume. 2) The signal may

induce a response in a cell exposed to the signal that manifests as biological damage. 3) The degree of damage induced in a cell by the signal is proportional to the time the cell is exposed to the signal above a threshold value. The response is binary, with responding cells experiencing a characteristic level of damage and non-responding cells receiving no damage. 4) Directly exposed and perfectly shielded cells both experience signal induced damage, and this damage is added to the damage induced by direct exposure to radiation.

3.5.3 Signal Production

Following exposure to radiation, cells release a bystander signal for a period of time, $\rho(t)$, modeled by equation 5.5 [93]:

$$\rho(t) = \frac{\rho_{max}}{1 + \frac{\lambda V}{\nu C}} \left(1 - exp\left(-t\left(\frac{\nu C}{V} + \lambda\right)\right)\right) + \rho_0 * exp\left(-\lambda t\right) \tag{3.1}$$

Here, $\rho(t)$ is the bystander signal concentration as function of time,ρ_{max} is the local bystander signal concentration equilibrium, λ is the signal decay constant, V is the volume, ν is substitution for $\frac{\eta}{\rho_{max}}$ where η is the rate of local signal production when the concentration is 0, C is the number of irradiated cells, and ρ_0 is the signal concentration at time t= 0.

Cells exposed to a signal above a threshold $\rho_{thresh} = \frac{\rho_t}{\rho_{max}}$ will accumulate potentially lethal damage. Here ρ_t is the absolute threshold and ρ_{max} is the local concentration of bystander signal, therefore ρ_{thresh} is the threshold value as it relates to the local bystander signal concentration.

3.5.4 Accumulation of Radiation Induced Damage

As stated earlier, cellular response to the model's signal is a binary event. Cells either respond to the signal or they do not. The number of hits induced is a function how long a cell has been exposed to a signal above the threshold. The probability that a cell will

respond to a radiation induced signal (P_B) is given by equation 5.6 [93]. Here τ is the time the cell is exposed to a bystander signal above a threshold and κ is a cell specific signal kinetic parameter.

$$P_B = 1 - exp\,(-\kappa\tau) \tag{3.2}$$

Cellular damage is quantified in terms of hits that accumulate in a sensitive structure within the cell. A hit could be interpreted as analogous to a potentially lethal DNA double strand break. Hits accumulate both as a function of local absorbed dose and exposure to signals from other irradiated cells that surpass their defined threshold. The total number of hits is determined by adding the hits induced by the absorbed dose with the hits induced by signals from other directly exposed cells. Signal-generated hits are determined by sampling from a Poisson probability distribution function (Poisson PDF) with an expectation value for bystander induced hits (HB) characteristic of the cell type. Similarly, local dose-generated hits are found by sampling from a Poisson PDF with an expectation value for radiation-induced hits (Hits/Gy) that is proportional to the delivered dose. Rules to translate the number of hits into cellular outcomes were developed by Partridge [109]. According to these rules cells that accumulate five or more hits immediately die, cells with three or more hits receive moderate damage and will become arrested in the G1 phase of the cell cycle, and any cell in the G2 phase of its cycle will become arrested if it receives even one hit. Note that in respect to the cell cycle in the delivery of multiple fractions, we assume that between delivery of subsequent fractions, the cells will have fully reassorted themselves such that the surviving cells from the previous fraction will be distributed according to the initial cell cycle distribution. The SF is determined by subtracting the percent of dead or arrested cells from 100 %.

Table 3.1: Initial input parameters for prostate cells (DU 145).

Parameter	Value and Standard Deviation
Signal decay constant -λ	0.019 $\pm$0.002
Signal threshold -$\frac{\rho_t}{\rho_{mas}}$	0.21$\pm$0.02
γ (min/Gy)	61$\pm$20
κ (min^{-1})	0.0028$\pm$0.001
ν (min^{-1})	0.00011$\pm$0.00004
Hits/Gy	0.78 $\pm$0.006
H_B	3.0$\pm$0.4
initial cells	4000
initial volume (ml)	17.5

Note $\lambda, \frac{\rho_t}{\rho_{max}}, \gamma, \kappa, \nu, \gamma\kappa$, hits/Gy, and HB are fitted parameters taken from McMahon et al. (2013). HB corresponds to the number of hits induced by the bystander effect in the responding cells and $\gamma\kappa$ characterizes how rapidly the bystander signal builds up.

3.5.5 Verification of our model with the model of McMahon

To test that our Matlab model of the bystander effect was consistent with that provided by McMahon et al., we looked at the results of both models when starting from the same input parameters. The initial inputs used are listed in Table 3.1. Using the initial input parameters listed in Table 3.1 we set up a scenario as depicted in Figure 3.1 whereby a volume of prostate cells was partially exposed to a photon beam of ionizing radiation. One part of the volume (right section of Figure 3.1) was directly exposed and received 100 % of a predetermined or prescribed dose. The other part of the volume (left section of Figure 3.1) was assumed to be shielded and received only a scatter dose contribution here modelled uniformly within the shielded volume as 3 % of the prescribed dose. The directly exposed volume was varied from 0 - 100 % and in each scenario the SF of cells was calculated. We looked at single doses of 8, 4 and 2 Gy radiation doses. We compared our results for the 4 and 8 Gy radiation exposure to data provided by McMahon et al.

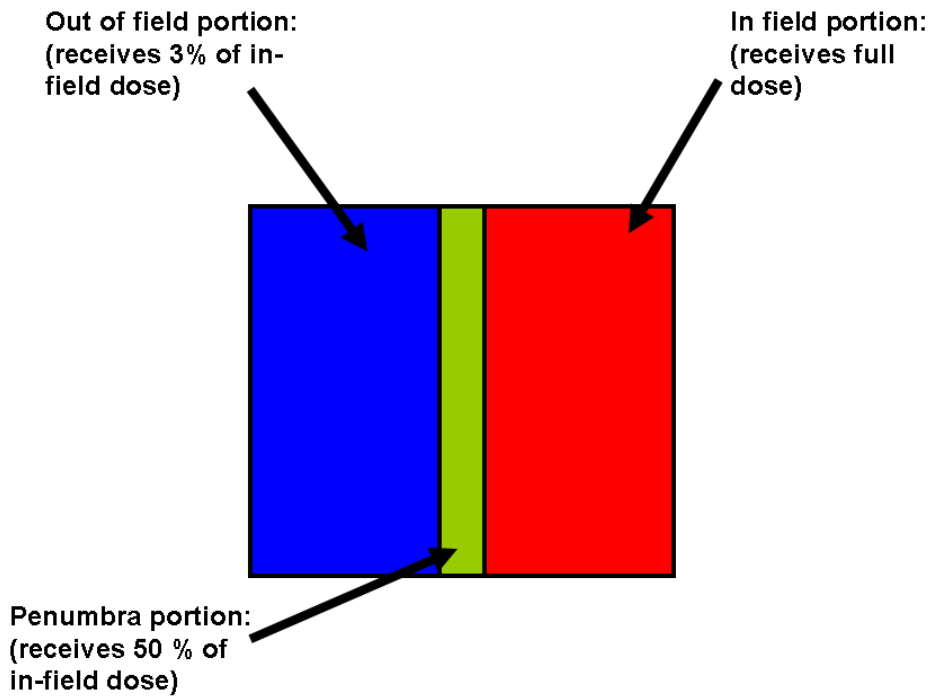

Figure 3.1: Model set-up of a 50% tumour exposure.

3.5.6 **Modelling of 39 fraction clinical treatment**

Random miss scenario. A typical prescription at our center for an intermediate risk prostate external beam radiation therapy treatment is 7800 cGy delivered in 39 fractions, with the expectation that at least 95% of the planning target volume (PTV) receives this dose. This is accomplished by delivering 2 Gy per fraction for a total of 39 fractions. This served as a starting point for our clinical modeling process. As above, for each fraction we assumed that a random portion of the tumour was shielded from the direct radiation while the remaining portion received the full 2 Gy in-field dose (see Figure 3.1). Again cells out-of-field received 3% of the dose delivered in-field as a result of scatter or transmission.

The models presented by [93, 86] assumed a step-function dose distribution. In a more realistic scenario dose between in and out-of-field is generally subject to a spatial gradient at the field edge. To account for this, we included an intermediate step to account for the penumbra. For simplicity, it was assumed this penumbra region extended 0.5 cm in the beams eye view between the directly exposed and shielded regions and that it uniformly receives 50 % of the in-field dose (middle section of Figure 3.1). When the exposed fraction is 0, no cells receive the in-field dose and the majority of cells receive the out-of-field dose with a small portion of cells receiving the penumbra dose. When the exposed fraction was 1, 100 % of cells receive the full in-field dose and no cells receive either the penumbra dose or out-of-field dose. Despite the larger volume, it was assumed that the signal emitted by the exposed cells traveled quickly through the entire volume, distributing itself evenly between both the directly exposed and shielded cells. We adjusted the hits/Gy response parameter of our model from 0.78 hits/Gy in the 4000 cells to 0.96 hits/Gy in the clinical scenario so that when all cells receive a uniform dose of 2 Gy (i.e., the exposed fraction is 1) the bystander and LQ models predict similar results.

Starting with an initial number of prostate tumour cells, for each exposed volume scenario, we calculated in-field SF, out-of-field SF, as well as a total SF for the tumour volume using both a LQ formalism (SF_{LQ}) as well the bystander formalism developed above for a 2 Gy dose and then propagated this through a 39 fraction scenario. The total SF was calculated by dividing the total number of surviving cells after a radiation treatment by the total number of cells prior to the radiation treatment. The LQ_{SF} was calculated using Equation 3 and is a function of local absorbed dose only. Here, α and β are the proportionality coefficients for the linear and quadratic components, respectively. Parameters of α, β ($\alpha = 0.15$ and $\beta = 0.048$), and initial number of tumour cells (3.0×10^6) were taken from Pedicini's set of self-consistent radiobiological parameters

for intermediate stage prostate cancer [24].

Using the SF, the number of remaining clonogenic cells was determined and this became the new initial number of cells prior to another radiation treatment fraction. This process was then repeated 39 times to simulate a 39 fraction treatment course consistent with clinical practice at our center. The time cells are exposed to a bystander signal above a specified threshold (tau) is different for each fraction because there is a unique number of a bystander signalling cells for each treatment fraction. In all cases we assumed a volume of 50 cm^3 for the prostate volume. To calculate the relative volumes of the in-field, out-of-field, and the penumbra portions of prostate we assumed a simple three dimensional square. However, the geometry of the prostate used is not important for this analysis, what is important is knowing the relative portions of the different volumes.

$$SF_{LQ} = exp\left(-\alpha D - \beta D^2\right) \tag{3.3}$$

3.5.7 Systematic miss scenario

In the methodology used above, cells were randomly exposed to the various in-field, penumbra, and out-of-field doses, without regard for their specific geometric position within the target volume. Alternatively, we considered a scenario where the in-field and out-of-field volumes did not vary geometrically between fractions cells that were missed on the first fraction were missed on the last fraction. This might be representative of a systematic offset in setup or an incorrectly delineated target volume.

Cell survival within each region was based on a region specific dose as well as a general bystander signal. The total number of surviving cells following the entire treatment course was found by adding the number of surviving cells for each individual region of the tumour.

3.5.8 TCP calculations

The TCP model assumed that the number of surviving clonogenic tumour cells follows a Poisson distribution and that even a single surviving clonogenic cell has the potential to grow into a viable tumour [51]. Therefore, the probability of tumour control is equal to the probability that no clonogens survive following a course of radiation and is given by Equation 4.10 [46].

$$TCP = exp\,(-SN) \tag{3.4}$$

Here S is the surviving fraction and N is the initial number of clonogens. After simulating 39 fractions radiotherapy treatment we calculated TCP using Equation 4.10 where for every fraction the in-field cells received the full 2 Gy dose, the out-of-field cells received 3 % of the in-field dose (i.e., 0.06 Gy), and the cells with the penumbra received 50 % of the infield dose (i.e., 1 Gy). We simulated this for varying exposed fractions ranging from 0 - 100 %. Total SF was used in the calculation of TCP.

3.6 Results

3.6.1 Surviving fraction vs. exposed fraction

Verification of our model with McMahon et al..

Figure 3.2 shows results for the SF of shielded or out-of-field cells vs. exposed fraction for 2, 4 and 8 Gy radiation doses (to the directly exposed volume). For 4 and 8 Gy radiation doses, the SF remains constant up to an exposed fraction of 0.2 then sharply drops off for larger exposed fractions. The bystander model shows that there is a threshold value of signal needed before any effect on SF is observed. For example, in Figure 3.2, when the exposed fraction is 0.15, the threshold signal has not been reached and the SF of cells (those receiving 3 % of the treatment dose) is around 0.99, however at exposed

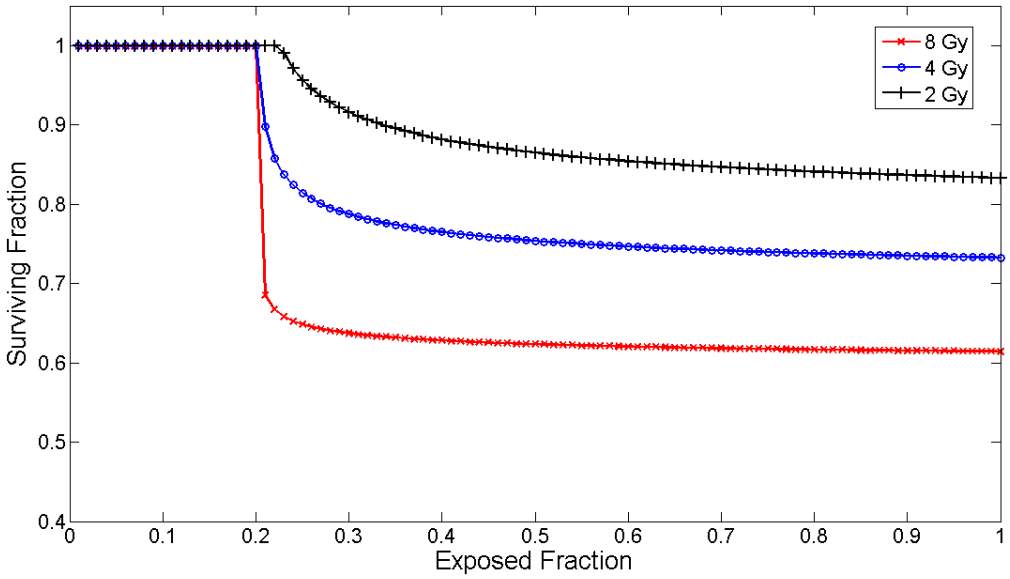

Figure 3.2: Out-of-field surviving fraction (SF) vs. exposed fraction using parameters from Table 3.1

fractions of 0.5 the threshold signal has been reached and the SF is drastically lower at around 0.88, 0.78, and 0.65 for 2, 4 and 8 Gy treatment scenarios. The bystander model shows the SF drops from 0.99 - 0.68 (33 %) and from 0.99 - 0.90 (9 %) between exposed fractions of 0.20 and 0.21 for cells receiving 8 and 4 Gy, respectively. These results are consistent with survival vs. exposed fraction of flask data published by McMahon et al. [93].

Figure 3.3 shows results for the directly exposed or in-field SF vs. exposed fraction for 2, 4 and 8 Gy radiation doses. Like the out-of-field results, cells exposed to 4 and 8 Gy radiation doses, the SF remains constant up to an exposed fraction of 0.2 then sharply drops off. The bystander model shows the SF drop from 0.20 - 0.10 (50 %) and from 0.65 - 0.56 (14 %) between exposed fractions of 0.20 and 0.21 for cells receiving 8 and 4 Gy, respectively. Cells receiving 2 Gy, have a drop in SF of around 6 % (0.90 -

0.85) between exposed fractions of 0.22 and 0.26.

Surviving fraction vs. exposed fraction for single exposures using 3.0×10^6 **cells**

SF vs. exposed fraction for 3.0×10^6 cells is shown in Figure 3.4. This work relates to the treatment of intermediate risk prostate treatment and the number of initial clonogenic tumour cells (3.0×10^6) is consistent with Wang et al. and Pedicini et al. estimate of initial number of clonogenic cells for intermediate risk prostate cancer [106, 24]. Unlike the experimental conditions modelled above with 4.0×10^3 cells, 3.0×10^6 cells are being irradiated, the bystander effect comes into play almost immediately as can be seen in the sharp initial drop in the bystander SF. At an exposed fraction of 1 % the SF given by the bystander model predicts a 5 % drop in SF compared to the SF when no cells are exposed to the in-field dose. As expected, when the exposed fraction of cells reaches 100 %, the total SF is consistent with that predicted by the in-field exposure model. When 100 % of the cells receive a dose of 2 Gy, the bystander and LQ models predict a SF of around 61 %. Between exposed fractions of 0.01 and 0.03, we see a very small drop in SF (around 1 %) then the SF remains relatively constant around 0.80 for out-of-field region, and 0.69 for the in-field regions. When only 1 % of the cells are exposed to direct radiation and 9 9% are shielded, our results showed that the total SF approach the SF for the out-of-field regions.

3.6.2 TCP vs. exposed fraction

Random miss scenario

Figure 3.5 gives the results of the TCP vs. exposed fraction for prostate cancer after delivering 7800 cGy to in-field portions of the tumour delivered over 39 fractions. The bystander model predicts a TCP of 50 % at an exposed fraction of 0.54 whereas the LQ model predicts that TCP 50 % occurs at an exposed fraction of 0.77. Similarly,

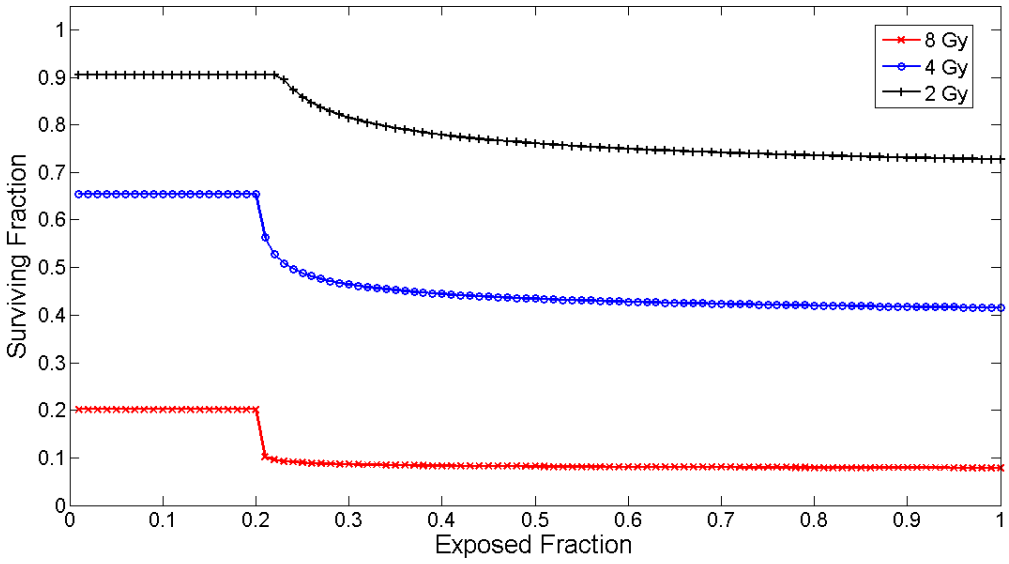

Figure 3.3: In-field surviving fraction (SF) vs. exposed tumour fraction using parameters from Table 3.1

the bystander model predicts that when the exposed fraction is 0.90, the TCP is 97 % compared with a TCP of 94 % as predicted by the LQ model. At an exposed fraction of 0.95, the TCP is 98 % and 97 % for the bystander and LQ models, respectively. When the exposed fraction is equal to 1, all cells are exposed to full radiation dose and both the bystander and LQ models predict a TCP of 0.99.

Systematic miss scenario

Figure 3.6 gives the results of TCP vs. exposed fraction for prostate cancer following systematic delivery of 7800 cGy to cells within the in-field portions of the tumour, 234 cGy to the outof- field portions, and 3900 cGy to cells with the penumbra region. The LQ model predicts a TCP of essential zero until the exposed reaches 1.0. This is consistent with a Poission based TCP model showing that if any portion of a tumour is consistently missed, the TCP is dramatically affected. However, our bystander-based model shows

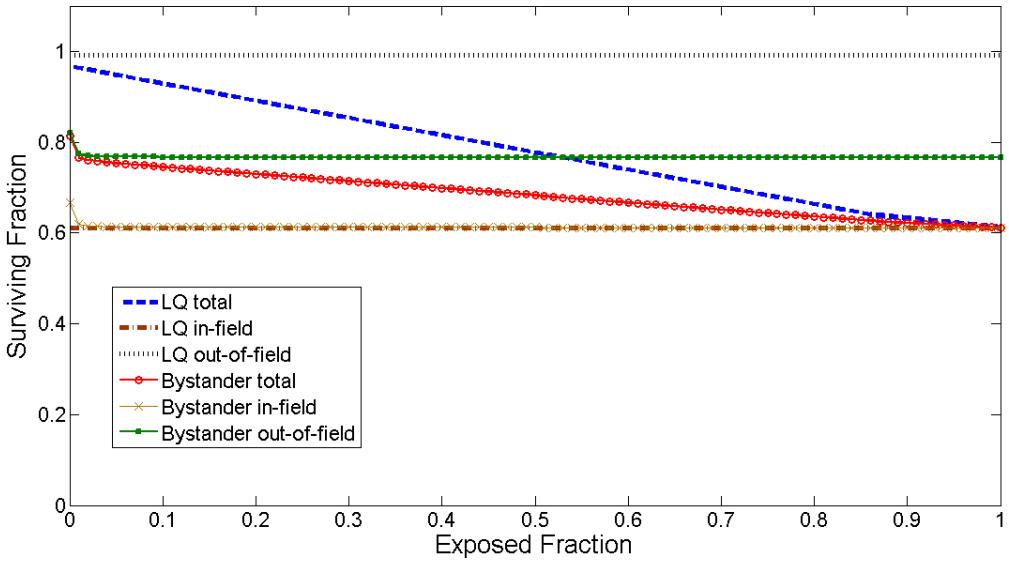

Figure 3.4: Surviving fraction (SF) vs. exposed tumour for in-field cells, out-of-field cells, and total cells for 3.0×10^6 initial tumour cells exposed to an in-field radiation dose of 2 Gy. The results for the linear-quadratic (LQ) in-field and Bystander in-field are overlapping except at the very lowest values of Exposed fraction.

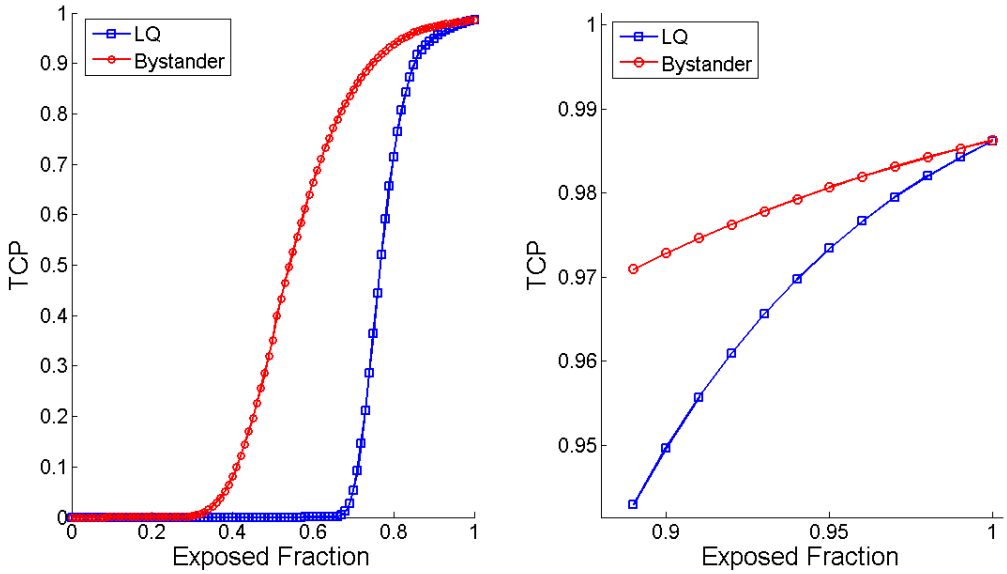

Figure 3.5: Tumour control probability (TCP) vs. exposed fraction for 39 fraction treatment radiotherapy course when considering random errors. On the left is the full TCP vs. exposed fraction graph showing how TCP changes when the exposed fraction ranges from 0 % and 100 %. On the right is a zoomed in portion of the graph showing how TCP changes for exposed fraction between 90 % and 100 %. Lq, linear-quadratic

that at an exposed fraction of 0.85, the TCP begins to deviate from the LQ-based model. The bystander model predicts a TCP of about 0.58 at an exposed fraction of 0.98 and a TCP of 0.76 at an exposed fraction of 0.99 whereas the LQ model predicts a TCP of essentially 0 for exposed fractions of both 0.98 and 0.99

3.7 Discussion

In this work we have investigated the consequences of a radiotherapy treatment course for prostate cancer across scenarios where portions of the tumour volume have not been directly exposed. Though tremendous efforts go into avoiding partial-irradiation scenarios in practice, they may at times be unavoidable. The tumour response has been modelled

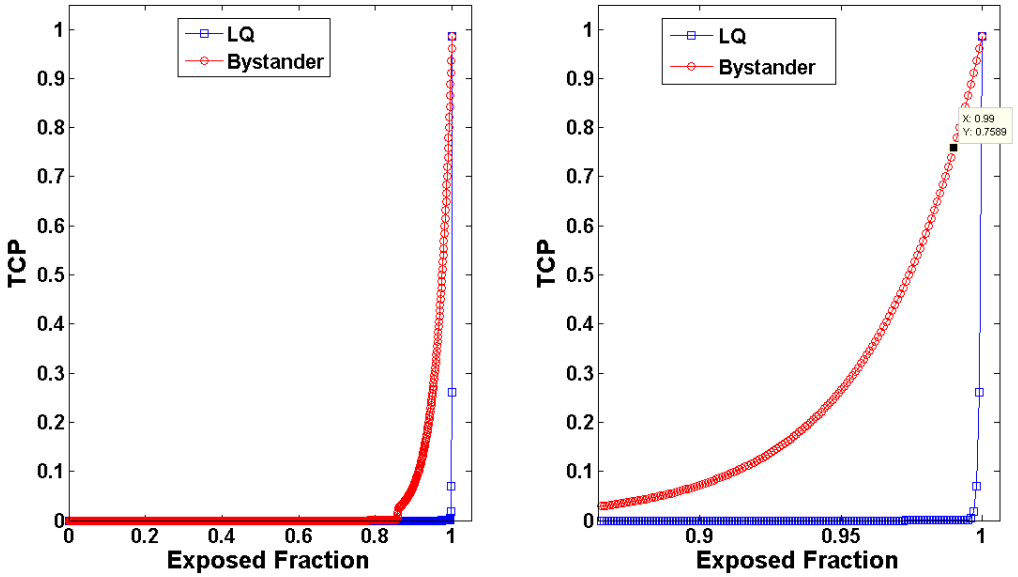

Figure 3.6: Tumour control probability (TCP) vs. exposed fraction for 39 fraction treatment radiotherapy course when considering systematic or geometric shifts. On the left is the full TCP vs. exposed fraction graph showing how TCP changes when the exposed fraction ranges from 0 % and 100 %. On the right is a zoomed in portion of the graph showing how TCP changes for exposed fraction between 90 % and 100 %. Lq, linear-quadratic.

in two ways, (i) by using model adapted from McMahon et al. [93] that incorporates a bystander signal and response that has proved valid in modelling in vitro experiments, and (ii) by using a more popular LQ model that relies completely on local absorbed dose. These outcomes have been translated into an overall TCP.

In this work we have limited our analysis to treatments of intermediate risk prostate cancer patients. We have considered in our analysis treatment plans consistent with the standard of care at our institutions, where a prostate radiotherapy patient would receive a treatment with a prescription dose of 78 Gy to be delivered in 39 fractions.

This work could be generalized to other cancers as well. So long as the basic assumptions in the model hold, we would expect to see generally increased TCP predictions compared to conventional LQ-based predictions under scenarios were small volumes are randomly or systematically missed. The degree of increase would depend on the specific details of the cancer in question. Generally speaking, it is required that the model be consistent with the data derived from experiments under uniform irradiation conditions from which the LQ models have been derived. The adjustable parameters in the bystander model allow for such tuning. The work here has focused on prostate cancer, which generally is considered a slow-growing cancer. In extending this work to other, faster growing cancers, re-population effects would need to be considered. Further, we have not considered heterogeneity of tumour response as would be induced by hypoxic subvolumes, for example, which could also play a strong role in predicting TCP under scenarios of geometric miss.

The bystander model predicts that there is a threshold bystander signal, which must be reached before the signal will have any effect on SF of clonogenic cells. In the in vitro (4000 cells) scenario, there is insufficient bystander signal to generate additional hits in the model until the exposed fraction reaches around 0.20 for doses of 8 Gy and 4 Gy and 0.22 for doses of 2 Gy. However, for greater exposed fractions, the bystander

signal reaches the threshold value triggers a drastic change to cell survival as can be seen in Figure 3.2 (the drop in survival of unexposed cells due signals from exposed cells) and Figure 3.3 (the self-induced drop in survival of exposed cells). When we model a more realistic clinical in vivo scenario with 3×10^6 cells, the cell density and number of cells are such that the threshold value for the bystander signal is reached for very small directly exposed volumes. When even only 1 % of the cells are exposed to the in-field dose, this still represents 30,000 cells, which is a factor of 7.5 times that of the entire in vitro case. As a result, the bystander model shows almost an immediate effect on SF regardless of the exposed fraction, as seen in Figure 3.4. Thus, this model implies that only a very small relative volume needs to be irradiated in a clinical scenario to induce a bystander effect. When modeling TCP for the 39 treatment course one of our assumptions was that at the start of each treatment fraction, the only effect from prior treatments is that of reduced number of tumour cells. We assume therefore that there are no residual bystander signals remaining from prior treatments. This assumption is, self-defensible within the model as the predicted effects depend on time above a threshold and the timescales over which the signal rises and drops are in the order of minutes to hours and much less than the 24-hour period assumed between fractions.

The bystander response model presented here explicitly incorporates an increased sensitivity of the cells in the G2 phase of the cell cycle. Cells in G2 will die with even one hit. This implies a sensitivity of the model to the assumptions (a) of the initial fraction of cells in G2 and (b) that that same fraction will be returned to between subsequent fractions. The results presented assumed that 5 % of the cells are in the G2 phase of the cell cycle for each fraction. The work of Scott et al. [111] suggests that the percentage of prostate cancer cells in the G2 and M phase combined is generally between 10 and 20 % and similar percentages are observed 24 h after irradiation, suggesting that the choice of 5 % explicitly in the G2 phase, and that this value is returned to between fractions, is

reasonable.

One of the challenges of going from in vitro to in vivo scenarios, is that we have assumed the biokinetics remain relatively similar. In practice, the assumption that a signal generated by directly exposed cells will efficiently spread through the entire tumour volume and reach an equilibrium concentration, though applicable to in vitro models, may not hold as the prostate gland is supported by a vascular framework. There are two points that support our assumption. First, the biological half-life of many substances introduced into the prostate is in the order of several hours to a few days [112, 113, 114]. The model applied here assumes that signal times above threshold are only maintained for a couple of hours at maximum because the signal is quickly metabolized. This timescale appears to be shorter than common biological half-life times. Secondly, if the signal released by the directly irradiated cells is subject to some degree of compartmentalization, the predictions of the model will be less accurate for the smaller exposed fractions, with increasing accuracy towards the larger exposed fractions and it is the latter scenarios (i.e., where 90 % or greater of the target volume is directly exposed) that are of greatest clinical relevance.

Another point of interest when considering bystander effects in an in vivo environment is recognition that because of the vascular framework with an in vivo scenario, it is possible that portions of the bystander signals will move outside the treatment volume and affect other normal tissues or lymphatic nodes down stream of the treatment volume. Indeed, other groups have reported bystander effects in distal organs in animal experiments [115]. The effect that bystander signals have outside the treatment volume, particularly on surrounding normal tissues, has not been looked at in this work but this is an important point to consider for future work. Another consideration when moving from in vitro to in vivo scenarios is that in an in vivo scenario, both normal tissue cells as well as cancer cells will be exposed to radiation and perhaps both cell types (normal

and cancerous) might send out a bystander signal compared to an in vitro environment where only specific cell lines have been grown in a medium. Heterogeneity of bystander signaling remains an open question.

Within the context of the model, Equation 5.5 incorporates a volume term. In Equation 5.5 , the volume term affects the maximum signal concentration (appears in the signal coefficient) as well as the rate at which the signal builds up.

However, McMahon et al. [93] has also shown that fixing the signal build-up rate to the decay coefficient l is a good approximation to the realistic kinetics of actual treatment volumes. The work shown assumed a target volume diameter of 5 cm. To test how sensitive our model was to the assumed volume, we looked at two extreme volumes: a 2 cm diameter prostate, and a 10 cm diameter prostate. We found the TCP changed by less than 1 % between these two extreme cases. Comparing our bystander model with a LQ model we found that to achieve probability of 50 % tumour control (TCP_{50}) can be achieved with our bystander model when 23 % more cells are shielded from direct exposure compared to the LQ model. For our specific modelling case, the maximum difference between the bystander model and the LQ model occurs at an exposed fraction of 0.70 where there is a huge difference in TCP prediction between the models. However, from a clinical perspective it would be very unlikely for 30 % of the tumour to be missed or underexposed. A more realistic case might be when say 90 - 95 % of the tumour gets the full infield dose and the rest is partially irradiated in a penumbra. The bystander model suggests a 3 % improvement in tumour control compared to that predicted by a LQ model when 90 % of the tumour receives the intended dose. When 95 % of the tumour is exposed to the in-field dose our bystander model shows a 1 % improvement in tumour control compared to a LQ model predication as shown in Figure 3.5. Generally, this model suggests that small segments of missed or partially exposed tumour may in fact not result in the loss of TCP that may be predicted by the LQ model.

3.8 Conclusions

Our modeling process uses a very simple model with some basic assumptions. We have taken a bystander model provided by McMahon et al. [93] which accurately reproduced SF for prostate cells consistent with experimental studies of Butterworth et al. [86] and have adapted the model to calculate TCP for a typical treatment course, including a penumbra region, for intermediate risk prostate cancer under conditions where sub-volumes of the target volume have been randomly or systematically missed. The results suggest that in clinical scenarios a bystander signal strong enough to modify LQ-based predictions may be induced even when very small relative volumes are directly irradiated. It also suggests the potential for a mitigated effect on TCP in scenarios where a small portion of the PTV may be missed or only partially irradiated. At a minimum, this model suggests that further study into bystander effects in clinical scenarios is warranted.

3.9 Acknowledgements

We would like to thank Dr. Derek Brown for his useful discussions and Dr. McMahon for providing the details of his groups work.

3.10 Declaration of interest

The authors report no conflicts of interest. The authors alone are responsible for the content and writing of the paper.

3.11 General conclusion to chapter 3

This chapter looked at how bystander effects can potentially modify biological outcome compared to the LQ model commonly employed in radiation biology when we consider systematic and random geometric shifts. This work demonstrates that the incorporation of bystander effects into models of treatment response potentially increases TCP under geometric miss scenarios. The bystander model was adapted from the published mechanistic model provided by McMahon et al. [93]. Dr. McMahon provide us with his original computer code written in the Python computer code environment. The bystander model we developed for this work was developed in the Matlab environment and was independently developed by myself under the supervision of Dr. Charles Kirkby. Our bystander model developed for this chapter was the starting point for looking at other potential bystander influenced outcomes in radiation therapy such as the effect of dose heterogeneity on biological outcomes. Dose heterogeneity and bystander effects will be the subject of the next chapter (chapter 4) in this work.

Chapter 4

Potential implications of the bystander effect on TCP and EUD when considering target volume dose heterogeneity

4.1 General introduction to chapter 4

The previous chapter looked at modelling potential consequences of geometric misses for intermediate risk prostate cancer assuming that bystander effects played a role *in vivo*. The results presented in chapter 3 demonstrated that bystander effects potentially improve TCP outcomes under geometric miss. This chapter expands upon the previous chapter and looks at the potential effect radiation induced bystander effects have under increasing dose heterogeneity scenarios. Typically radiation plans attempt to deliver a homogeneous dose to the target volume. This chapter investigates to what extent dose homogeneity constraints can be relaxed because of bystander effects.

The work presented in this chapter has been peer reviewed and published in the *International Journal of Radiation Biology (IJRB)*[116]. I was the first author of this work and the other contribution author was Dr. Charles Kirkby. I developed the models used in this work and prepared the main manuscript for this work. I collaborated closely with Dr. Charles Kirkby on the design and implementation of this bystander biological modeling under increasing dose heterogeneity scenarios. Both Dr. Kirkby and I contributed to the review of the results as well as the draft of the final manuscript.

4.2 Potential implications of the bystander effect on TCP and EUD when considering target volume dose heterogeneity

MJ Balderson[1,2,4], **C Kirkby**[1,2,3,4]

[1] Department of Medical Physics, Tom Baker Cancer Centre, Calgary, Alberta, Canada

[2] Department of Physics and Astronomy, and [3]Oncology, University of Calgary, Alberta

[4] Department of Medical Physics, Jack Ady Cancer Centre, Lethbridge, Alberta, Canada,

4.3 Abstract

Purpose: In light of *in vitro* evidence suggesting that radiation induced bystander effects may enhance non-local cell killing, there is potential for impact on radiotherapy treatment planning paradigms such as the goal of delivering a uniform dose throughout the clinical target volume (CTV). This work applies a bystander effect model to calculate equivalent uniform dose (EUD) and tumour control probability (TCP) for external beam prostate treatment and compares the results with a more common model where local response is dictated exclusively by local absorbed dose. The broad assumptions applied in the bystander effect model are intended to place an upper limit on the extent of the results in a clinical context.

Materials and methods: EUD and TCP of a prostate cancer target volume under conditions of increasing dose heterogeneity were calculated using two models: one incorporating bystander effects derived from previously published *in vitro* bystander data [93, 94]; and one using a common linear-quadratic (LQ) response that relies exclusively on local absorbed dose. Dose through the CTV was modelled as a normal distribution, where the degree of heterogeneity was then dictated by changing the standard deviation (SD). Also, a representative clinical dose distribution was examined as cold (low dose) sub-volumes were systematically introduced.

Results : The bystander model suggests a moderate degree of dose heterogeneity throughout a target volume will yield as good or better outcome compared to a uniform dose in terms of EUD and TCP. For a typical intermediate risk prostate prescription of 78 Gy over 39 fractions maxima in EUD and TCP as a function of increasing SD occurred at SD 5 Gy. The plots only dropped below the uniform dose values for SD 10 Gy, almost 13% of the prescribed dose. Small, but potentially significant differences in the outcome metrics between the models were identified in the clinically-derived dose distribution as cold sub-volumes were introduced.

Conclusions: In terms of EUD and TCP, the bystander model demonstrates the potential to deviate from the common local LQ model predictions as dose heterogeneity through a prostate CTV varies. The results suggest, at least in a limiting sense, the potential for allowing some degree of dose heterogeneity within a CTV, although further investigation of the assumptions of the bystander model are warranted.

Key words: Bystander Effect; Prostate Cancer; Modelling; Tumour Control Probability (TCP), Equivalent Uniform Dose (EUD).

4.4 Introduction

The general goal of radiation therapy is to kill clonogenic tumour cells while at the same time minimizing radiation dose to healthy normal tissues. This is typically done by delivering a homogenous prescription dose to the tumour. Dose heterogeneity within the tumour volume is discouraged because, under the assumption that cell killing is only a function of locally absorbed dose, more heterogeneous dose distributions will likely result in lower clonogenic cell kill. Under the above assumption, it has been proven that a uniform dose distribution produces the highest tumour control probability (TCP) [117, 118]. Under the assumptions of Uniform Dose Theory there have been numerous

studies that look at what effect heterogeneous dose distributions have on outcome [119, 117, 120, 118, 121, 122]. Generally speaking, unless the dose heterogeneity of a model can be positively correlated to the tumour response heterogeneity (i.e. the more resistant cells within a target volume get a higher dose), the planning goal should be a homogeneous dose distribution.

In the current era of radiation therapy, there is increasing awareness that factors other than locally absorbed dose play a role in the overall survival of biological cells exposed to radiation. Most mathematical and biological models are developed under the assumption that cell survival is based solely on the locally absorbed dose [43]. One of the other factors that influences cell killing, other than the locally absorbed dose, is commonly referred to the radiation induced bystander effect or just the bystander effect, where cell survival and other biological consequences are influenced by signals from other irradiated cells. Generally speaking, the bystander effect may actually be a set of effects where directly damaged cells communicate with undamaged cells via factors transmitted through the extracellular matrix or via more direct gap junction intercellular signalling (GJIC) [123]. Other long-range abscopal effects have been reported [124, 76, 125]. Current models of biological outcomes based solely on locally absorbed radiation dose might be inaccurate if the bystander effect plays a significant role in vivo [33, 126].

The radiation-induced bystander effect has been extensively studied since the 1990s and there is growing interest in better understanding this effect [127, 77, 76, 78, 81, 84, 80, 82, 86]. Most investigations into the radiation induced bystander effect are based on *in vitro* studies as well as various proposed mathematical models [89, 81, 92, 88, 94, 87, 109, 90, 110]. To our knowledge, there is a limited amount of information regarding how the bystander effect plays a role in an in vivo environment [108, 115].

Our group recently published a model describing the potential implication that the bystander effect might have on TCP in an in vivo environment under the conditions of a

partial geometric miss [33]. The model applied was adapted from the work of McMahon et al. [93]. In this work, we expand our study of the potential implications of this bystander model, under the assumption it behaves in vivo similarly to the conditions under which it was originally proposed *in vitro* and consider the specific problem of dose heterogeneity within a target volume. Dose heterogeneity, both in planning and delivery, naturally arises from a number of factors. These include: the transport of radiation through radiologically heterogeneous media and tissues, the competing goals of hitting a target and avoiding or limiting doses to critical organs, inter- and intra-fraction variation in patient anatomy, as well as physical constraints in the production and shaping of each radiation field. An in-house assessment of 15 different intermediate risk prostate patients treated at our centre found a range of standard deviations (SD) between 48 cGy and 113 cGy with an average SD of 67 cGy about an intended dose of 7800 cGy. The SD was found by fitting the differential dose volume histogram (dDVH) data to a normal distribution. The dDVH had been exported from our treatment planning system, Eclipse, (Varian, Palo Alto, CA, USA) using sub volumes with dimensions of 2.5 x 2.5 x 2.5 mm.

In a clinical radiotherapy context radiation-induced bystander effects illicit some natural speculation. If within a target volume, a smaller sub-volume receives a hot dose (above the mean to the whole target volume), the cells in that sub-volume may emit a signal that influences the response of other cells that received lower doses. Therefore when a heterogeneous dose is delivered, to some degree the hot sub-volumes may compensate for the low sub-volumes. The extent to which this occurs is difficult to predict, but certainly warrants investigation because of the potential to impact on radiation therapy treatment delivery. Expansion in the allowable dose heterogeneity in a target volume may permit more avoidance of sensitive critical structures, for example. We propose in this work, that the *in vitro* model of bystander effects represents an upper limit to the in vivo case. Influences of vasculature, and in vivo metabolism will quite likely mitigate or

dilute the signalling observed *in vitro*. Therefore, if the calculated biological responses suggest no clinical relevance based on an *in vitro* -derived model, there is unlikely to be any. But results to the contrary would suggest further investigation is warranted. Specifically this study considers how current TCP and equivalent uniform dose (EUD) might be influenced under conditions of increasing dose heterogeneity under competing models of response.

4.5 Methods and Materials

4.5.1 Bystander model

Our bystander model was taken and adapted from the published mechanistic model developed by McMahon at el, [93]. An overview of the model and its assumptions is given below. More specific details are available elsewhere [33, 93, 94]. We explore, via this model, the potential role bystander effects could play under situations of heterogeneous dose distributions.

Bystander Signal Production

Following exposure to a radiation, cells release a bystander signal for a period of time, $\rho(t)$, modeled by equation 4.1 [93]:

$$\rho(t) = \frac{\rho_{max}}{1 + \frac{\lambda V}{\nu C}} \left(1 - exp\left(-t\left(\frac{\nu C}{V} + \lambda\right)\right)\right) + \rho_0 * exp\left(-\lambda t\right) \tag{4.1}$$

Here, $\rho(t)$ is the bystander signal concentration as function of time, ρ_{max} is the local bystander signal concentration equilibrium, λ is the signal decay constant, V is the volume, ν is substitution for $\frac{\eta}{\rho_{max}}$ where η is the rate of local signal production when the concentration is 0, C is the number of irradiated cells, and ρ_0 is the signal concentration at time t= 0.

According to the model proposed by McMahon et al. [93] irradiated cells emit a signal for a fixed amount of time after exposure. Cells exposed to this signal will accumulate biological damage (additional to any induced by direct irradiation) in a quantity proportional to the time the cells experience the signal above a defined threshold. The probability that a cell will respond to a radiation induced signal (P_B) is given by equation 4.2 [93]. Here τ is the time the cell is exposed to a bystander signal above a threshold and κ is a cell specific signal kinetic parameter.

$$P_B = 1 - exp\left(-\kappa\tau\right) \tag{4.2}$$

Cells experience damage from radiation dose as well as bystander signal that translate into a various number of hits on sensitive structures of the cell. Rules to translate the number of hits were developed by Patridge [109]. Signal-generated hits are determined by sampling from a Poisson probability distribution function (Poisson PDF) with an expectation value for bystander induced hits (HB) characteristic of the cell type. Similarly, local dose-generated hits are found by sampling from a Poisson PDF with an expectation value for radiation-induced hits (Hits/Gy) that is proportional to the delivered dose. Parameter values used in our model are found in table 4.1

Basic Assumptions

In the bystander model damage accumulates as an integer number of hits to a sensitive target within the cell. The precise definition of a hit is purposefully left ambiguous as it is simply a convenient quantity by which damage can accumulate, allowing for end-points to be determined. 1) Cells exposed to radiation will both experience damage directly from the radiation and generate a signal for an extended period of time which is proportional to the delivered dose (D). The amount of time the cells signal (T_{sig}) is governed by the following relationship.

Table 4.1: Initial input parameters for prostate cells (DU 145).

Parameter	**Value and Standard Deviation []**
Signal decay constant -λ	0.019 $\pm$0.002
Signal threshold -$\frac{\rho_t}{\rho_{mas}}$	0.21$\pm$0.02
γ (min/Gy)	61$\pm$20
κ (min^{-1})	0.0028$\pm$0.001
ν (min^{-1})	0.00011$\pm$0.00004
ν (min^{-1})	0.00011$\pm$0.00004
Hits/Gy	0.96 $\pm$0.006
H_B	3.0$\pm$0.4
Number of cells	3×10^6
initial volume (ml)	50

Initial input parameters used in our model for prostate cells (DU 145). Note $\lambda, \frac{\rho_t}{\rho_{max}}, \gamma, \kappa, \nu, \gamma\kappa$, hits/Gy, and HB are fitted parameters taken from McMahon et al. (2013). HB corresponds to the number of hits induced by the bystander effect in the responding cells and $\frac{Hits}{Gy}$ corresponds to the hits induced from direct radiation, and $\gamma\kappa$ characterizes how rapidly the bystander signal builds up.

$$T_{sig} = \gamma D \tag{4.3}$$

Here γ is a cell line specific parameter. This signal enters the medium in which the exposed cells are suspended and freely moves to other cells. Diffusion of the signal is assumed to be efficient, such that an equilibrium concentration is quickly obtained within the target volume. 2) The bystander signal above a threshold value may induce a response in a cell exposed to the signal that manifests as biological damage. 3) The degree of damage is proportional to the time the cells are exposed to a signal above a threshold value. The response is binary, with responding cells experiencing a characteristic level of damage and non-responding cells receiving no damage. 4) This damage is added to the damage induced by direct exposure to radiation.

4.5.2 Equivalent Uniform Dose (EUD) calculations

EUD calculations for increasing dose heterogeneity

Niemierko [69] developed the concept of EUD as a way to analyze and compare different heterogeneous dose distributions. The full details of the derivation of EUD can be found elsewhere [69]. The basic idea of the EUD is to determine what uniform dose would have the same surviving fraction (SF) as some heterogeneous dose distributions of interest (D_i).

$$SF\left(EUD\right) = SF\left(\{D_i\}\right) \tag{4.4}$$

Here, $SF\left(\{D_i\}\right)$ is the overall SF from a heterogeneous dose distribution. If there is a heterogeneous dose distribution where N portions of the tumour volume each receive a homogeneous dose, characterized by the dDVH, the overall SF is the weighted average of all SF's for the various subvolumes (v_i) and is given by equation 4.5,

$$SF\left(\{D_i\}\right) = \sum_{i=1}^{N} \nu_i \times SF\left(D_i\right) \tag{4.5}$$

SF are calculated one of two ways: 1) using standard methods that assume the SF is a function of dose alone and 2) using our numerical bystander model. The SF for uniform doses is given by equation 4.6.

$$SF\left(D\right) = \left(SF_2\right)^{\frac{D}{D_{ref}}} \tag{4.6}$$

Here, SF_2 is the SF following a uniform 2 Gy radiation dose (D_{ref}). In the spirit of EUD, *after* the SF for the heterogeneous dose distribution has been determined, the question we consider is "What EUD would give the same overall SF" If the SF has been determined by our bystander model or has been calculated using linear quadratic (LQ)

models, the EUD approach at this point would be the same. Using equation 4.4, 4.5, and 4.6 we have:

$$(SF_2)^{\frac{EUD}{D_{ref}}} = \sum_{i=1}^{N} \nu_i \times SF(D_i) \tag{4.7}$$

which can be easily arranged to determine EUD;

$$EUD = D_{ref} \frac{ln[\sum_{i=1}^{N} \nu_i \times SF_i]}{ln(SF_2)} \tag{4.8}$$

We come up with a new form of EUD that we have defined as EUD_{byst} (see equation 4.9). EUD_{byst} represents what uniform radiation dose would have the same biological effect when we consider that the overall SF is a function of both locally absorbed dose as well as a bystander component as determined by our bystander model. Therefore, EUD_{byst} is a function of both dose as well a bystander signal.

$$EUD_{byst}(D, byst) = D_{ref} \frac{ln[\sum_{i=1}^{N} \nu_i \times SF_{byst}]}{ln(SF_2)} \tag{4.9}$$

It is important to note that under conditions of uniform dose, the predictions of the bystander model with respect to surviving fraction reduce to those predicted by the common linear quadratic model. Hence, an actual uniform dose means the same whether the bystander model is invoked or not. We looked at how the EUD as well as our EUD_{byst} change when the dose heterogeneity increases as measured by systematically increasing the SD of our dose distributions.

EUD calculations for increasing cold spot volume within CTV

In some prostate plans, there is an overlap between the clinical tumour volume (CTV) and the volumes associated with the normal tissues like the rectum or bladder. For example, if the PTV region overlaps with planning rectal volume (PRV) then the overlap region can be problematic for the optimization of the plan during the planning stages.

The problem occurs because one objective during the optimization is trying to put dose in that region to satisfy the CTV dose requirements, while at the same time another constraint is attempting to reduce the dose to the same region to satisfy the PRV dose constraints. This often results in a portion of the CTV getting a lower prescription dose which we call a cold spot. We investigate how the standard EUD as well as EUD_{byst} change as the cold spot volume increases for cold spots receiving only 95%, 90%, 85%, and 80% of mean (prescription) dose of 78 Gy delivered over 39 fractions. For the cold spot cases, we fixed the SD of the dose heterogeneity at 0.67 Gy, but then change the volume of the CTV that receives the particular cold spot dose.

4.5.3 **TCP calculations**

The TCP model assumes that even a single surviving clonogen will have the potential of growing into a viable tumour and that the cells will follow a Poisson type distribution [51]. Therefore, the probability of tumour control is equal to the probability that no clonogens survive following a course of radiation and is given by equation 10 [46].

$$TCP = exp\,(-SF \times N) \tag{4.10}$$

Here SF is the surviving fraction and N is the initial number of clonogens. After simulating a fractionated radiotherapy treatment for each different dose heterogeneity scenario, we calculate the total number of expected surviving cells and then using equation 10 calculate a final TCP for each dose heterogeneity scenario. We ignore any repopulation effects. We assumed an initial number of clonogenic prostate cells of 3×10^6 with alpha ($\alpha = 0.15Gy^{-1}$) and beta ($\beta = 0.048Gy^{-2}$) values. Our initial number of prostate clonogenic cells as well as alpha and beta parameters were consistent with that of others for intermediate risk prostate cancer [106, 24].

Using equation 4.10, we calculate the TCP under the assumption that the surviving

fraction is a function of dose alone as well as under the assumption the surviving fraction is a function of both the absorbed dose as well as some bystander signal. We investigated how TCP changes with increasing dose heterogeneity for both TCP calculation methods mentioned above.

4.6 Results

4.6.1 Bystander adjusted EUD

Prescription of 60 Gy in 30 fractions

The work originally presented by Niemierko was used as a test case [69]. Niemierko presented the results of EUD for a test case where the prescription dose of 60 Gy was delivered over 30 equal fractions. Niemierko simulated dose heterogeneity by increasing the SD of the normal density function from 0 Gy to 18 Gy. In all cases, the mean of the normal density function remained at the prescription dose of 60 Gy.

In our work, the test case scenario described by Niemierko was reproduced and a bystander adjusted EUD was calculated and compared with the standard calculation of EUD as presented by Niemierko [69]. To be consistent with Niemierkos results, we adjusted the parameters of our bystander model such that a uniform dose of 2 Gy would represent an overall SF of 0.5.

Figure 4.1, shows the results of both the EUD as well as the EUD_{byst} vs. increasing dose heterogeneity as measured by the SD. When a bystander component to cell kill is considered, the EUD_{byst} shows a 1% increase as the SD increases from 0 to 2 Gy and then EUD_{byst} drops slowly as the SD increases from 2 Gy to 18 Gy. According to our results, the maximum EUD_{byst} occurs at a SD of around 2 Gy, and at a SD of 4 Gy the EUD_{byst} drops back down to the starting value at a SD of 0 Gy. By contrast, the normal EUD has a maximum value at a SD of 0 Gy and then slowly decreases as the

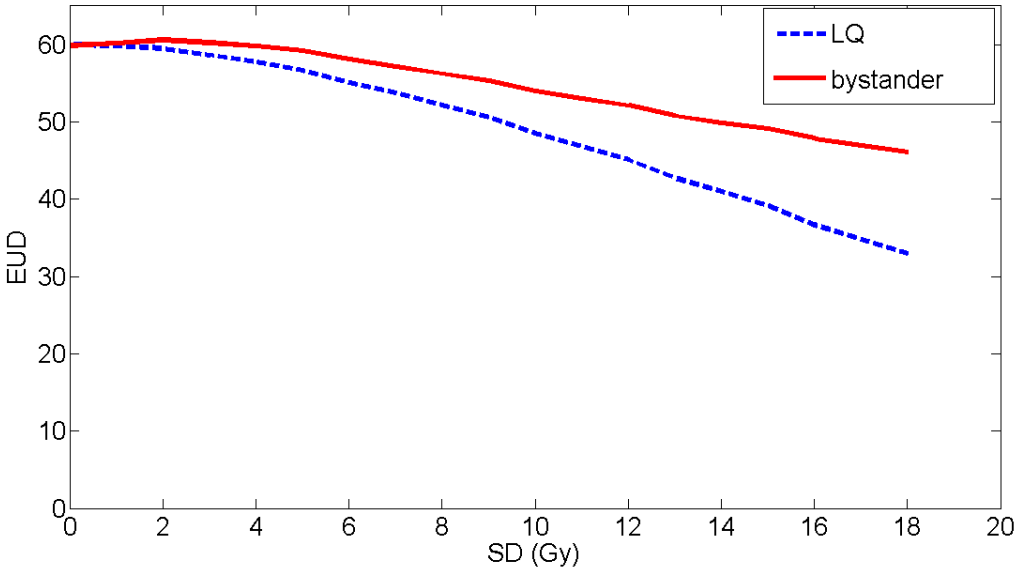

Figure 4.1: EUD and EUD_{byst} vs. SD for a prescription dose of 60 Gy delivered over 30 fractions.

SD increases. As expected, at a SD of 0 Gy the EUD would equal the prescription dose of 60 Gy and then drop as the dose heterogeneity increases which is consistent with the uniform dose idea.

Prescription of 78 Gy in 39 fractions

The standard of care for intermediate risk prostate cancer at our institution is a prescription dose of 78 Gy delivered over 39 fractions. Dose heterogeneity for the intermediate risk prostate cancer case was simulated as before by taking dose values from a normal density function with a mean value of 78 cGy while increasing the SD from 0 Gy up to 18 Gy (see figure 4.2).

Figure 4.3 shows the results of EUD vs. SD for the intermediate risk prostate scenario. As with the test case presented by earlier, a homogeneous dose distribution is equal to the prescription dose, which is 78 Gy for our intermediate risk prostate case.

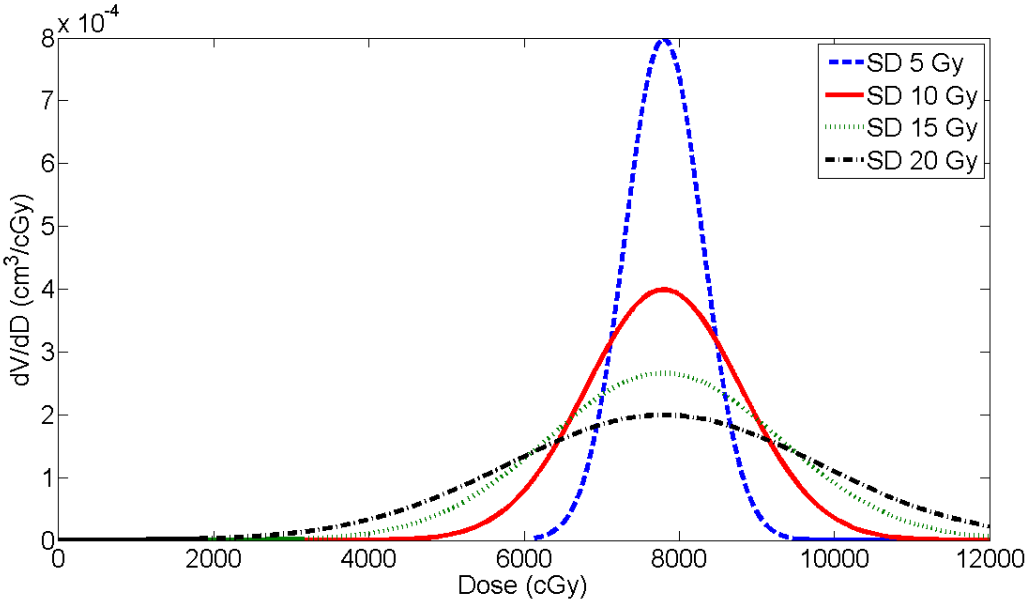

Figure 4.2: The differential dose volume histograms for different heterogeneous dose distributions. All distributions have a mean value of 78 Gy but with different SD.

The EUDbyst slightly increases reaching a maximum value of 80.58 Gy for a dose heterogeneity associated with a SD of 5 Gy and then the EUDbyst slowly drops as the SD increases beyond 5 Gy. Interestingly the SD can increase to as much as 12.5 Gy before the EUDbyst drops below the uniform dose (SD = 0) prediction. When the bystander effect is not considered, EUD starts at the prescription dose of 78 Gy at a SD of 0 then immediately begins to decrease as the dose heterogeneity increases. At a SD of 18 Gy the EUD has dropped to 55 Gy which is a 30% drop in EUD for a perfectly homogeneous dose distribution. For the bystander model, the EUDbyst at a SD of 18 Gy has dropped by around 6% from the 0 SD case to an EUD_{byst} of 73 Gy.

Increasing cold spot volume scenario

Figure 4.4 shows the results of EUD vs. percent of CTV volume receiving the cold spot dose. As expected both the EUD as well as the EUDbyst drop as the cold spot volume

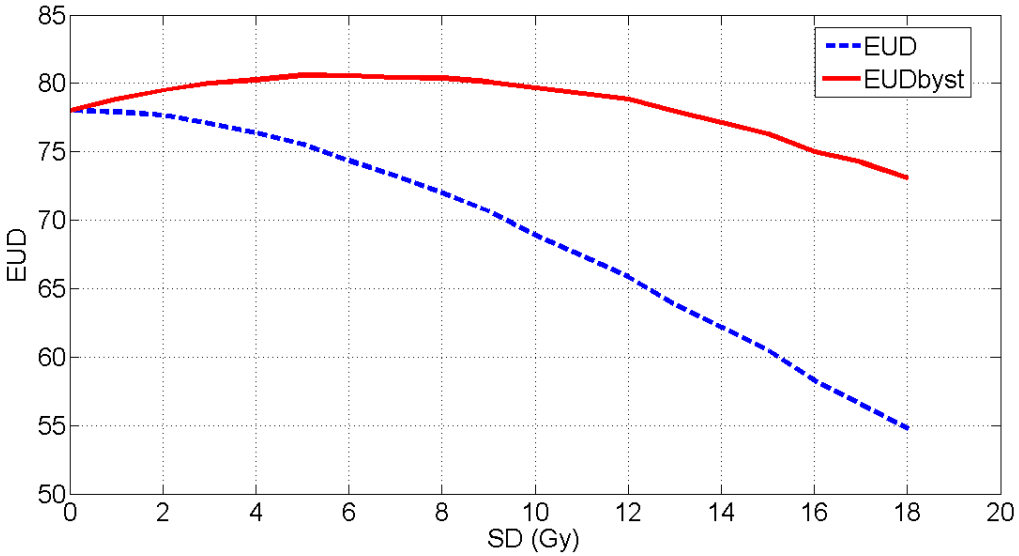

Figure 4.3: EUD and EUD_{byst} vs. SD for a prescription dose of 78 Gy delivered over 39 fractions for our intermediate risk prostate scenario.

increases. However, for the same percent of cold spot volume, our results show that the EUDbyst value drops less than the EUD value. For example, if a CTV cold volume of 20% receives 80% of the mean dose, the EUDbyst is about 2% greater then EUD and for a cold volume dose that is 95% of the mean dose, our results show that the EUDbyst is only about 0.5% higher than the EUD.

4.6.2 Bystander adjusted TCP when considering increasing dose heterogeneity.

TCP vs. SD is shown in figures 4.5 and 4.6. Under the assumption of the LQ models of cell killing, the maximum TCP occurs when a perfectly homogeneous dose distribution (SD is 0) is delivered to the tumour volume. According to the LQ model the TCP value begins to drop in a sigmoid type fashion as the dose heterogeneity increases. For example,

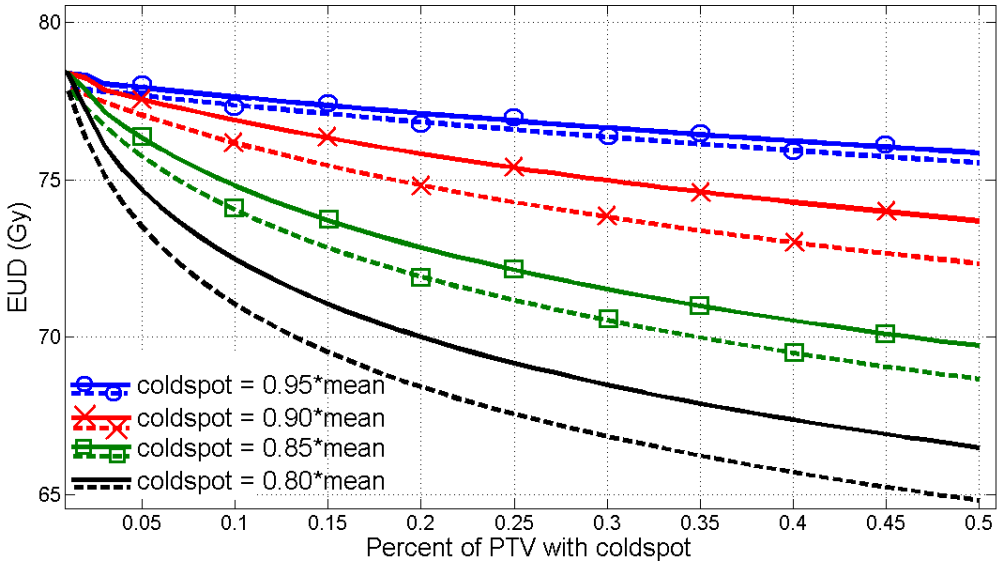

Figure 4.4: EUD vs Percent of CTV volume receiving coldspot dose. The dashed lines represent the standard EUD formulism and the solid lines represent the bystander influenced (EUD_{byst})

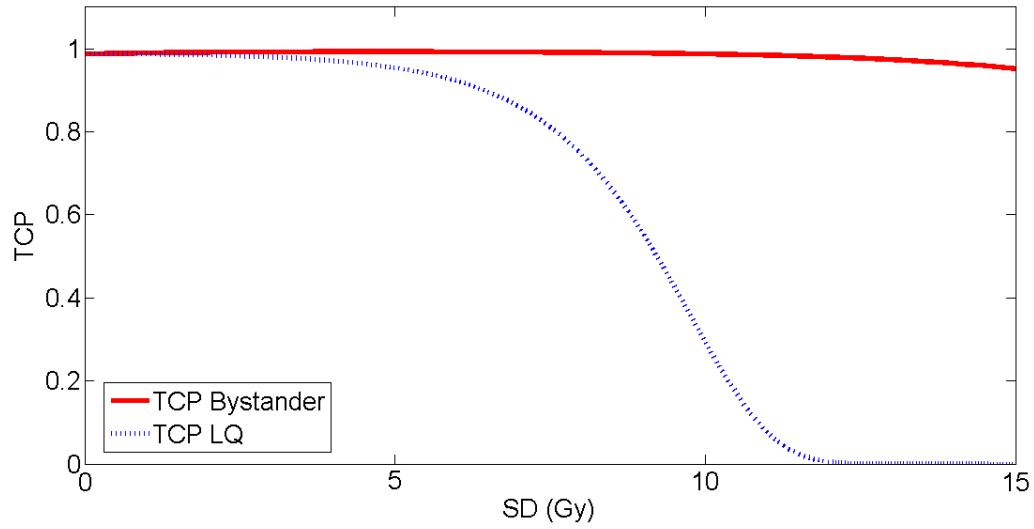

Figure 4.5: TCP vs. SD for a typical intermediate risk prostate prescription of delivering 78 Gy over 39 fractions.

at a SD of 0 cGy the LQ model predicts a high TCP value of 99% and slowly drops to a TCP value of 97% at a SD of 4 Gy and then the TCP drops more rapidly dropping to a value of .75 at a SD of 8 Gy. At a SD of 12 Gy, the LQ model predicts essentially a TCP of around 0.

By comparison, when a bystander effect is considered the results are quite different. Unlike the LQ model, TCP actually shows a slight increase as the dose heterogeneity begins to increase. According to our bystander model, the maximum TCP occurs at a dose heterogeneity of SD = 5 Gy and then slowly begins to drop as the dose heterogeneity increases further. Under the assumptions of our bystander model, our results show that the TCP will remain as good as or even better than a perfectly homogeneous dose distribution up to a heterogeneous dose distribution of around 10 Gy.

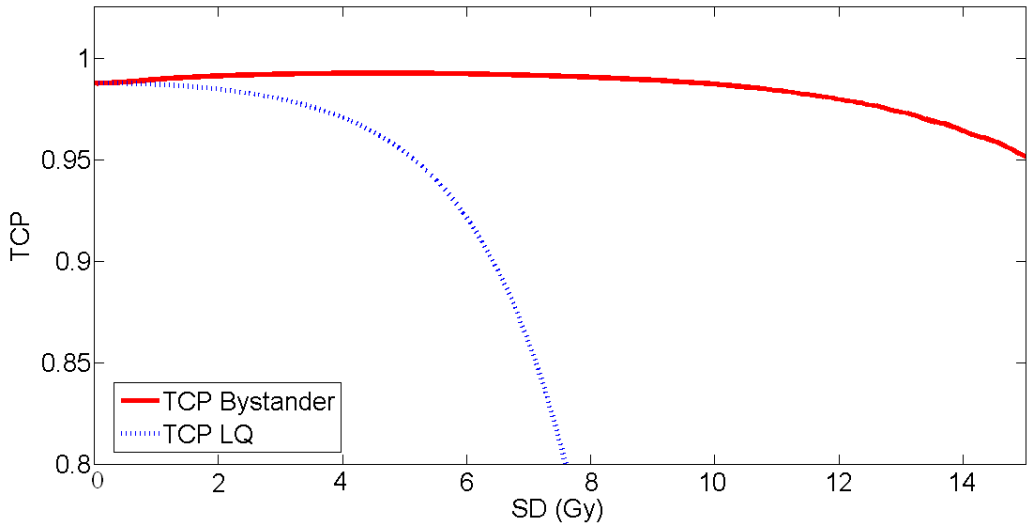

Figure 4.6: A zoomed in figure of TCP vs. SD for a typical intermediate risk prostate prescription of delivering 78 Gy over 39 fractions.

4.7 Discussion

In this work, we have investigated the potential consequences of a radiation-induced bystander effect on the biological outcomes of EUD as well as TCP across scenarios of increasing dose heterogeneity as well as increasing cold spot volumes within an otherwise clinically realistic CTV. The current radiation therapy planning paradigm includes minimizing dose heterogeneities over a target volume, but because of normal tissue constraints, radiologically heterogeneous media and mechanical limitations of equipment, there tends to be some dose heterogeneity across the target volume. In this work TCP and EUD have been calculated in two ways, (i) by using model adapted from McMahon et al. [93] that incorporates a bystander signal and response, and (ii) by using more popular LQ and EUD models that assume cell killing is a function only of locally absorbed dose.

The results generated using the bystander model herein demonstrate that some degree

of dose heterogeneity may yield acceptable outcomes (as good or better) compared to perfectly homogeneous dose distributions. The model shows acceptable outcomes of TCP to an upper limit of around SD of 10 Gy about a mean dose of 78 Gy. In the test case presented by Niemierko [69], the maximum EUDbyst occurs at a dose heterogeneity corresponding to a SD of 2 Gy. Under the intermediate risk prostate scenario, the highest EUD_{byst} occurs at a SD of 5 Gy. The slight increases ($\sim$1% and 3% respectively) are not large enough to warrant attempts at heterogeneity optimization.

The explanation for this behavior is reasonably intuitive in terms of the model. In a heterogeneous dose distribution through a particular volume, those cells exposed to higher doses will generate stronger bystander signals. These signals will then influence the response of the cells receiving less dose. However, as the dose heterogeneity continues to increase, the effects from bystander signals on the cells that received lower doses eventually become insufficient to compensate for the lack of damage due to the lower dose. As a result, a turning point is reached. The overall cell survival goes up as the dose heterogeneity continues to increase.

For the cases considered in this work, the highest EUD_{byst} values are 60.57 Gy and 80.58 Gy for the 60 Gy prescriptions and the 78 Gy dose prescriptions respectively. For the 60 Gy prescription, the maximum EUD_{byst} is about 1% higher than the maximum EUD. Similarly, for the 78 Gy scenario, our results show that the maximum EUD_{byst} is about 3% higher than the maximum EUD. It is interesting to note that under the intermediate risk prostate case, if the dose heterogeneity is such as to maximize EUD_{byst}, our bystander model suggest it would have a similar biological effect as one might expect if an extra 2 Gy fraction were delivered. Further, in the 78 Gy case, it was shown that a SD of $\sim$ 16% of the prescribed dose resulted in as good or better EUD values. In context, typical plans (created with the goal of a uniform dose distribution) have an SD on the order of 1%. For the case of the cold volume within the CTV, the EUD_{byst} was consistently

higher than the EUD. The model of the bystander effect therefore suggests the potential for mitigating decreases in treatment outcome when cold spots are unavoidable.

Based on the results of our bystander model, the bystander effect might play a more significant role at higher mean doses, assuming the dose heterogeneity is normally distributed around the mean value. As a result, the bystander effect increased the EUD by 1% for a 60 Gy prescription and by 3% for the 78 Gy prescriptions. The bystander model assumes that cells generate a bystander signal proportional to the absorbed dose. Therefore, higher dose prescriptions will results in cells exposed to higher radiation doses, which in turn translate into higher bystander signals.

One assumption made in this work is that the bystander signal above a specific threshold will have a negative impact on cell survival. Bystander signals do not always have a negative impact on cell survival and there have been studies where proliferative [128] and other beneficial effects have been reported [129]. In this study, we focused on potential bystander effects within the target volume of a confined gland. Our approach was first to model potential damage from bystander effects and then second model the potential consequence of that damage within a target volume. Looking at bystander effects on normal tissues was beyond the scope of this work. However, a much deeper understanding of bystander effects on clonogenic as well as normal tissues is needed before any current clinical practice would be modified because of bystander effects.

It is important to underscore the fact that the results presented here are based on the assumption that the cells in an in vivo, three dimensional (3D), vascular tumour volume will behave in a manner consistent with the in vitro conditions under which the form of this model was derived. As mentioned, this work is expected to define a maximum extent a bystander effect might play in terms of outcome for clinical scenarios because, as the assumptions of the bystander model break down, we are likely to see a diminished effect on cell response. For example, we assumed that the bystander signal is highly efficient

such that a signal released by one cell will have influence on all cells within the CTV regardless of location. We looked at the sensitivity of the results to initial parameter values in the bystander model by analyzing how a 10% increase and 10% decrease would affect our results. According to our model, the results were most sensitive to the response parameters hits per Gy (HPG) as well as (HB). When there is little dose heterogeneity (ie. SD is close to 0) the results were most sensitive to the HPG parameter. However, as the dose heterogeneity increased, the HB parameter became more influential. For example, in the case of the EUD results, a 10% change in HPG would cause about a 9% change in our results at SD of 0 and only a 4% change in our results at a SD of 18 Gy. A 10% change in HB would results in a 5% change at SD of 0, and a 8% change at a SD of 18 Gy.

The assumption that the bystander signal instantly equilibrates throughout the entire target volume is not unreasonable in vitro, but in a 3D vascular tissue, factors released into the extracellular matrix may be transported out of the tissue or tumour completely and diluted through the rest of the body, and hence diminish any effect on cell response. For example, work by Belyakov [130] showed that in a 3D artificial human skin for both the highly differentiated model of the human epidermis (EPI−200) and full thickness skin model (EFT−300) bystander effects were only observed up to ∼1mm away from directly irradiated cells. However, signal transport is still a very open-ended question and is likely to depend on the specific properties of the tissue or organ involved. Regardless, the predictions of model herein establish an upper bound on bystander effects in vivo. In our intermediate risk prostate scenario, all cells within the PTV receive some radiation dose. If a spatial limit to bystander signal diffusion were to be applied, this would localize the predicted responses such that more highly modulated spatial dose distributions would behave more consistently with this model, but less modulated doses (i.e. a large dose gradient across the target volume) would experience less overall damage as there would be

larger distances between the longest- and shortest-time signalling cells. Ultimately even if the results presented hold only in a qualitative context, they may relax the planning constraint of aiming for a uniform dose distribution and potentially open up new planning approaches such as introducing small, hot volumes to compensate for cold ones. At a minimum, our results suggest that further research into this area is warranted.

4.8 Conclusion

Our modeling process uses a very simple model with some basic assumptions. We have expanded on a recently published in vivo bystander model [33] that was originally adapted from the in vitro bystander provided model by McMahon et al.[93]. The results demonstrate the potential to deviate from both EUD and TCP predictions of the common local LQ model and standard EUD models when considering dose heterogeneity in the treatment volume of a prostate radiotherapy treatment. The bystander model suggests that a large amount of dosimetric heterogeneity through a treatment volume may be acceptable in a treatment plan and that a moderate amount may even be optimal. At a minimum, this model suggests that further study into bystander effects in clinical scenarios is warranted especially when considering different heterogeneous dose distributions.

4.9 General conclusion to chapter 4

This chapter looked TCP and EUD models to determine to what extent dose homogeneity planning constraints may be relaxed because of bystander effects. This work demonstrates that the incorporation of bystander effects into models of treatment response can potentially relax homogeneity constraints. Chapter 3 and this chapter have shown that bystander effects potentially have important implications when it come to radiotherapy treatment. Bystander effects have been known to play an important role in low dose regions such as those which may be found out-of-field of the primary treatment site [131, 132]. The objective of the next chapter was to relatively compare to what extent bystander effects play in low dose out-of-field regions compared to other known low dose effects such as low dose hypersensitivity effects, and this was the focus of the chapter 5.

Chapter 5

The Relative Biological Effectiveness of Out-of-Field Dose

5.1 General introduction to chapter 5

The work presented in this chapter investigated the relative biological effectiveness different low dose phenomena have on out-of-field radiation dose. A simple single arc treatment was used to simulate a typical prostate VMAT treatment where the physical out-of-field dose was compared with an equivalent out-of-field dose, assuming that low dose hypersensitivity effects, bystander effects, spectral effects, play a role in the biological effectiveness out-of-field. RBE are then compared for the different out-of-field effects.

This work has been submitted to the peer-reviewed journal *Physics in Medicine and Biology*. I was the first author of this work and prepared the main manuscript. The other contributing authors were Brandon Koger and Dr. Charles Kirkby. I developed the main algorithm for modeling the consequences of low dose hypersensitivity and bystander effects, and Dr. Charles Kirkby developed the main algorithm for modeling the consequences for spectral effects. Brandon Koger provided the source code modifications used in the Monte Carlo dosimetry simulations. All authors contributed to the review of the results and development of the final manuscript.

5.2 The Relative Biological Effectiveness of Out-of-Field Dose

Michael Balderson[1,2,3],MSc, Brandon Koger[1,2], BSc, and Charles Kirkby [1,2,3], PhD

[1] Department of Medical Physics, Tom Baker Cancer Centre, Calgary, Alberta, Canada

[2] Department of Physics and Astronomy, and [3]Oncology, University of Calgary, Alberta

[3] Department of Medical Physics, Jack Ady Cancer Centre, Lethbridge, Alberta, Canada,

Running title:

Key words: Low Dose Hypersensitivity ; Prostate Cancer; Bystander Effects, Monte Carlo

Declaration of Interest: The authors declare no conflicts of interest with the work presented herein.

5.3 Abstract

Purpose : Using simulations and models derived from existing literature, this work investigates the relative biological effectiveness (RBE) for out-of-field radiation and attempts to quantify the relative magnitudes of different contributing phenomena (spectral, bystander, and low dose hypersensitivity effects) . Specific attention is paid to external beam radiotherapy treatments for prostate cancer.

Materials and methods: Using different biological models that account for spectral, bystander, and low dose hypersensitivity effects, we calculate the RBE for different points

moving radially out from isocentre for a typical single arc VMAT prostate case. The RBE was found by taking the ratio of the equivalent dose to the physical dose. Equivalent doses were calculated by determining what physical dose would be necessary to produce the same overall biological effect as that predicted using the different biological models.

Results : Spectral effects changed the RBE out-of-field less than 2 %, whereas low dose hypersensitivity and bystander effects had much more profound changes of the RBE for out-of-field doses. The bystander effect had the largest RBE for points located just outside edge of the primary radiation beam in the cranial caudal (z-direction) compared to low dose hypersensitivity and spectral effects. In the coplanar direction, bystander effect played the largest role in enhancing the RBE for points up to 8.75 cm from isocentre.

Conclusions: Spectral, bystander, and low dose hypersensitivity effects can all increase the RBE for out-of-field radiation doses. In most cases, bystander effects seem to play the largest role followed by the low dose hypersensitivity. Spectral effects were unlikely to be of any clinical significance. Bystander, low dose hypersensitivity, and spectral effect increased the RBE much more in the cranial caudal direction (z-direction) compared with the coplanar directions.

5.4 Introduction

In recent years there have been many advances in radiotherapy techniques such as Intensity Modulated Radiotherapy (IMRT) and Volumetric Modulated Arc Therapy (VMAT). These techniques offer significant improvement in delivering highly conformal radiation doses to the target. In order to accurately predict the responses of tumours or normal

tissues to external beam radiation therapy, it is important to understand the survival response of cells to a given absorbed dose, not only in the volume where the highest doses of radiation accumulate (which generally corresponds to the target volume of the therapy plus a surrounding margin), but also outside of this volume where dose arises due to the combination of entry and exit dose, scatter, and leakage. entry and exit dose, scatter, and leakage. We define out-of-field dose as any dose that arises in the patient that arises outside of the collimated treatment field. Generally, organs-at-risk "those organs particularly sensitive to radiation" and other healthy tissues that surround the directly irradiated volume will receive this out-of-field dose. On rare occasions, even with properly defined margins, the clinical target volume (CTV the gross tumour volume plus the microscopic extension of the disease) can be located outside of the directly irradiated volume (which could for example be defined as the volume confined by the delivered 95% iso-surface), a situation commonly referred to as a partial geometric miss. Partial geometric misses can occur due to an accumulation of extreme errors in setup, motion, and/or errors in accurately delineating the CTV, and can have tremendous impact on the intended outcome of a treatment. Additionally an accurate understanding of how tissues respond to out-of-field dose is important for predicting and understanding the risk of radiation-induced secondary malignancies. In this work, we examine several factors that have been identified as having a role in modifying the common linear quadratic (LQ) survival response to absorbed dose in out-of-field scenarios. These include spectral effects [133, 134], low dose hypersensitivity effects[72, 135], and bystander effects [136, 137, 86, 93]. Others have suggested that these low dose phenomena work in concert with each other and are not mutually exclusive [131, 138, 139, 140].

The purpose of this work is to examine common models for predicting these effects in an external beam radiotherapy treatment scenario (we place specific emphasis on the treatment of prostate cancer), and compare their relative magnitudes in terms of relative

biological effectiveness or RBE. This will offer insight into their relative magnitudes and suggest on which effect(s) emphasis should be placed in future research.

From the outset it is important to recognize that some groups have suggested that these low dose phenomena work in concert with each other and may not be not mutually exclusive [131, 138, 139, 140]. For the purpose of this study, we have assumed that these low dose effects are independent of each other.

5.4.1 Spectral Effects

At the physical level, the radiation outside the primary radiation field results primarily from scatter. As a result the mean energy outside the primary field is less than that within. Small differences in biological effectiveness are observed when comparing the effects of kilovoltage radiation to megavoltage radiation or Co-60 gamma rays [141]. As mean electron energy decreases, the track structure changes resulting in increased in lineal energy, which in turn increases the biological damage induced per unit absorbed dose. There is some evidence to suggest that a similar, yet scaled down, phenomenon may occur on the periphery of megavoltage photon beam [134, 142, 133]. Using a previously developed simulation technique that translates a Monte Carlo generated spectrum into an estimate of DNA double strand breaks,[143, 144] we quantify the relative magnitude of this effect.

Low Dose Hypersensitivity

It is generally well accepted that radiation doses above 2 Gy are well described by the LQ model. However, over the past three decades or so different scientific investigators have noticed many cell lines have shown an increased radiosensitivity to radiation doses below 1 Gy compared with what would be predicted from the backward extrapolation of LQ response derived for high doses [72, 73]. It has been shown that over fifty different cells lines exhibit this increased radiation sensitivity at low doses [74, 75].

Surviving fractions (SF, the fraction of clonogens remaining after receiving an absorbed dose) at very low doses are much better fit using a modification to the LQ model called the induced-repair mode [36], see equation 5.4. In the LQ model, α is a constant, parameterizing the linear component of the survival response. Similarly a constant β parameterizes the quadratic component of the curve, both in response to an absorbed dose, D, such that the surviving fraction is given by $e^{(-\alpha D-\beta D^2)}$. In the induced repair model, α becomes a function of dose as shown in equation 5.3.

According to this empirical model, at low doses (at approximately 10 cGy and below) cells experience a hyper-radiosensitivity (HRS) and as the dose increases they begin to experience an increased radio-resistance (IRR) [36]. On a cell survival curve the increase in radiosensitivity at low doses is manifest as a steeper initial slope on the survival curve (α_s) compared with what would be extracted from extrapolating back from higher dose regions using the LQ model, which have more gradual slope (α_r). The more radiosensitive phase happens for doses up to around 10 cGy. As the dose increases the cells become more radio resistant. The point where the transition from α_s to α_r is 63% complete is defined by a parameter D_c. The transition from the more sensitive to more resistant biological response typically happens between approximately 20 cGy - 80 cGy [36]. At high doses ($>$ 100 cGy) the induced repair model and the LQ model predict the same overall cell killing.

5.4.2 **Bystander Effects**

Radiation-induced bystander effects cause cells to respond to the fact that neighboring cells have been irradiated [76] and therefore do not necessarily respond to radiation dose in isolation [33, 116]. Bystander effects are assumed to result from cell to cell communication through gap junction intercellular communication (GJIC) or through signals released into the surrounding medium [145, 146]. Bystander effects potentially play an important role

in low doses regions (< 0.2 Gy)[131, 132] and have the potential to influence the width of the margins used in radiotherapy, but much more work in needed to understand how bystander effects actually work *in vivo* [147].

Bystander effects have been shown in the many different experiments ([84, 86, 76, 92, 33, 116]. Bystander effects seem to attack the fundamental assumption of the prevalent LQ model (i.e. SF is a function of absorbed dose alone) and there is increasing interest to better understand the implications these effects have on radiotherapy treatment [147].

5.5 Methods and Materials

Irradiation Geometry

For this work we considered an irradiation geometry for a simplified VMAT treatmentas depicted in figure **??**. A planning target volume (PTV) of radius 2.5 cm was assumed to be centred inside a cylinder of radius 15.0 cm and length 70.0 cm. All materials were assumed to be radiologically equivalent to water. A 6 MV photon source was used to deliver a circular field of radius 3.0 cm (PTV radius + 0.5 cm) at isocenter. The source was delivered in an arc-therapy context with uniform fluence at all gantry angles. Attenuation from a patient support device was assumed negligible. Our model assumed a Varian iX linear accelerator with a 100 cm source to axis distance. The z-axis was defined as representative of a cranial-caudal direction along the length of the cylinder and is perpendicular to the plane of beam delivery. The radial or r-axis was defined as any direction away from isocentre within the plane of beam delivery.

Dose profiles used for the low dose hypersensitivity and bystander effect models were generated in this geometry using the Eclipse treatment planning system (version 11.01) with the Acuros XB (AXB) radiation transport and dose calculation algorithm applied (Varian Medical Systems, Palo Alto, CA, USA). Details of the Monte Carlo model used

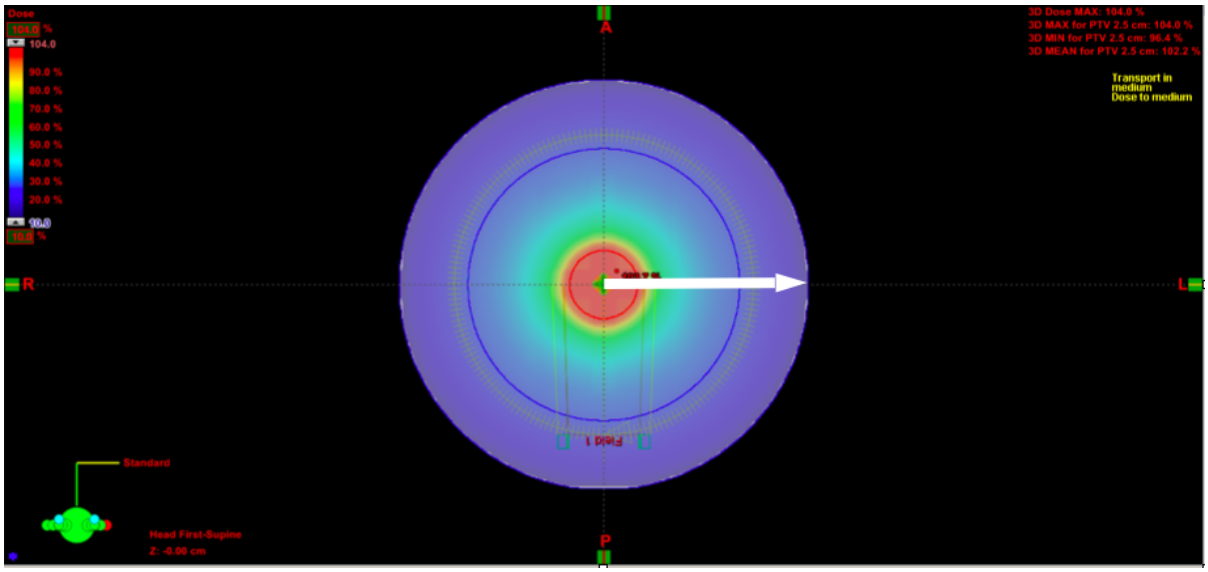

Figure 5.1: Dose map on an axial slice through isocentre as planned on the Eclipse TPS. The extracted dose profile in the r-dimension (indicated by the white arrow) starts at the origin of our target then moves outward in the radial direction. The z-dimension points in toward the page. The 6 MV photon beam was collimated to deliver a uniform fluence to the target volume. Because this was an arc-therapy geometry the source rotates though 360 degrees (gantry angles of 180E through 180 on a Varian scale).

to examine the spectral fluences are given below.

5.5.1 **Spectral Effects**

To quantify the approximate magnitude of spectral variation effects on a 6 MV photon beam in the geometry specified above, we used a technique for the coupled simulation of radiation transport on a macroscopic level and then simulated the induction of genetic damage on a microscopic level. Following the methods specified in earlier work [143, 144, 149] the Penetration and Energy Loss (PENELOPE) Monte Carlo package (version 2011) [150] was used to model radiation transport through the geometry depicted in figure 5.1. The source model used was a modified form of the penEasy "source-boxisotropicgaussspectrum" source sourceBoxIsotropicGaussSpectrum source which as-

sumed a point source that uniformly emitted photons within a pre-defined aperture angle. This angle was set to define a 3.0 cm circle at isocentre. The code was modified to randomly shift the position and angle of the source according to gantry angle, with each gantry angle having a uniform probability of occurring. Effectively, this simulated an arc delivery with uniform fluence at all angles. The photon spectrum was that derived by Sheikh-Bagheri and Rogers [148], which we note was scored for the central axis ($r \leq 2.25$ cm) for a Varian Clinac linear accelerator with a 10 by10 cm^2 field. Effects such as scatter from the jaws, MLC leakage, or contaminant electrons were considered higher order and not incorporated into the model. Simulation parameters were set as followes. The parameters C1 and C2, which establish the mean free path between hard elastic events and the maximum average fractional energy loss in a single step, respectively were both set to values of 0.1 as per the penEasy default. Photon absorption energies were set to 100 eV, while electron absorption energies were set to 100 keV (for the first stage simulations). Particles below these thresholds are considered locally absorbed. Threshold energies for radiative events, W_{cr}, and the separation of hard and soft elastic collisions, W_{cc}, tracked with the absorption energies.

This source and geometry reproduced the treatment planning system dose profiles as shown in figure 5.1. As shown, the MC dose profiles are sharper than those produced by the treatment planning system, an effect that is due to the simplified source model. The treatment planning system incorporates the collimator jaws, multileaf collimator leaves, etc. to produce a more realistic penumbra. Distance to agreement in the penumbra is generally within 3 mm and for the purposes of this work the differences in photon spectra as a function of position at 10 mm intervals are not likely to have a strong dependence on these details.

In the first set of simulations, the PENELOPE code scored photon fluence, differential in energy. In the $z = 0$ plane the fluence was symmetric for all gantry angles, thus it was

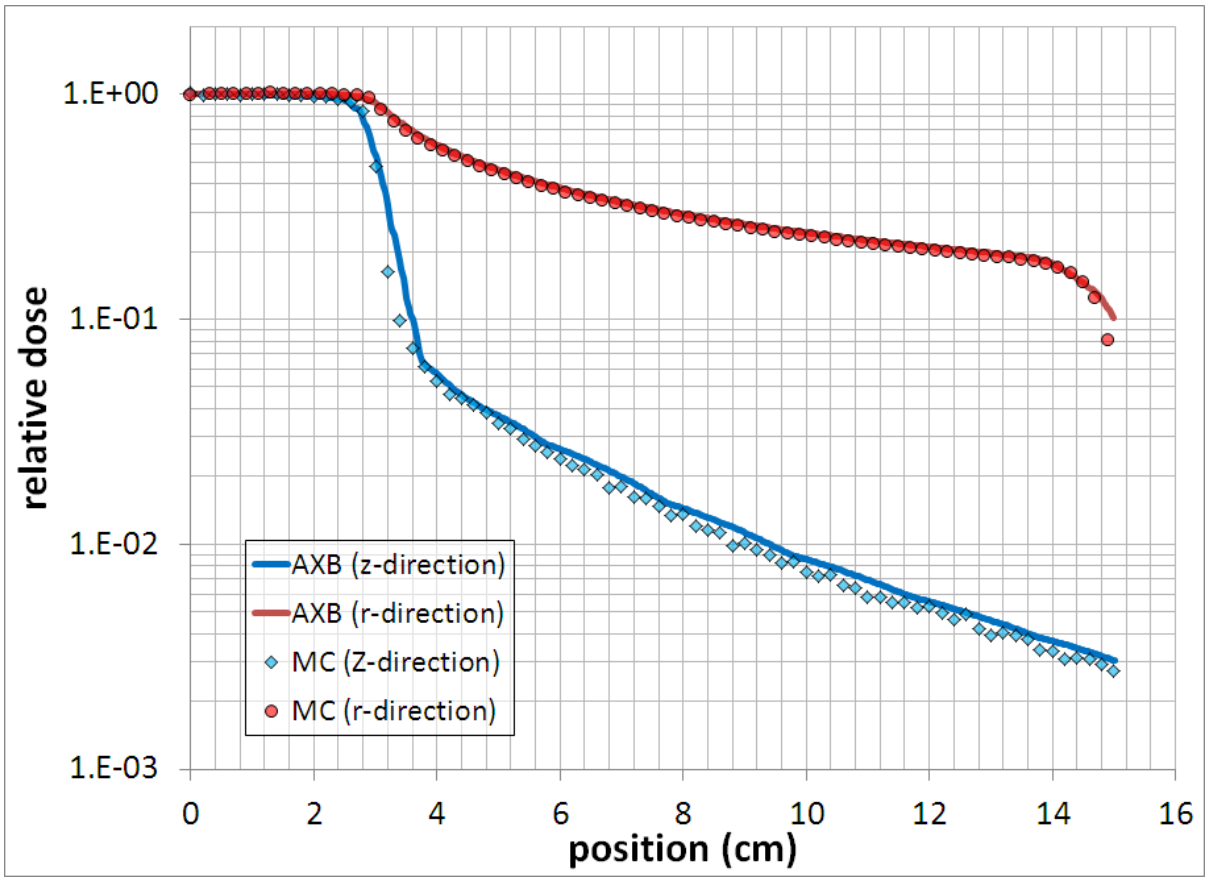

Figure 5.2: A comparison of the dose profiles in the radial (r) and longitudinal or cranial-caudal (z) dose profiles between the treatment planning system (AXB) and the simplified MC model. At the field edge, the MC results show a slightly sharper fall-off due to the source aperture defining the edge rather than a beam-shaping device (MLC). This difference should not significantly affect the results.

scored in radially concentric annular volumes with $\triangle r = 3$ mm, $\triangle z = 4$ mm in the axial plane at 10 mm intervals. Llongitudinally in 2 mm radius, $\triangle z = 4$ mm cylinders at 10 mm intervals. Energy bins were 20 keV wide.

The scored photon fluence was then used as input into a second set of simulations that used a unique tally written to estimate the expected value of genetic damage induced at a given site in response to the calculated photon fluence, differential in energy. The tally relies on a set of tabulated data taken directly from the Monte Carlo Damage Simulation (MCDS) software [144, 151, 152] (version 3.1) for a series of monoenergetic electrons. The MCDS is not a radiation transport code. For a particle characterized by its charge and kinetic energy, the code randomly distributes lesions along a DNA segment and then groups those lesions together estimating the number of double strand breaks (DSBs) as well as other forms of genetic damage (single strand breaks and base pair damages) and damage complexity.

In the second set of simulations the PENELOPE-scored photon fluence was used as a source incident on a (3.3 μm) cube of water, representative of a cell nucleus. As photons pass through and interact with the small volume, electrons are generated. These electrons are tracked by the tally. The MC simulation parameters were set to run with absorption energies of 100 eV (photons and electrons), C1 = C2 =0 (detailed simulation) and W_{cc} and W_{cr} tracked with absorption energy. We introduced a modification to the code where electrons were translocated immediately on escaping the volume, and set, without any modification to the direction vector to the opposite side of the cube. (Informally this is referred to as an electron "Pac-Man Universe" after the popular 1980s video game). Note that photons freely escape the volume. In this way, the code simulates an environment under charged particle equilibrium in response to a given photon spectrum in a computationally efficient manner. Each time a new electron is either (i) created, or (ii) translated, its incident energy is recorded. The electron and its progeny are tracked

until they are either absorbed or the escape the volume. The tally looks up the MCDS estimate of genetic damage based on the electron‘s energy at incidence and this value is incorporated into an average, weighted by the dose deposited by the electron track. The dose weighting is necessary to properly account for the low energy electrons with ranges much less than the scoring volume. This general approach successfully predicts genetic damage induced over a variety of energies and radiation types. Benchmarking has been reported elsewhere [143].

The code yields an estimate of the mean number of double-strand breaks (DSBs) induced per Gy per gigabase pair (Gbp) for a given photon spectrum. Elsewhere in this paper we derive RBE as a ratio of doses required to generate the same surviving fraction as an end point. For this particular effect, for convenience, we limit the RBE end point to the estimated number DSBs induced

$$RBE = \frac{D_0}{D_{r,z}} = \frac{DSB_{r,z}}{DSB_0} \tag{5.1}$$

where D_0 and $D_{r,z}$ are the doses required to induce the same number of DSBs under the different photon spectra at point r,z compared to the origin at 0. This different end point opens up some uncertainty for a relative comparison. The repair or misrepair of induced DSBs into cell survival is complex and may need to account for such details as the complexity of the induced DSBs, the fraction of the breaks that are repairable, or pairwise interactions of the DSBs [153]]. That said, the complexity of the induced damage is generally a more significant factor when dealing with larger particles such as protons, alpha particles, or heavy ions, and not expected to vary to a great extent for differences in photon spectra. Further differences in repair kinetics should not be so great as to change the result by an order of magnitude.

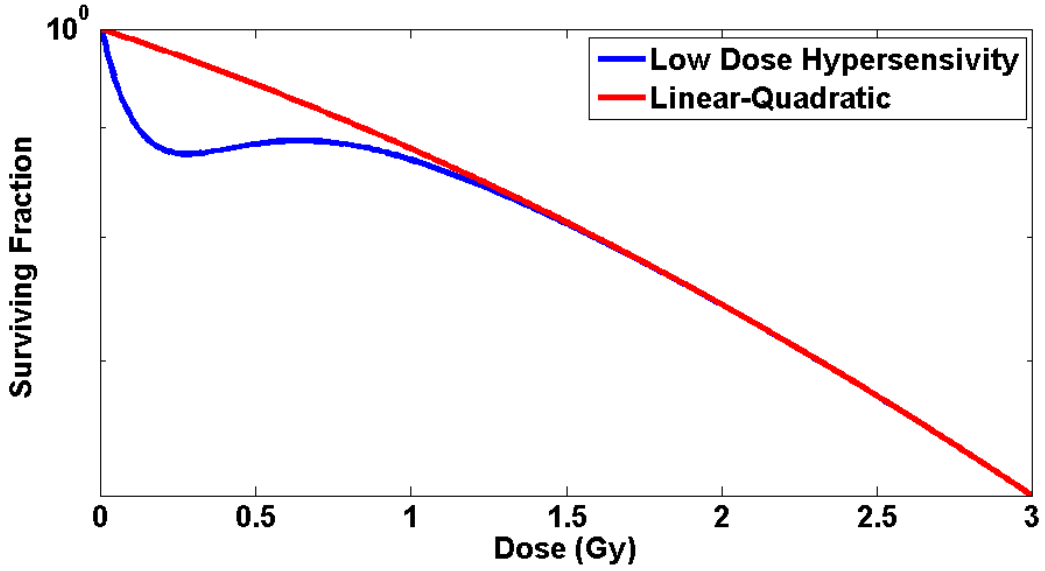

Figure 5.3: Surviving fraction vs. Dose using both the Linear-Quadratic model as well as the Induced Repair model for doses between 0 and 3 Gy. Parameters used in the figure are those for normal tissue prostate cells RWEP1 [2].

5.5.2 Low Dose Hypersensitivity

To investigate the effects of low dose hyper-sensitivity, SF were calculated using the induced repair model for low dose hypersensitivity cases using equation 5.4. To begin, a correlation map that relates SF and dose for doses between 0 Gy and 3 Gy was developed (see figure 5.3).

In this analysis we looked at dose profiles for both the radial and longitudinal directions). Dose profiles were extracted from the treatment planning system, with each line profile starting at the isocentre and then moved out toward the phantom edges (see the white arrow in figure 5.1 for the radial profile). For each point along our line profile we convert the physical dose to an equivalent dose assuming the presence of low dose hypersensitivity. The RBE is determined by taking the ratio of the equivalent does D_{eq} to the physical dose D_{phy}. D_{phy} is the physical dose absorbed in the tissue and D_{eq} is

Cell Line (Prostate)	α_s [Gy^{-1}]	α_r [Gy^{-1}]	β [Gy^{-2}]	D_c [Gy]	Source
Prostate Cancer (DU145)	0.930	0.173	0.023	0.137	[73]
Prostate Cancer (PC3)	0.77	0.12	0.03	0.18	[2]
Prostate Normal (RWPE1)	2.10	0.06	0.07	0.16	[2]

Table 5.1: Cell specific parameters used in the low dose hypersensitivity analysis.

the equivalent physical dose that would be necessary to produce the same effect when spectral, low dose hypersensitity, and bystander effects are considered.

$$RBE = \frac{D_{eq}}{D_{phy}} \tag{5.2}$$

.

$$\alpha(D) = \alpha_r - (\alpha_r - \alpha_s)\, e^{\frac{D}{D_c}} \tag{5.3}$$

$$SF = e^{\left(\alpha_r - (\alpha_r - \alpha_s) e^{\frac{D}{D_c}} D - \beta D^2\right)} \tag{5.4}$$

Low dose hypersensitivity effects are cell-line specific. Parameters used for cell-line specific parameters came from published results and are listed in table 5.1.

5.5.3 **Bystander Effects**

Our bystander model was adapted from the bystander model developed originally by McMahon et al. [93, 126, 33, 116]. The original bystander model proposed by McMahon et al., was developed from *in vitro* experiments for prostate (DU 145), lung (H460), human fibroblast (AGO-1522), and malignant melanoma (MM576) cells [93, 126, 86, 85]. Specific details on the bystander development are available elsewhere [126, 93, 116, 33]. In overview the basic premise and assumptions used in the bystander model are:

1. Cells exposed to radiation will release a bystander signal into the surrounding medium.

2. Cells will release a bystander signal for a specific period of time which is proportional to the absorbed dose.

3. The overall bystander signal concentration $\rho(t)$ increases while cells are actively signaling and then decays after the cells cease signaling. The overall bystander signal concentration is governed by equation 5.5.

$$\rho(t) = \frac{\rho_{max}}{1 + \frac{\lambda V}{\nu C}} \left(1 - exp\left(-t\left(\frac{\nu C}{V} + \lambda\right)\right)\right) + \rho_0 * exp\left(-\lambda t\right) \tag{5.5}$$

Here, $\rho(t)$ is the bystander signal concentration as function of time, $\rho_{max}$is the local bystander signal concentration equilibrium, λ is the signal decay constant, V is the volume, ν is substitution for $\frac{\eta}{\rho_{max}}$ where η is the rate of local signal production when the concentration is 0, C is the number of irradiated cells, and ρ_0 is the signal concentration at time t= 0.

4. If cells get exposed to a bystander signal above a defined threshold, there is a probability that these cells will receive additional biological damage in addition to any damage induced directly by the absorbed dose. Note that damage in this model does not necessarily imply DSBs as in the spectral effect model, although it could. Instead damage is scored as a set of arbitrary hits to a given cell, described below. The probability that a cell will experiences this additional biological damage is proportional to the length of time the cell has been exposed to a bystander signal concentration above the threshold τ.

$$P_B = 1 - exp\left(-\kappa\tau\right) \tag{5.6}$$

Here P_B is the probability of a cell receiving biological damage, τ is the time the cell is exposed to a bystander signal above a threshold and κ is a cell specific signal kinetic parameter.

5. Biological damage is manifest as an integer number of "hits" on the cell. A "hit" can be induced by absorbed radiation and from exposure to a bystander signal above the threshold. The total amount of "hits" is found by adding "hits" induced by radiation with the "hits" induced from bystander effects.

6. Finally, the total number of "hits" induced on a cell is translated to SF using specific rules published by Patridge et al. [109].

In this work, we introduced a limiting radius to the bystander model such that a bystander signal generated by one cell can affect the bystander signal concentration for cells up to one cm away. Starting at the origin of our PTV, we calculate the bystander signal concentration for all points along our profile for both coplanar as well as out of field directions. The bystander model then calculates the overall surviving fraction for cells at each point along the profile taking into account the absorbed radiation dose as well as bystander signal concentration at each point. The overall bystander surviving fraction can then be translated back to an equivalent dose using the LQ model by solving the quadratic equation. The RBE then is found by taking the ratio of the equivalent dose to the physical dose using equation 5.2.

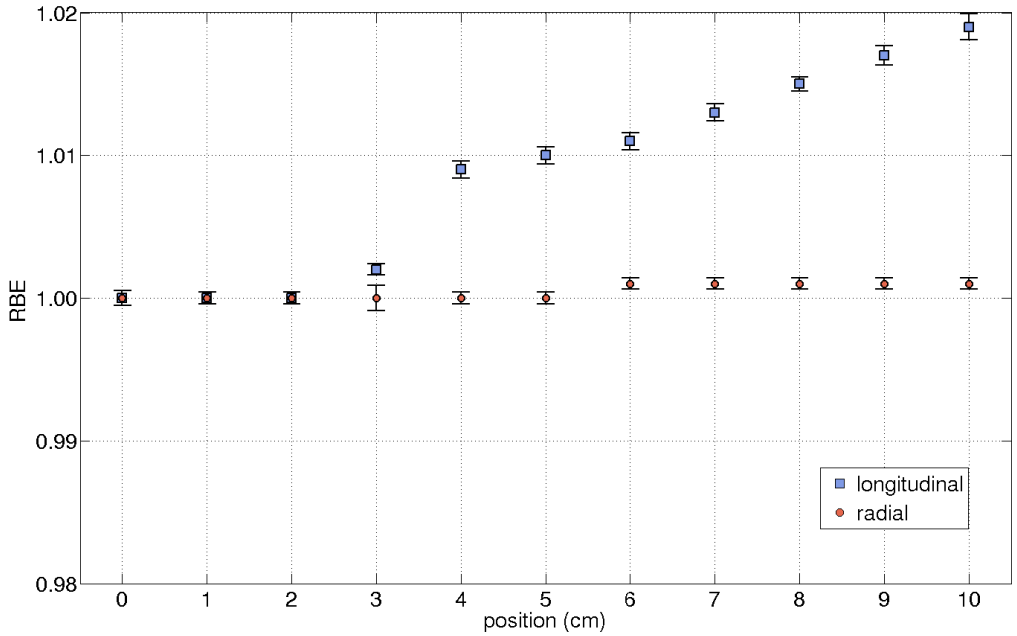

Figure 5.4: The relative biological effectiveness defined as a function of radial or longitudinal position moving outward from the isocentre due to spectral effects. Moving radially (coplanar with the primary field) there is very little change (~ 0.1 %) in the relative numbers of DSBs induced. Moving longitudinally the RBE increases with increasing distance once outside the target volume, but the difference is less than 2%. Error bars represent statistical uncertainty (two standard deviations) in the simulation results.

5.6 Results

5.6.1 Spectral Effects

The results of the RBE derived from the differences in DSB induction predicted for the calculated photon spectra are summarized in figure 5.4. For reference, the mean photon energy at isocentre was scored as 1.656 MeV and varied by less than 2% within the target volume under the conditions simulated. The mean energy decreased to 1.481 MeV and 1.188 MeV at r = 5 cm and r = 10 cm, respectively. Moving in the z-direction however, mean photon energies were reduced to 455 keV and 266 keV at z = 5 cm and z = 10 cm, respectively, and these values likely represent extreme (low end) cases of mean energy reduction out-of-field because head scatter and leakage, which were not modelled, are likely to have higher energies. However, despite what appear to be large differences in mean photon energy, figure5.4 illustrates that the relative differences in the induced number of DSBs was calculated to be very small.

The induced number of DSBs at the isocentre was approximately 8.4 DSBs/Gy/Gbp. This value remained constant within approximately 0.1 % as a function of position in the radial direction. This is because the photon spectra in the different radial positions (and therefore the resulting electrons spectra) are dominated by the photons from the incident field and so the mean energy remains above approximately 1.2 MeV. Dose in this region is a function of entry and exit dose as well as scatter and leakage, and though the lower energy scatter radiation may account for a significant portion of the delivered dose, it does not appear to be enough of a change to affect the induced DSB yield beyond a trivial level.

In the longitudinal direction the dose outside of 3 cm is delivered entirely by scatter and leakage. As a result the photon spectrum shifts towards lower energies. Again, the mean photon energy within the target volume (z = 0 cm) was 1.66 MeV, while at 10 cm

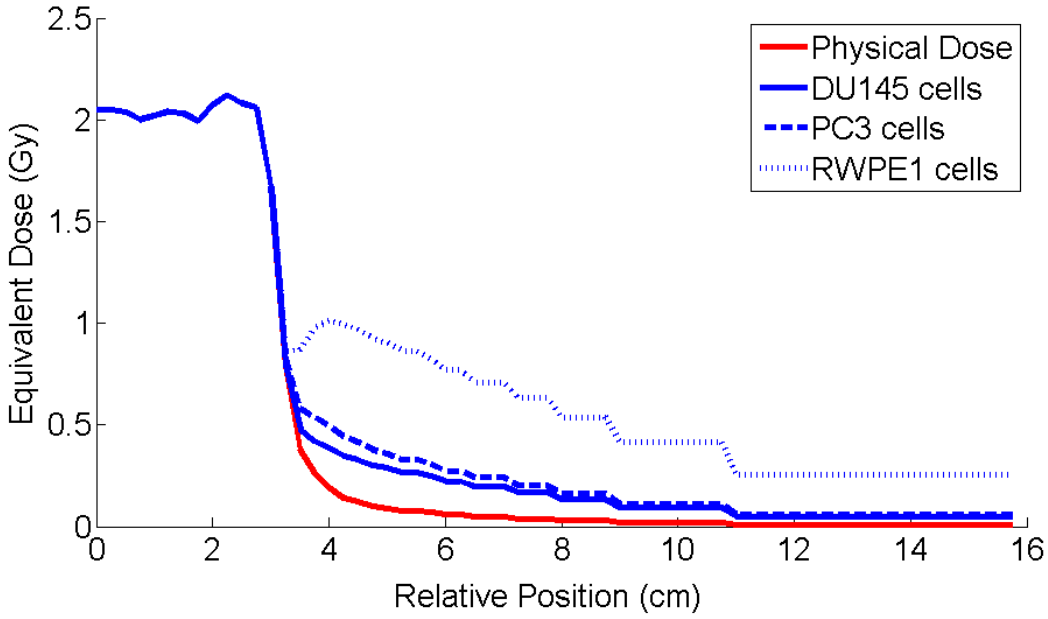

Figure 5.5: The Equivalent Dose (Gy) vs. Relative Position (cm) moving in the cranial–caudal direction (z direction). The red line is the physical dose reported from eclipse and the blue lines represent the equivalent dose for different cell lines assuming the presence of low dose hypersensitivity.

it was only 266 keV. Small changes in the DSB yield are consequently observed, increasing with distance from the target volume. Differences, according to these simulations, demonstrate that this change is less than 2 %. Even though a change was resolved it is likely of little consequence when attempting to predict the biological responses of tissues because this change is of a similar magnitude to common dosimetric uncertainties.

5.6.2 **Low Dose Hypersensitivity**

Figure 5.5 shows the biologically equivalent dose vs. relative position moving across the target volume in the z direction. The low dose hypersensitivity curves for the different cell lines remain consistence with each other to a relative position of 3.25 cm then the curves begin to diverge. The relative position of 3.25 cm from isocentre represents a

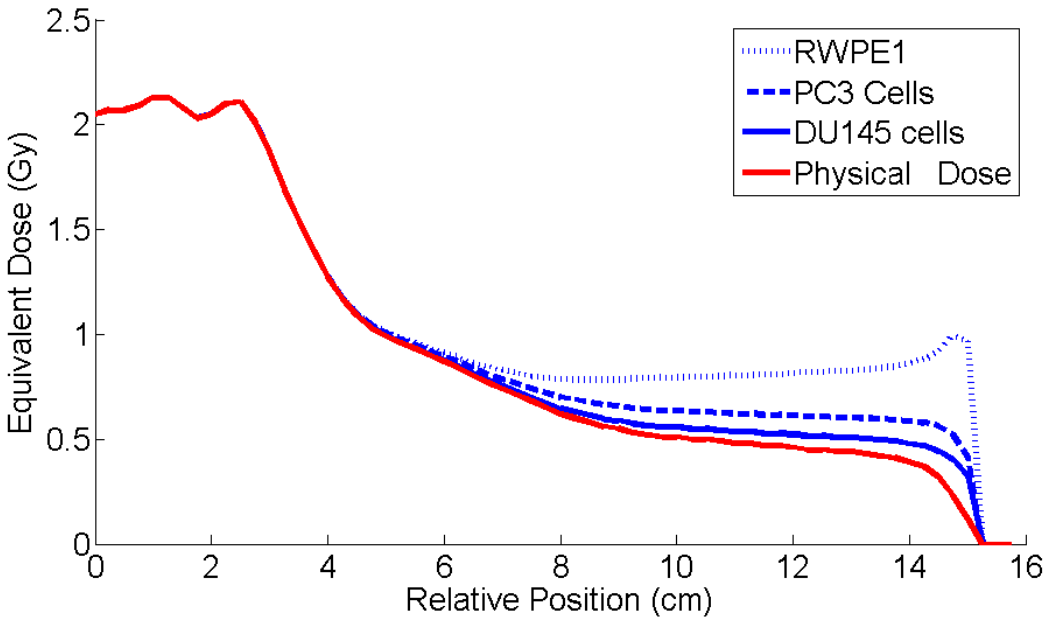

Figure 5.6: The Equivalent Dose (Gy) vs. Relative Position (cm) moving in the coplanar direction. The red line is the physical dose reported from eclipse and the blue lines represent the equivalent dose for different cell lines assuming the presence of low dose hypersensitivity.

point 0.75 cm beyond the edge of the PTV and 0.25 cm beyond the edge of the 3.0 cm circular field of radiation. The relative difference between the different cell lines in the z-direction at 4 cm was 1.01 Gy, 0.5 Gy, and 0.38 Gy for RWPE1, PC3, and DU145 cells respectively compared to a physical dose of 0.19 Gy. RWPE1 cells had the largest low dose hypersensitivity effect and DU145 cells showed the least response to hypersensitivity for low radiation doses. According to these results at 4 cm the RBE is 5.3, 2.6, and 2 times larger than the physical dose for RWPE1, PC3, and DU145 cells respectively (see figure 5.9).

Figure 5.6 shows the biological equivalent dose vs. relative position moving across the target coplanar with the radiation beam (radial direction). The low dose hypersensitivity curves for the different cell lines remain consistent with each other to a relative position

of 4.25 then the curves begin to diverge. In the coplanar direction the physical dose does not drop off as rapidly as it does in the out of field z-direction. For example in the z - direction the physical dose drops from 1 Gy to 0.5 Gy over a distance a few mm in the out of field direction compared to 5 cm in the coplanar directions for the same drop in dose. The total range of relative positions in low dose regions is much larger than the out of field directions. This has the effect of lifting the tail of the dose drop off curve slightly compared to the physical dose. At 10 cm from isocentre the physical dose is roughly 50 cGy where as biologically equivalent dose for RWPE1, PC3, and DU145 cells at 10 cm are 79 cGy, 64 cGy, and 56 cGy respectively.

5.6.3 **Bystander Effects**

Figure 5.7 shows the results of the biologically equivalent dose vs. the relative position from isocentre for the out of field direction. The biologically equivalent dose curve from the bystander effect widens the shoulder of the physical dose curve. Looking at a 50% drop in dose, the physical dose dropped to 1 Gy at a relative position of 3.2 cm from isocentre whereas the bystander effect biologically equivalent dose curve dropped to 1 Gy at around 4 cm from isocentre.

Figure 5.8 shows the results of biologically equivalent dose vs. relative position in the coplanar direction for the bystander effect. The biologically equivalent bystander curve drops to 1 Gy at relative positions of 6.5 cm compared to 5 cm for the physical dose. According to our model, at 10 cm from isocentre the bystander effect increased the dose by about 19 cGY compared to the physical dose (50 cGy to 69 cGy). In other words, at 10 cm from isocentre our results predict that the bystander effect is equivalent to about a 38 % higher dose than what would be reported by the treatment planning system for the out of field dose in the coplanar direction at 10 cm from isocentre. Similarly, at 5 cm from isocentre the biologically equivalent bystander dose is 23 % higher than the physical

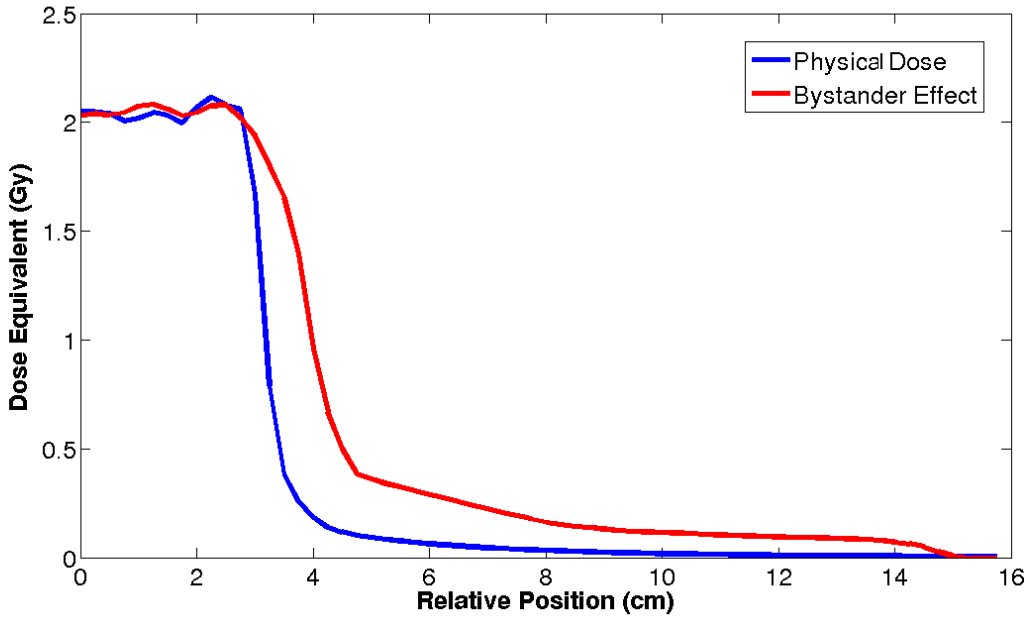

Figure 5.7: The Equivalent Dose (Gy) vs. Relative Position (cm) moving in the cranial–caudal direction (z direction). The red line is the physical dose reported from eclipse and the blue lines represent the equivalent dose for DU145 cells assuming the presence of bystander effects.

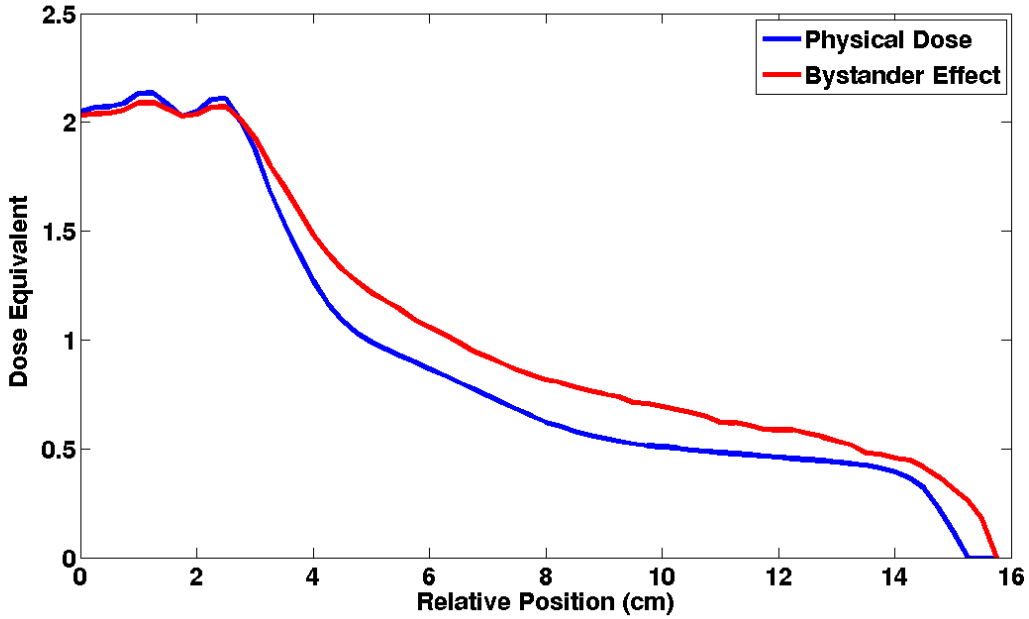

Figure 5.8: The Equivalent Dose (Gy) vs. Relative Position (cm) moving coplaner to the radiation beam (x or y direction). The red line is the physical dose reported from eclipse and the blue lines represent the equivalent dose for DU145 cells assuming the presence of bystander effects.

dose.

5.7 Discussion

In aggregate the results demonstrate that spectral effects result in RBE changes of less than 2 % outside of the primary target volume. Changes predicted by the low-dose hypersensitivity model are cell-line dependent, but appear to be capable of inducing RBEs 20 times higher at 10 cm from isocentre and 5 times higher $\sim$ 1 cm from the edge of the primary beam. Bystander effects, again, while expected to be cell-line dependent were predicted to be on the order of 5 times higher out of the field. These relative magnitudes are important. Earlier work experimentally demonstrated a difference in DSB induction in out-of-field beams, and this was initially attributed to the out-of-field spectral changes [133]. Other groups have pointed out that these results were more likely explained by RIBEs [154]. While both effects are likely at play, these calculations demonstrate the RIBEs are by far the more dominant effect.

As expected the low dose hypersensitivity did not have any effect on the equivalent dose until the physical dose dropped below 1 Gy. Even when the physical doses dropped below 1 Gy the results depended on the biological parameters used for different cell lines. The physical dose predicted by eclipse dropped to 1 Gy at 7 mm beyond the edge of the PTV for the out of field directions and 2.5 cm for the coplanar direction. Cells located within 7 mm in the out of field direction and within 2.5 cm of the PTV in the coplanar direction will not be sensitive to low dose hypersensitivity effects and only cells beyond those limits will see an increased biologically equivalent dose. The bystander effect however seems to effect the biologically equivalent dose of cells on the edge of the PTV. In this model low dose hypersensitivity will not affect the biologically equivalent dose for cell located up to about 7 mm beyond the edge of the PTV and only play a

role for cells located more than 7 mm from the edge of the PTV. The bystander effect however has an effect on cells located on the periphery of the PTV. In the out of field direction, cells located 5 mm from the PTV edge will receive an absorbed dose of 1.67 Gy but if bystander effects are considered they would receive a biologically equivalent dose of 1.94 Gy. At 1 cm from the edge of the PTV cells will receive an adsorbed physical dose of 0.38 Gy but an equivalent bystander adjusted dose of 1.65 Gy. In the coplanar directions, the physical dose at 0.5 cm and 1 cm from the PTV edge are 1.88 Gy and 1.54 Gy respectively. Considering bystander effects, the biologically equivalent dose at 0.5 cm and 1 cm are 1.93 Gy and 1.71 Gy respectively which is about 3% and 11% higher than physical doses at those locations.

The results for the low dose hypersensitivity seem to be strongly cell line dependent. For example, Martin et al., [2] looked at clonogenic survival following irradiation for 3 prostate cancer cell lines (DU145, PC3, and 22RV1) and two prostate epithelial (PWR1E and RWPE1) cell lines [2]. In their study only PC3 as well as RWPE1 cells showed increased hypersensitivity at low doses and that DU145, 22RV1, and PWR1E cells did not. However, Wouters and Skarsgard found that DU145 cells did however show a slight increase in radiosensitiviy at low doses [73]. Currently, the only available prostate specific response parameters for our bystander model were DU145 cell line parameters [93]. If we compare DU 145 bystander effects with DU 145 low dose hypersensitivity effects, it appears that bystander effects make a larger difference in RBE compared with low dose hypersensitivity effects. For example at 4 cm from isocenter, the RBE for the bystander effect in the coplanar direction was 1.17 compared with 1.0 for low dose hypersensitivity effects. At 10 cm from isocentre the RBE for bystander effects was 4.8 compared with 2.0 for low dose hypersensitivity effects. In the z-direction, at 4 cm from isocentre the RBE for bystander effects was 1.4 compared with 1.1 for low dose hypersensitivity. At 10 cm from isocenter the RBE for bystander effects and low dose hypersensitivity was much

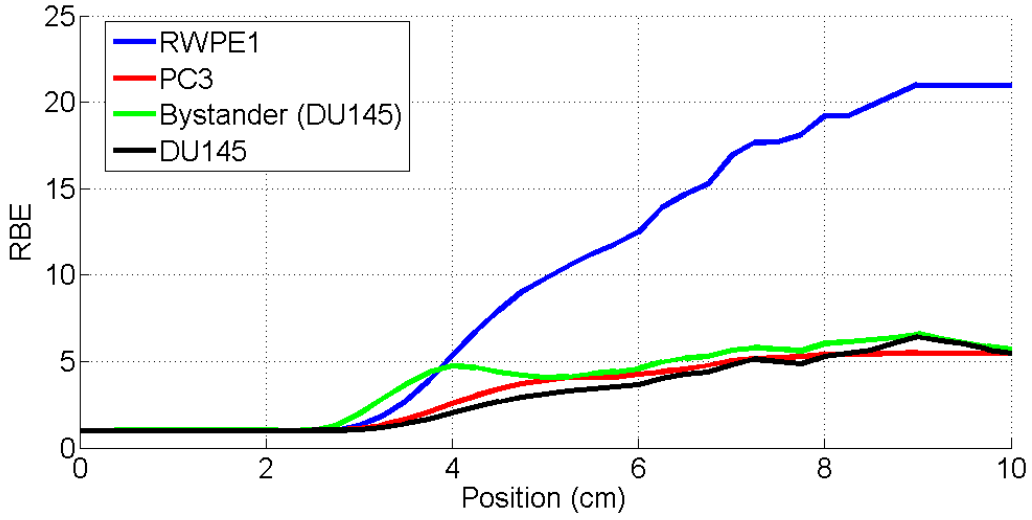

Figure 5.9: The RBE in a cranial-caudal direction (z direction) moving outward from the isocentre due to low dose hypersensitivity, bystander, and spectral effects. LDH (RWPE1), LDH (PC3), and LDH (DU 145) are the RBE for low dose hypersensitivity. Bystander (DU 145) is the RBE for the bystander effect and "Spectral" represents the RBE for spectral out-of-field effects when moving in the cranial-caudal (z direction).

closer but the bystander effect still had a higher RBE of 5.7 compared with an RBE of 5.5 for low dose hypersensitivity.

This study looked at the RBE for out-of-field doses as we move radially away from isocentre. An important point to note is that in reality, moving radially from isocentre we are likely traversing different cell types. For example, the RBE of prostate cancer DU 145 cells 10 cm from isocentre is an oversimplification as 10 cm from isocenter is beyond the edges of the PTV and into the surrounding normal tissues. The focus of this work was on prostate cancer and used prostate specific parameters. To get a full picture of the RBE for out-of-field doses, a follow up study could look at the surrounding normal tissues using biological parameters for both bladder and rectum.

In this work we introduced a limiting radius to the bystander signal of 1 cm. To test the sensitivity of our results to the limiting radius of the bystander signal the results in

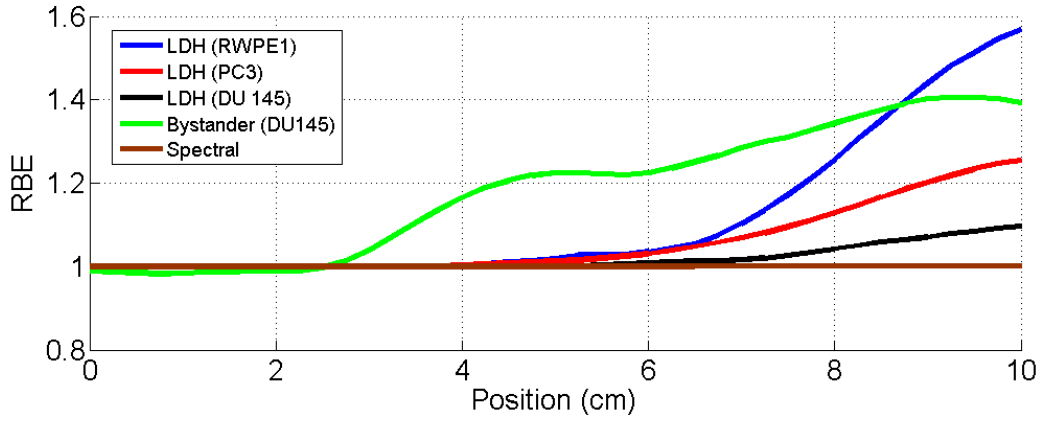

Figure 5.10: The RBE in a coplanar direction moving outward from the isocentre due to low dose hypersensitivity and the bystander effect. LDH (RWPE1), LDH (PC3), and LDH (DU 145) are the RBE for low dose hypersensitivity. Bystander (DU 145) is the RBE for the bystander effect and "Spectral" represents the RBE for spectral out-of-field effects when moving in the coplanar direction.

the coplanar direction were repeated for limiting radius of 2 mm, 5 mm, 1 cm, 2 cm, and 3 cm. The results of this sensitivity analysis are shown in figure 5.11. At a distance of 10 cm from isocentre, the bystander effect resulted in a biologically equivalent dose of 59 cGy for a bystander signal range limited to 2 mm compared to 79 cGy when the bystander single range was limited to 3 cm which is a 33 % larger biologically equivalent dose. General speaking, the bystander effect played a larger role in out of fields when the signal range was largest.

5.8 Conclusion

Spectral, Bystander, and low dose hypersensitivity effects all increased the RBE outside the primary target volume. Spectral effects seem to play a smaller role than bystander and low dose hypersensitivity effects in changing the RBE. These results however are dependent on cell-line as well as their location out-of-field. RWPE1 cells showed the

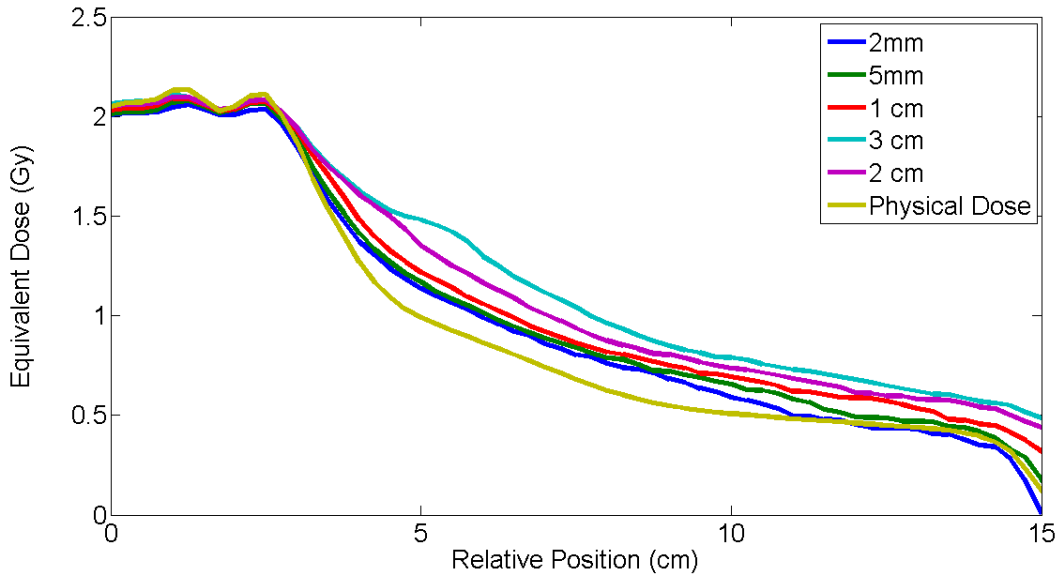

Figure 5.11: A sensitivity analysis of the bystander range parameter. We looked at how the results changed when we assumed the bystander signal range was 2 mm, 5 mm, 1 cm, 2 cm, and 3 cm. In this work we assumed a 1 cm signal range for the bystander effect.

largest low dose hypersensitivity effects. For a single arc VMAT prostate treatments, the RBE in the cranial-caudal direction (z direction) is about 3 to 4 times larger than the RBE in the coplaner direction. If we look solely at prostate DU145 cells, our results show that bystander effects enhances the RBE more than low dose hypersensitivity especially for cells located just outside the edge of the PTV.

5.9 General Conclusions to chapter 5

This work quantified the relative magnitude bystander effects and low dose hypersensitivity effects have on out-of-field radiation doses. Both bystander, low dose hypersensitivity, and spectral effects increased the biologically equivalent out-of-field radiation doses. Bystander effects seemed to play a large role on the periphery of the PTV. Periphery doses would be inherently sensitive to geometric miss errors such as those presented in chapters 2 and 3.

Chapter 6

Conclusion

6.1 Review of the thesis

This work looked at different modelling approaches for EBRT for prostate cancer. Initially, we were interested in understanding what effects large geometric misses would have on TCP for common treatment modalities of IMRT and VMAT. Better imaging techniques in recent years have lead to many investigations regarding how motion, geometric uncertainty, and treatment margins have on patient outcome [30, 155, 156, 157]. The motivation of many of these studies was to determine the most reasonable treatment margins to maximize tumour control while minimizing normal tissue complications [32, 17, 18]. In our initial work, we assumed appropriate treatment margins, but wanted to study cases where the geometric miss was much larger than what would be accounted for in the treatment margins and specifically investigated if IMRT was more robust then VMAT. This initial study used the standard LQ model to predict treatment outcomes in terms of TCP. This initial investigation lead us to consider how other biological models, specifically ones that accounted for bystander effects changed predicted outcomes under geometric miss error (see chapter 3) as well as dose heterogeneity scenarios (see chapter 4). Our final study was based on the fact we had shown in the work presented in chapters 2 and 4 that bystander effects potentially played an important role in treatment and should not be disregarded. The final chapter looked at the RBE of bystander effects in low dose out-of-field regions compared to other low dose effects such as low dose hypersensitivity and the effects of changing photon energy spectrum.

6.2 Summary of Results

The work presented in chapter 2 investigated cases where geometric miss errors went beyond the uncertainties typically accounted for in treatment planning and resulted in less than optimal tumour control for two common approaches to treatment of prostate cancer: static gantry IMRT and VMAT. We used a Monte Carlo-based model of biological response to predict how mean TCP changes when systematic and random geometric miss errors were introduced into a model test case. Directly comparing static gantry IMRT with VMAT treatment deliveries suggests that static gantry IMRT can result in higher mean TCP values than VMAT for given large errors, or that the static gantry IMRT approach offers an increased latitude for forgiveness, to the order of 2 mm, over VMAT.

Chapter 3 suggested that in clinical scenarios, a bystander signal strong enough to modify LQ-based predictions may be induced even when small volumes of the target have been directly irradiated. It also suggests the potential for a mitigated effect on TCP where small portions of the PTV have been missed or only partially irradiated. Under these conditions of geometric miss, bystander effects potentially increase TCP predictions compared with the LQ model predictions.

The results presented in chapter 4 demonstrate that bystander effects potentially deviate from both EUD and TCP predictions of the common local LQ model and when considering dose heterogeneity in the treatment volume of prostate radiotherapy treatments. The bystander model suggests that a large amount of dosimetric heterogeneity through a treatment volume may be acceptable in a treatment plan and that a moderate amount may even be optimal. These results suggest that incorporation of bystander effects into models of treatment response, can potentially relax dose homogeneity constraints.

The relative magnitude that bystander effects have on biological response in out-of-

field regions has been quantified compared to other effects such as low dose hypersensitivity effects, and spectral effects. Spectral, bystander, and low dose hypersensitivity effects all increased the RBE outside the primary target volume. Spectral effects seem to play a much smaller role than bystander and low dose hypersensitivity effects in changing the RBE. These results however are dependent on cell-line as well as their location out-of-field. RWPE1 cells showed the largest low dose hypersensitivity effects. For a single arc VMAT prostate treatment, the RBE in the cranial-caudal direction (z direction) is about 3 to 4 times larger than the RBE in the coplaner direction. If we look solely at prostate DU145 cells, our results show that bystander effects enhances the RBE more than low dose hypersensitivity especially for cells located just outside the edge of the PTV. Spectral effects are largely expected to be independent of human cell type.

6.3 Future Work

6.3.1 Normal Tissue Complication Probability Studies

Radiotherapy treatments consider both dose to clonogenic cells as well as dose to surrounding normal tissues. It is the interplay between these two aspects of radiotherapy treatments which determines the most appropriate treatment approach. Dose optimization schemes are applied to cover the tumour with a lethal treatment dose while minimizing dose to surrounding normal tissues. This work focused on biological models of tumour control, primarily TCP. The other important question is how would the simulations presented in this work effect healthy normal tissues. Normal tissue complications can be quantified using common normal tissue complication probabilities (NTCP) models. Common NTCP models would include Lyman-Kutcher-Burman (LKB) Model [158] and the Relative Seriality Model [159]. In radiotherapy prostate treatment, the two main organs at risk in EBRT are the rectum and bladder. At our centre for example, to min-

imize radiation dose to these sensitive organs at risk, radiation treatments for prostate cancer are delivered when patients have full bladders and empty rectums. An important question to answer in future work would be how much do radiation induced bystander effect increase NTCP particularly for the bladder and rectum.

6.3.2 **Experimental Validation**

Like any biological or mathematical model, the predicted outcomes of the biological model need to be experimentally validated. In order for the results presented in this work to be truly accepted, the results need to be experimentally validated for *in vivo* scenarios. Much of this work dealt with biological modelling of radiation induced bystander effects. Our bystander model was adapted from a bystander model that was based on *in vitro* experimental evidence [94, 93, 126] and we have applied our model to *in vivo* prostate treatment scenarios.

As a starting point for experimental validation of this model, prostate cancer cells would have to be acquired to test our results. Our bystander model was developed using response and signal parameters derived from prostate carcinoma cells (DU-145)[93]. DU-145 and other cell lines such as A549 (lung carcinoma), MDA-MB-231 (breast adenocarcinoma), A375 (melanoma), and T98G (glioblastoma multiform) are commonly available from supplies such as Sigma-Aldrich (USA). Experimental validation of this model *in vivo* is much more challenging than *in vitro*. However, a good starting point for *in vivo* validation could be acquiring 3D tissue models from companies such as MatTek (USA). At a minimum, similar simulations such as those modelled in this study would need to be repeated experimentally with 3D tissue cultures and the results tallied and quantified. For example, cells could be irradiated with different field sizes in a manner that some cells are directly exposed to radiation while others are shielded. Similarly you could keep a constant field size but shield the centre of the the cells using differ-

ent diameters of circular shielding. Changing the diameter of the circular shielding will change the the ratio of cells exposed the full 2 Gy radian with cells exposed to a much lower shielded dose. Experiments such as this will in part validate the work presented herein and justify further study into how radiation induced bystander effects play a role in EBRT of prostate cancer.

Bibliography

[1] Robert Meier. Dose-escalated robotic sbrt for stage i-ii prostate cancer. *Front Oncol*, 5:48, 2015.

[2] Lynn Martin, Brian Marples, Mary Coffey, Mark Lawler, Donal Hollywood, and Laure Marignol. Recognition of o6meg lesions by mgmt and mismatch repair proficiency may be a prerequisite for low-dose radiation hypersensitivity. *Radiat Res*, 172(4):405–413, Oct 2009.

[3] Canadian Cancer Societys Advisory Committee on Cancer Statistics. Canadian cancer statistics 2014. toronto, on: Canadian cancer society; 2014. 2014.

[4] Ihe in your pocket 2008: A handbook of health economic statistics.

[5] Management of localised prostate cancer: watchful waiting, surgery or radiation therapy, depending on the natural course, which is often relatively slow. *Prescrire Int*, 21(131):242–248, Oct 2012.

[6] G. Delaney, S. Jacom, C. Fetherstone, and M. Barton. The role of radiotherapy in cancer treatmetn: estimating optimal utilization from a review of evidance-based clinical guidelines. *Cancer*, 104(6):1129–37, 2005.

[7] American Cancer Society. web, June 2015.

[8] Stephen A. Boorjian, R Jeffrey Karnes, Rosalia Viterbo, Laureano J. Rangel, Eric J. Bergstralh, Eric M. Horwitz, Michael L. Blute, and Mark K. Buyyounouski. Long-term survival after radical prostatectomy versus external-beam radiotherapy for patients with high-risk prostate cancer. *Cancer*, 117(13):2883–2891, Jul 2011.

[9] Nicholas Hardcastle, Wolfgang A. Tom, Kerwyn Foo, Andrew Miller, Martin Carolan, and Peter Metcalfe. Comparison of prostate imrt and vmat biologically optimised treatment plans. *Med Dosim*, 36(3):292–298, 2011.

[10] Enzhuo M. Quan, Xiaoqiang Li, Yupeng Li, Xiaochun Wang, Rajat J. Kudchadker, Jennifer L. Johnson, Deborah A. Kuban, Andrew K. Lee, and Xiaodong Zhang. A comprehensive comparison of imrt and vmat plan quality for prostate cancer treatment. *Int J Radiat Oncol Biol Phys*, 83(4):1169–1178, Jul 2012.

[11] Pengpeng Zhang, Laura Happersett, Margie Hunt, Andrew Jackson, Michael Zelefsky, and Gig Mageras. Volumetric modulated arc therapy: planning and evaluation for prostate cancer cases. *Int J Radiat Oncol Biol Phys*, 76(5):1456–1462, Apr 2010.

[12] M. Teoh, C. H. Clark, K. Wood, S. Whitaker, and A. Nisbet. Volumetric modulated arc therapy: a review of current literature and clinical use in practice. *Br J Radiol*, 84(1007):967–996, Nov 2011.

[13] D. Verellen and F. Vanhavere. Risk assessment of radiation-induced malignancies based on whole-body equivalent dose estimates for imrt treatment in the head and neck region. *Radiother Oncol*, 53(3):199–203, Dec 1999.

[14] Jeremy D. Ruben, Sidney Davis, Cherie Evans, Phillip Jones, Frank Gagliardi, Matthew Haynes, and Alistair Hunter. The effect of intensity-modulated radiotherapy on radiation-induced second malignancies. *Int J Radiat Oncol Biol Phys*, 70(5):1530–1536, Apr 2008.

[15] Eric J. Hall and Cheng-Shie Wuu. Radiation-induced second cancers: the impact of 3d-crt and imrt. *Int J Radiat Oncol Biol Phys*, 56(1):83–88, May 2003.

[16] A. L. McKenzie, M. van Herk, and B. Mijnheer. The width of margins in radiotherapy treatment plans. *Phys Med Biol*, 45(11):3331–3342, Nov 2000.

[17] M. van Herk, Peter Remeijer, and Joos V. Lebesque. Inclusion of geometric uncertainties in treatment plan evaluation. *Int J Radiat Oncol Biol Phys*, 52(5):1407–1422, Apr 2002.

[18] Marcel van Herk. Errors and margins in radiotherapy. *Semin Radiat Oncol*, 14(1):52–64, Jan 2004.

[19] Alan McKenzie, Marcel van Herk, and Ben Mijnheer. Margins for geometric uncertainty around organs at risk in radiotherapy. *Radiother Oncol*, 62(3):299–307, Mar 2002.

[20] M. Mangoni, I. Desideri, B. Detti, P. Bonomo, D. Greto, F. Paiar, G. Simontacchi, I. Meattini, S. Scoccianti, T. Masoni, C. Ciabatti, A. Turkaj, S. Serni, A. Minervini, M. Gacci, M. Carini, and L. Livi. Hypofractionation in prostate cancer: radiobiological basis and clinical appliance. *Biomed Res Int*, 2014:781340, 2014.

[21] J Martin Brown, David J. Carlson, and David J. Brenner. The tumor radiobiology of srs and sbrt: are more than the 5 rs involved? *Int J Radiat Oncol Biol Phys*, 88(2):254–262, Feb 2014.

[22] David J. Brenner, Alvaro A. Martinez, Gregory K. Edmundson, Christina Mitchell, Howard D. Thames, and Elwood P. Armour. Direct evidence that prostate tumors show high sensitivity to fractionation (low alpha/beta ratio), similar to late-responding normal tissue. *Int J Radiat Oncol Biol Phys*, 52(1):6–13, Jan 2002.

[23] J. Fowler, R. Chappell, and M. Ritter. Is alpha/beta for prostate tumors really low? *Int J Radiat Oncol Biol Phys*, 50(4):1021–1031, Jul 2001.

[24] Piernicola Pedicini, Lidia Strigari, and Marcello Benassi. Estimation of a self-consistent set of radiobiological parameters from hypofractionated versus standard

radiation therapy of prostate cancer. *Int J Radiat Oncol Biol Phys*, 85(5):e231–e237, Apr 2013.

[25] T. Pawlicki, P.B. Dunscombe, A.J. Mundt, and P. Scalliet, editors. *Quality and Safety in Radiotherapy*. CRC Press, Taylor and Francic Group, 2010.

[26] Tim Craig, Vitali Moiseenko, Jerry Battista, and Jake Van Dyk. The impact of geometric uncertainty on hypofractionated external beam radiation therapy of prostate cancer. *Int J Radiat Oncol Biol Phys*, 57(3):833–842, Nov 2003.

[27] Thomas E. Byrne. A review of prostate motion with considerations for the treatment of prostate cancer. *Med Dosim*, 30(3):155–161, 2005.

[28] Theodore F. Mutanga, Hans C J. de Boer, Gerard J. van der Wielen, Mischa S. Hoogeman, Luca Incrocci, and Ben J M. Heijmen. Margin evaluation in the presence of deformation, rotation, and translation in prostate and entire seminal vesicle irradiation with daily marker-based setup corrections. *Int J Radiat Oncol Biol Phys*, 81(4):1160–1167, Nov 2011.

[29] G. S. Mageras, G. J. Kutcher, S. A. Leibel, M. J. Zelefsky, E. Melian, R. Mohan, and Z. Fuks. A method of incorporating organ motion uncertainties into three-dimensional conformal treatment plans. *Int J Radiat Oncol Biol Phys*, 35(2):333–342, May 1996.

[30] Valeria Landoni, Bianca Saracino, Simona Marzi, Michaele Gallucci, Maria G. Petrongari, Enrico Chianese, Michaela Benassi, Giuseppe Iaccarino, Antonella Soriani, and Giorgio Arcangeli. A study of the effect of setup errors and organ motion on prostate cancer treatment with imrt. *Int J Radiat Oncol Biol Phys*, 65(2):587–594, Jun 2006.

[31] J. M. Balter, H. M. Sandler, K. Lam, R. L. Bree, A. S. Lichter, and R. K. ten Haken. Measurement of prostate movement over the course of routine radiotherapy using implanted markers. *Int J Radiat Oncol Biol Phys*, 31(1):113–118, Jan 1995.

[32] M. van Herk, A. Bruce, A. P. Kroes, T. Shouman, A. Touw, and J. V. Lebesque. Quantification of organ motion during conformal radiotherapy of the prostate by three dimensional image registration. *Int J Radiat Oncol Biol Phys*, 33(5):1311–1320, Dec 1995.

[33] Michael John Balderson and Charles Kirkby. Potential implications on tcp for external beam prostate cancer treatment when considering the bystander effect in partial exposure scenarios. *Int J Radiat Biol*, 90(2):133–141, Feb 2014.

[34] N. Barthelemy-Brichant, J. Sabatier, W. Dew, A. Albert, and J. M. Deneufbourg. Evaluation of frequency and type of errors detected by a computerized record and verify system during radiation treatment. *Radiother Oncol*, 53(2):149–154, Nov 1999.

[35] R. L. Warters and K. G. Hofer. Radionuclide toxicity in cultured mammalian cells. elucidation of the primary site for radiation-induced division delay. *Radiat Res*, 69(2):348–358, Feb 1977.

[36] Michael C. Joiner. *Basic Clinical Radiobiology*. Hodder Arnold, 2009.

[37] H.R. Withers. The four r's of radiotherapy. in: Letter to editor. *Advancees in Radiation Biology*, 5:241–271, 1975.

[38] G. G. Steel, T. J. McMillan, and J. H. Peacock. The 5rs of radiobiology. *Int J Radiat Biol*, 56(6):1045–1048, Dec 1989.

[39] L.H. Gray, A.D. Conger, M. Ebert, S. Hornsey, and O.C. Scott. The concentration of oxygen dissolved in tissues at the time of irradiation as a factor in radiotherapy. *Br J Radiol*, 26:638–48, 1953.

[40] E. A. WRIGHT and P. HOWARD-FLANDERS. The influence of oxygen on the radiosensitivity of mammalian tissues. *Acta radiol*, 48(1):26–32, Jul 1957.

[41] David J. Carlson, Paul J. Keall, Billy W Loo, Jr, Zhe J. Chen, and J Martin Brown. Hypofractionation results in reduced tumor cell kill compared to conventional fractionation for tumors with regions of hypoxia. *Int J Radiat Oncol Biol Phys*, 79(4):1188–1195, Mar 2011.

[42] Otilia Nuta Firouz Darroudi. The impact of the bystander evect on the low-dose hypersensitivity phenomenon. *Radiat Environ Biophys*, 47:265–274, 2008.

[43] E.J Hall and A.J. Giaccia. *Radiobiology for the Radiologist*. Lippincott Williams & Wilkins, 2006.

[44] H. R. Withers, J. M. Taylor, and B. Maciejewski. The hazard of accelerated tumor clonogen repopulation during radiotherapy. *Acta Oncol*, 27(2):131–146, 1988.

[45] Alfred North Whitehead. *AN: Introduction to mathematics*. Oxford University Press, 1911.

[46] X. Allen Li, Markus Alber, Joseph O. Deasy, Andrew Jackson, Kyung-Wook Ken Jee, Lawrence B. Marks, Mary K. Martel, Charles Mayo, Vitali Moiseenko, Alan E. Nahum, Andrzej Niemierko, Vladimir A. Semenenko, and Ellen D. Yorke. The use and qa of biologically related models for treatment planning: short report of the tg-166 of the therapy physics committee of the aapm. *Med Phys*, 39(3):1386–1409, Mar 2012.

[47] C Clifton Ling and Li X.A. Over the next decade the success of radiation treatment planning will be judged by the immediate biological response of tumor cells rather than by surrogate measures such as dose maximization and uniformity. *Medical Physics*, 32(7):2189–2192, 2005.

[48] Brad Warkentin, Pavel Stavrev, Nadia Stavreva, Colin Field, and B Gino Fallone. A tcp-ntcp estimation module using dvhs and known radiobiological models and parameter sets. *J Appl Clin Med Phys*, 5(1):50–63, 2004.

[49] B. Sanchez-Nieto and A. E. Nahum. Bioplan: software for the biological evaluation of. radiotherapy treatment plans. *Med Dosim*, 25(2):71–76, 2000.

[50] M. Langer, S. S. Morrill, and R. Lane. A test of the claim that plan rankings are determined by relative complication and tumor-control probabilities. *Int J Radiat Oncol Biol Phys*, 41(2):451–457, May 1998.

[51] T. R. MUNRO and C. W. GILBERT. The relation between tumour lethal doses and the radiosensitivity of tumour cells. *Br J Radiol*, 34:246–251, Apr 1961.

[52] J. F. Fowler. The linear-quadratic formula and progress in fractionated radiotherapy. *Br J Radiol*, 62(740):679–694, Aug 1989.

[53] R. G. Dale. The application of the linear-quadratic dose-effect equation to fractionated and protracted radiotherapy. *Br J Radiol*, 58(690):515–528, Jun 1985.

[54] R. K. Sachs, P. Hahnfeld, and D. J. Brenner. The link between low-let dose-response relations and the underlying kinetics of damage production/repair/misrepair. *Int J Radiat Biol*, 72(4):351–374, Oct 1997.

[55] M. V. Williams, J. Denekamp, and J. F. Fowler. A review of alpha/beta ratios for experimental tumors: implications for clinical studies of altered fractionation. *Int*

J Radiat Oncol Biol Phys, 11(1):87–96, Jan 1985.

[56] L. B. Marks. Extrapolating hypofractionated radiation schemes from radiosurgery data: Regarding hall et al.,. *International of Radiation Oncology Biologoy Physics*, 21:819–824, 1995.

[57] E. Hall and Brenner. Extrapolating hypofractionated radiation schemes from radiosurgery data. *IJROBP*, 25:381–385, 1993.

[58] David J. Brenner. The linear-quadratic model is an appropriate methodology for determining isoeffective doses at large doses per fraction. *Semin Radiat Oncol*, 18(4):234–239, Oct 2008.

[59] John P. Kirkpatrick, Jeffrey J. Meyer, and Lawrence B. Marks. The linear-quadratic model is inappropriate to model high dose per fraction effects in radiosurgery. *Semin Radiat Oncol*, 18(4):240–243, Oct 2008.

[60] John P. Kirkpatrick, David J. Brenner, and Colin G. Orton. Point/counterpoint. the linear-quadratic model is inappropriate to model high dose per fraction effects in radiosurgery. *Med Phys*, 36(8):3381–3384, Aug 2009.

[61] Jack F. Fowler. Linear quadratics is alive and well: in regard to park et al. (int j radiat oncol biol phys 2008;70:847-852). *Int J Radiat Oncol Biol Phys*, 72(3):957; author reply 958, Nov 2008.

[62] J Martin Brown, David J. Brenner, and David J. Carlson. Dose escalation, not "new biology," can account for the efficacy of stereotactic body radiation therapy with non-small cell lung cancer. *Int J Radiat Oncol Biol Phys*, 85(5):1159–1160, Apr 2013.

[63] J Martin Brown, David J. Carlson, and David J. Brenner. Dose escalation, not new biology, can account for the efficacy of stereotactic body radiation therapy with non-small cell lung cancer. in reply to rao et al. *Int J Radiat Oncol Biol Phys*, 89(3):693–694, Jul 2014.

[64] Shyam S. Rao, Jung Hun Oh, Andrew Jackson, and Joseph O. Deasy. Dose escalation, not new biology, can account for the efficacy of stereotactic body radiation therapy with non-small cell lung cancer. in regard to brown et al. *Int J Radiat Oncol Biol Phys*, 89(3):692–693, Jul 2014.

[65] M. Guerrero and X Allen Li. Extending the linear-quadratic model for large fraction doses pertinent to stereotactic radiotherapy. *Phys Med Biol*, 49(20):4825–4835, Oct 2004.

[66] Clint Park, Lech Papiez, Shichuan Zhang, Michael Story, and Robert D. Timmerman. Universal survival curve and single fraction equivalent dose: useful tools in understanding potency of ablative radiotherapy. *Int J Radiat Oncol Biol Phys*, 70(3):847–852, Mar 2008.

[67] Jian Z. Wang, Zhibin Huang, Simon S. Lo, William T C. Yuh, and Nina A. Mayr. A generalized linear-quadratic model for radiosurgery, stereotactic body radiation therapy, and high-dose rate brachytherapy. *Sci Transl Med*, 2(39):39ra48, Jul 2010.

[68] Frederick W. McKenna and Salahuddin Ahmad. Isoeffect calculations with the linear quadratic and its extensions: An examination of model-dependent estimates at doses relevant to hypofractionation. *J Med Phys*, 36(2):100–106, Apr 2011.

[69] A. Niemierko. Reporting and analyzing dose distributions: a concept of equivalent uniform dose. *Med Phys*, 24(1):103–110, Jan 1997.

[70] G. J. Kutcher, C. Burman, L. Brewster, M. Goitein, and R. Mohan. Histogram reduction method for calculating complication probabilities for three-dimensional treatment planning evaluations. *Int J Radiat Oncol Biol Phys*, 21(1):137–146, May 1991.

[71] Prescribing, recording and reporting photon beam therapy (report 62). Technical report, International Commission on Radiation Units & Measurements, 1999.

[72] M. C. Joiner, B. Marples, and H. Johns. The response of tissues to very low doses per fraction: a reflection of induced repair? *Recent Results Cancer Res*, 130:27–40, 1993.

[73] B. G. Wouters and L. D. Skarsgard. Low-dose radiation sensitivity and induced radioresistance to cell killing in ht-29 cells is distinct from the "adaptive response" and cannot be explained by a subpopulation of sensitive cells. *Radiat Res*, 148(5):435–442, Nov 1997.

[74] M. C. Joiner, B. Marples, P. Lambin, S. C. Short, and I. Turesson. Low-dose hypersensitivity: current status and possible mechanisms. *Int J Radiat Oncol Biol Phys*, 49(2):379–389, Feb 2001.

[75] Patrick D. Beauchesne, Suzanne Bertrand, Robert Branche, Steven P. Linke, Roland Revel, Jean-Franois Dore, and Rmy M. Pedeux. Human malignant glioma cell lines are sensitive to low radiation doses. *Int J Cancer*, 105(1):33–40, May 2003.

[76] Kevin M. Prise and Joe M. O'Sullivan. Radiation-induced bystander signalling in cancer therapy. *Nat Rev Cancer*, 9(5):351–360, May 2009.

[77] D.J. Brenner, J.B. Little, and R.K. Sachs. The bystander effect in radiation oncogenesis: Ii. a quantitative model. *Radiation Research*, 155:402–408, 2001.

[78] William F. Morgan. Non-targeted and delayed effects of exposure to ionizing radiation: I. radiation-induced genomic instability and bystander effects in vitro. *Radiat Res*, 159(5):567–580, May 2003.

[79] William F. Morgan. Non-targeted and delayed effects of exposure to ionizing radiation: Ii. radiation-induced genomic instability and bystander effects in vivo, clastogenic factors and transgenerational effects. *Radiat Res*, 159(5):581–596, May 2003.

[80] Carmel Mothersill and Colin B. Seymour. Radiation-induced bystander effects–implications for cancer. *Nat Rev Cancer*, 4(2):158–164, Feb 2004.

[81] Nobuyuki Hamada, Hideki Matsumoto, Takamitsu Hara, and Yasuhiko Kobayashi. Intercellular and intracellular signaling pathways mediating ionizing radiation-induced bystander effects. *J Radiat Res*, 48(2):87–95, Mar 2007.

[82] Zelanna Goldberg and Bruce E. Lehnert. Radiation-induced effects in unirradiated cells: a review and implications in cancer. *Int J Oncol*, 21(2):337–349, Aug 2002.

[83] Rajamanickam Baskar. Emerging role of radiation induced bystander effects: Cell communications and carcinogenesis. *Genome Integr*, 1(1):13, 2010.

[84] H. Nagasawa and J. B. Little. Induction of sister chromatid exchanges by extremely low doses of alpha-particles. *Cancer Res*, 52(22):6394–6396, Nov 1992.

[85] C. Mothersell and C Seymour. Medium from irradiated human epithelial cells but not human fibroblasts reduces the clonogenic survival of unirradiated cells. *Int J Radiat Biol*, 71:421–427, 1997.

[86] Karl T. Butterworth, Conor K. McGarry, Colman Trainor, Stephen J. McMahon, Joe M. O'Sullivan, Giuseppe Schettino, Alan R. Hounsell, and Kevin M. Prise.

Dose, dose-rate and field size effects on cell survival following exposure to non-uniform radiation fields. *Phys Med Biol*, 57(10):3197–3206, May 2012.

[87] Hooshang Nikjoo and Igor K. Khvostunov. Biophysical model of the radiation-induced bystander effect. *Int J Radiat Biol*, 79(1):43–52, Jan 2003.

[88] M. P. Little, J A N. Filipe, K. M. Prise, M. Folkard, and O. V. Belyakov. A model for radiation-induced bystander effects, with allowance for spatial position and the effects of cell turnover. *J Theor Biol*, 232(3):329–338, Feb 2005.

[89] F. Ballarini, D. Alloni, A. Facoetti, A. Mairani, R. Nano, and A. Ottolenghi. Modelling radiation-induced bystander effect and cellular communication. *Radiat Prot Dosimetry*, 122(1-4):244–251, 2006.

[90] R. D. Stewart, R. K. Ratnayake, and K. Jennings. Microdosimetric model for the induction of cell killing through medium-borne signals. *Radiat Res*, 165(4):460–469, Apr 2006.

[91] Igor Shuryak, Rainer K. Sachs, and David J. Brenner. Biophysical models of radiation bystander effects: 1. spatial effects in three-dimensional tissues. *Radiat Res*, 168(6):741–749, Dec 2007.

[92] Martin A. Ebert, Natalka Suchowerska, Michael A. Jackson, and David R. McKenzie. A mathematical framework for separating the direct and bystander components of cellular radiation response. *Acta Oncol*, 49(8):1334–1343, Nov 2010.

[93] Stephen J. McMahon, Karl T. Butterworth, Colman Trainor, Conor K. McGarry, Joe M. O'Sullivan, Giuseppe Schettino, Alan R. Hounsell, and Kevin M. Prise. A kinetic-based model of radiation-induced intercellular signalling. *PLoS One*, 8(1):e54526, 2013.

[94] Stephen J. McMahon, Karl T. Butterworth, Conor K. McGarry, Colman Trainor, Joe M. O'Sullivan, Alan R. Hounsell, and Kevin M. Prise. A computational model of cellular response to modulated radiation fields. *Int J Radiat Oncol Biol Phys*, 84(1):250–256, Sep 2012.

[95] A. Brown and E. Day. Assessment of motion and field placement verification of the prostate using gold seed fiducial markers: a feasibility study. *The Radiographer*, 57:12–20, 2010.

[96] P. B. Greer, K. Dahl, M. A. Ebert, C. Wratten, M. White, and J. W. Denham. Comparison of prostate set-up accuracy and margins with off-line bony anatomy corrections and online implanted fiducial-based corrections. *J Med Imaging Radiat Oncol*, 52(5):511–516, Oct 2008.

[97] Marco Krengli, Simone Gaiano, Eleonora Mones, Andrea Ballar, Debora Beld, Cesare Bolchini, and Gianfranco Loi. Reproducibility of patient setup by surface image registration system in conformal radiotherapy of prostate cancer. *Radiat Oncol*, 4:9, 2009.

[98] E. K. Osei, R. Jiang, R. Barnett, K. Fleming, and D. Panjwani. Evaluation of daily online set-up errors and organ displacement uncertainty during conformal radiation treatment of the prostate. *Br J Radiol*, 82(973):49–61, Jan 2009.

[99] T. R. Siow, C. L. Ngoi, and W. K. Tan. Inter-fraction prostate motion during intensity-modulated radiotherapy for prostate cancer. *Singapore Med J*, 52(6):405–409, Jun 2011.

[100] Sabine Levegrn, Andrew Jackson, Michael J. Zelefsky, Ennapadam S. Venkatraman, Mark W. Skwarchuk, Wolfgang Schlegel, Zvi Fuks, Steven A. Leibel, and

C Clifton Ling. Risk group dependence of dose-response for biopsy outcome after three-dimensional conformal radiation therapy of prostate cancer. *Radiother Oncol*, 63(1):11–26, Apr 2002.

[101] Rex Cheung, Susan L. Tucker, Lei Dong, and Deborah Kuban. Dose-response for biochemical control among high-risk prostate cancer patients after external beam radiotherapy. *Int J Radiat Oncol Biol Phys*, 56(5):1234–1240, Aug 2003.

[102] S. M. Oliveira, N. J. Teixeira, and L. Fernandes. What do we know about the alpha/beta for prostate cancer? *Med Phys*, 39(6):3189–3201, Jun 2012.

[103] J. T. Booth and S. F. Zavgorodni. The effects of radiotherapy treatment uncertainties on the delivered dose distribution and tumour control probability. *Australas Phys Eng Sci Med*, 24(2):71–78, Jun 2001.

[104] Henk B. Kal and Marion P R. Van Gellekom. How low is the alpha/beta ratio for prostate cancer? *Int J Radiat Oncol Biol Phys*, 57(4):1116–1121, Nov 2003.

[105] Raymond. Miralbell, S. Roberts, E. Zubizarreta, and J.H. Hendry. Dose fractionation sensitivity of of prostate cancer deduced from radiotherapy outcomes of 5969 patients in seven international institution data sets. *Int J Radiat Oncol Biol Phys*, 82:e17–e24, 2012.

[106] Wang J.Z., Guerrero M., and Li X.A. How low is the alpha/beta ratio for prostate cancer? *Int J Oncol Biol Phys*, 55:194–203, 2003.

[107] Manish D. Shah and Ken Balderson. A manic episode associated with efavirenz therapy for hiv infection. *AIDS*, 17(11):1713–1714, Jul 2003.

[108] Y. Ilnytskyy and O. Koturbash, I. Kovalchuk. Radiation-induced bystander effects in vivo are epigenetically regulated in a tissue-specific manner. *Environmental and*

Molecular Mutagenesi, 50:105–13, 2009.

[109] Mike Partridge. A radiation damage repair model for normal tissues. *Phys Med Biol*, 53(13):3595–3608, Jul 2008.

[110] Fernando P. Faria, Ronald Dickman, and Carlos H C. Moreira. Models of the radiation-induced bystander effect. *Int J Radiat Biol*, 88(8):592–599, Aug 2012.

[111] S. Scott, P. Gumerlock, L. Beckett, Y. Li, and Z. Goldberg. Survival and cell cycle kinetics of human prostate cancer cell lines after single and multifraction exposures to ionizing radiation. *Int J Radiat Oncol Biol Phys*, 59:219–227, 2004.

[112] H. Washida, M. Tsugaya, N. Hirao, H. Sakagami, and Y. Iwase. [pharmacokinetic study of cefmenoxime concerning its transfer into tissues]. *Jpn J Antibiot*, 38(6):1648–1653, Jun 1985.

[113] D. Kaushal, M. L. Garg, M. R. Bansal, and M. P. Bansal. Biokinetics of lead in various organs of rats using radiotracer technique. *Biol Trace Elem Res*, 53(1-3):249–260, 1996.

[114] C. Spitzweg, A. B. Dietz, M. K. O'Connor, E. R. Bergert, D. J. Tindall, C. Y. Young, and J. C. Morris. In vivo sodium iodide symporter gene therapy of prostate cancer. *Gene Ther*, 8(20):1524–1531, Oct 2001.

[115] Igor Koturbash, Jonathan Loree, Kristy Kutanzi, Clayton Koganow, Igor Pogribny, and Olga Kovalchuk. In vivo bystander effect: cranial x-irradiation leads to elevated dna damage, altered cellular proliferation and apoptosis, and increased p53 levels in shielded spleen. *Int J Radiat Oncol Biol Phys*, 70(2):554–562, Feb 2008.

[116] Michael J. Balderson and Charles Kirkby. Potential implications of the bystander effect on tcp and eud when considering target volume dose heterogeneity. *Int J*

Radiat Biol, 91(1):54–61, Jan 2015.

[117] S. Webb and A. E. Nahum. A model for calculating tumour control probability in radiotherapy including the effects of inhomogeneous distributions of dose and clonogenic cell density. *Phys Med Biol*, 38(6):653–666, Jun 1993.

[118] S. Webb, P. M. Evans, W. Swindell, and J. O. Deasy. A proof that uniform dose gives the greatest tcp for fixed integral dose in the planning target volume. *Phys Med Biol*, 39(11):2091–2098, Nov 1994.

[119] M. Goitein. Causes and consequences of inhomogeneous dose distributions in radiation therapy. *Int J Radiat Oncol Biol Phys*, 12(4):701–704, Apr 1986.

[120] L. Strigari, L. C. Orlandini, I. Andriani, A. d'Angelo, M. Stefanacci, A. M. Di Nallo, and Marcello Benassi. A mathematical approach for evaluating the influence of dose heterogeneity on tcp for prostate cancer brachytherapy treatment. *Phys Med Biol*, 53(18):5045–5059, Sep 2008.

[121] R. J. Yaes. The biological effect of inhomogeneous dose distributions in fractionated radiotherapy. *Int J Radiat Oncol Biol Phys*, 19(1):203–207, Jul 1990.

[122] E. D. Yorke. Modeling the effects of inhomogeneous dose distributions in normal tissues. *Semin Radiat Oncol*, 11(3):197–209, Jul 2001.

[123] E. I. Azzam, S. M. de Toledo, and J. B. Little. Direct evidence for the participation of gap junction-mediated intercellular communication in the transmission of damage signals from alpha -particle irradiated to nonirradiated cells. *Proc Natl Acad Sci U S A*, 98(2):473–478, Jan 2001.

[124] Joseph M. Kaminski, Eric Shinohara, James Bradley Summers, Kenneth J. Niermann, Allan Morimoto, and Jeffrey Brousal. The controversial abscopal effect.

Cancer Treat Rev, 31(3):159–172, May 2005.

[125] Svetlana Sjostedt and Eva Bezak. Non-targeted effects of ionising radiation and radiotherapy. *Australas Phys Eng Sci Med*, 33(3):219–231, Sep 2010.

[126] Stephen J. McMahon, Conor K. McGarry, Karl T. Butterworth, Joe M. O'Sullivan, Alan R. Hounsell, and Kevin M. Prise. Implications of intercellular signaling for radiation therapy: a theoretical dose-planning study. *Int J Radiat Oncol Biol Phys*, 87(5):1148–1154, Dec 2013.

[127] E. I. Azzam, S. M. de Toledo, T. Gooding, and J. B. Little. Intercellular communication is involved in the bystander regulation of gene expression in human cells exposed to very low fluences of alpha particles. *Radiat Res*, 150(5):497–504, Nov 1998.

[128] E Claridge Mackonis, N. Suchowerska, M. Zhang, M. Ebert, D. R. McKenzie, and M. Jackson. Cellular response to modulated radiation fields. *Phys Med Biol*, 52(18):5469–5482, Sep 2007.

[129] William M. Bonner. Phenomena leading to cell survival values which deviate from linear-quadratic models. *Mutat Res*, 568(1):33–39, Dec 2004.

[130] Oleg V. Belyakov, Stephen A. Mitchell, Deep Parikh, Gerhard Randers-Pehrson, Stephen A. Marino, Sally A. Amundson, Charles R. Geard, and David J. Brenner. Biological effects in unirradiated human tissue induced by radiation damage up to 1 mm away. *Proc Natl Acad Sci U S A*, 102(40):14203–14208, Oct 2005.

[131] Kevin M. Prise, Melvyn Folkard, and Barry D. Michael. Bystander responses induced by low let radiation. *Oncogene*, 22(45):7043–7049, Oct 2003.

[132] C. B. Seymour and C. Mothersill. Relative contribution of bystander and targeted cell killing to the low-dose region of the radiation dose-response curve. *Radiat Res*, 153(5 Pt 1):508–511, May 2000.

[133] A. Syme, C. Kirkby, R. Mirzayans, M. MacKenzie, C. Field, and B. G. Fallone. Relative biological damage and electron fluence in and out of a 6 mv photon field. *Phys Med Biol*, 54(21):6623–6633, Nov 2009.

[134] C. Kirkby, C. Field, M. MacKenzie, A. Syme, and B. G. Fallone. A monte carlo study of the variation of electron fluence in water from a 6 mv photon beam outside of the field. *Phys Med Biol*, 52(12):3563–3578, Jun 2007.

[135] B. Marples. Is low-dose hyper-radiosensitivity a measure of g2-phase cell radiosensitivity? *Cancer Metastasis Rev*, 23(3-4):197–207, 2004.

[136] Carmel Mothersill and C. B. Seymour. Radiation-induced bystander effects and the dna paradigm: an "out of field" perspective. *Mutat Res*, 597(1-2):5–10, May 2006.

[137] Carmel Mothersill and Colin Seymour. Radiation-induced bystander effects: evidence for an adaptive response to low dose exposures? *Dose Response*, 4(4):283–290, 2006.

[138] Carmel Mothersill, C. B. Seymour, and M. C. Joiner. Relationship between radiation-induced low-dose hypersensitivity and the bystander effect. *Radiat Res*, 157(5):526–532, May 2002.

[139] Brian Marples, Michael C. Joiner, and Kirsten A. Skov. The effect of oxygen on low-dose hypersensitivity and increased radioresistance in chinese hamste v79-379a cells. *Radiation Research*, 138:S17–S20, 1994.

[140] A.C Heuskin, A-C.and Were, H Riguier, C. Micheles, and S. Lucas. Low-dose hypersensitivity and bystander effect are not mutually exclusive in a549 lung carcinoma cells after irradiation with charged particles. *Radiat R*, 180:491–8, 2013.

[141] Hooshang Nikjoo and Lennart Lindborg. Rbe of low energy electrons and photons. *Phys Med Biol*, 55(10):R65–109, May 2010.

[142] H. H. Liu and F. Verhaegen. An investigation of energy spectrum and lineal energy variations in mega-voltage photon beams used for radiotherapy. *Radiat Prot Dosimetry*, 99(1-4):425–427, 2002.

[143] C. Kirkby, E. Ghasroddashti, Y. Poirier, M. Tambasco, and R. D. Stewart. Rbe of kv cbct radiation determined by monte carlo dna damage simulations. *Phys Med Biol*, 58(16):5693–5704, Aug 2013.

[144] R. D. Stewart, S. Streitmatter, D.C. Argento, C. Kirkby, J.T. Goorley, and G. Moffitt. Rapid multiscale simulation of dna double strand break (dsb) relative biological effectiveness (rbe) for photons, neutrons, and light ions. *Phys Med Biol (submitted April 2015)*, 2015.

[145] R. A. McMasters, R. L. Saylors, K. E. Jones, M. E. Hendrix, M. P. Moyer, and R. R. Drake. Lack of bystander killing in herpes simplex virus thymidine kinase-transduced colon cell lines due to deficient connexin43 gap junction formation. *Hum Gene Ther*, 9(15):2253–2261, Oct 1998.

[146] C. Denning and J. D. Pitts. Bystander effects of different enzyme-prodrug systems for cancer gene therapy depend on different pathways for intercellular transfer of toxic metabolites, a factor that will govern clinical choice of appropriate regimes. *Hum Gene Ther*, 8(15):1825–1835, Oct 1997.

[147] Stephen J. McMahon, Conor K. McGarry, Karl T. Butterworth, Suneil Jain, Joe M. O'Sullivan, Alan R. Hounsell, and Kevin M. Prise. Cellular signalling effects in high precision radiotherapy. *Phys Med Biol*, 60(11):4551–4564, Jun 2015.

[148] Daryoush Sheikh-Bagheri and D W O. Rogers. Monte carlo calculation of nine megavoltage photon beam spectra using the beam code. *Med Phys*, 29(3):391–402, Mar 2002.

[149] Y. Hsiao and R. D. Stewart. Monte carlo simulation of dna damage induction by x-rays and selected radioisotopes. *Phys Med Biol*, 53(1):233–244, Jan 2008.

[150] Josep Sempau, Andreu Badal, and Lorenzo Brualla. A penelope-based system for the automated monte carlo simulation of clinacs and voxelized geometries-application to far-from-axis fields. *Med Phys*, 38(11):5887–5895, Nov 2011.

[151] V. A. Semenenko and R. D. Stewart. Fast monte carlo simulation of dna damage formed by electrons and light ions. *Phys Med Biol*, 51(7):1693–1706, Apr 2006.

[152] Robert D. Stewart, Victor K. Yu, Alexandros G. Georgakilas, Constantinos Koumenis, Joo Han Park, and David J. Carlson. Effects of radiation quality and oxygen on clustered dna lesions and cell death. *Radiat Res*, 176(5):587–602, Nov 2011.

[153] David J. Carlson, Robert D. Stewart, Vladimir A. Semenenko, and George A. Sandison. Combined use of monte carlo dna damage simulations and deterministic repair models to examine putative mechanisms of cell killing. *Radiat Res*, 169(4):447–459, Apr 2008.

[154] Karl T. Butterworth, Conor K. McGarry, Colman Trainor, Joe M. O'Sullivan, Alan R. Hounsell, and Kevin M. Prise. Out-of-field cell survival following exposure to intensity-modulated radiation fields. *Int J Radiat Oncol Biol Phys*, 79(5):1516–1522, Apr 2011.

[155] Gilles Crehange, Celine Mirjolet, Melanie Gauthier, Etienne Martin, Gilles Truc, Karine Peignaux-Casasnovas, Caroline Azelie, Franck Bonnetain, Suzanne Naudy, and Philippe Maingon. Clinical impact of margin reduction on late toxicity and short-term biochemical control for patients treated with daily on-line image guided imrt for prostate cancer. *Radiother Oncol*, 103(2):244–246, May 2012.

[156] Ingelise Jensen, Jesper Carl, Bente Lund, Erik H. Larsen, and Jane Nielsen. Radiobiological impact of reduced margins and treatment technique for prostate cancer in terms of tumor control probability (tcp) and normal tissue complication probability (ntcp). *Med Dosim*, 36(2):130–137, 2011.

[157] Arthur L Boyer and Timothy Schultheiss. Effects of dosimetric and clinical uncertainty on complication-free local tumor control. *Radiotherapy and Oncology*, 11(1):65–71, 1988.

[158] J. O. Deasy. Comments on the use of the lyman-kutcher-burman model to describe tissue response to nonuniform irradiation. *Int J Radiat Oncol Biol Phys*, 47(5):1458–1460, Jul 2000.

[159] P. Kllman, A. Agren, and A. Brahme. Tumour and normal tissue responses to fractionated non-uniform dose delivery. *Int J Radiat Biol*, 62(2):249–262, Aug 1992.